Internal Representations for the Generalization of Motor Memories

Thesis Advisor
Professor Maurice A. Smith

Author
Jordan B. Brayanov

INTERNAL REPRESENTATIONS FOR THE GENERALIZATION OF MOTOR MEMORIES

ABSTRACT

Movement and memory are two of the most fundamental components of our existence. From the moment of birth, we rely on a variety of movements to interact with people and objects around us, and as we grow, we continuously form new motor memories to improve the fidelity of these interactions by exploring and learning more about our environment, especially in unfamiliar situations, ultimately becoming better equipped to handle novel and unknown environments.

In this dissertation, we explore four facets of motor memory associated with voluntary movement and postural control in the upper limbs:

(1) Optimal motor memory formation via sensorimotor integration. We ask whether the motor system combines prior memories with new sensory information to produce statistically-optimal weight estimates. We find that the weight estimate that the motor system makes in order to re-stabilize one's arm posture when an object is rapidly removed from the hand that supports it, reflected information integration in a Bayesian, statistically-optimal fashion. Remarkably, we demonstrate that when experiencing the well-known size-weight illusion, the motor and perceptual system's weight estimates are biased in opposite directions, suggesting two divergent modes for information integration within the central nervous system.

(2) Movement features important for the learning and generalization of motor memories. We show that, velocity-dependent adaptation generalizes across different movements, even from discrete straight point-to-point to continuous circular movements, however the amount of generalization is limited and context-dependent. In a series of experiments, we quantified the contributions of different movement features to the elicited adaptation transfer. In particular, we

show that other movement states (i.e. position and acceleration) make only minor contributions whereas, the contexts provided by movement geometry and movement continuity are critical.

(3) Internal representation of motor memories in intrinsic-extrinsic coordinates. We show that motor memories are based not on fully intrinsic or extrinsic representations but on a gain-field (multiplicative) combination the two. This gain-field representation generalizes between actions by effectively computing movement similarity based on the Mahalanobis distance across both intrinsic and extrinsic coordinates, in line with neural recordings showing mixed intrinsic-extrinsic representations in motor and parietal cortices.

(4) Motor memories with local and global generalization. We demonstrate the existence of two distinct components of motor memory displaying different generalization footprints: One generalizes only locally, around the trained movement direction and with the trained end-effector, whereas the other generalizes broadly across both., We proceed to show that broad generalization results from a rapidly-learning adaptive process, dominates on easier-to-learn tasks, and performs high-level processing, producing adaptation vectors that integrate multiple sources of information, in line with a recent theory for perceptual learning.

TABLE OF CONTENTS

Acknowledgements

First, I would like to thank my advisor, Professor Maurice Smith, for his mentorship, training, and intellectual challenges which have defined the last 6.5 years of my life. The quantitative and analytic rigor which he brings to every situation has been one of his greatest gifts, and I can only hope that some of it has rubbed off onto me. Moreover, his personal generosity, inclusiveness, and giving nature have set an example for me and every person who has worked within the lab. I would also like to thank the other members of my committee, Professor Dan Press, Professor Bence Ölveczky, and Professor Robert Howe, for their guidance and support, and in particular, Dan for his contributions and collaboration on the gain-field representation project described in Chapter 4.

Next, I thank my fellow graduate students (Luis Nicolas Gonzalez-Castro, Howard Wu, Gary Sing, Alkis Hadjiosif, Yohsuke Miyamoto, and Andrew Brennan) and post-docs (Bijan Najafi, Wilsaan Joiner, Thrishantha Nanayakkara, and Biljana Petreska) in the Harvard Neuromotor Control Lab for the countless hours of relaxation time, collaborative work, and intense discussions and debates we have shared both inside and outside of lab. In particular, I would like to thank Alkis Hadjiosif and Biljana Petreska for designing, running, and analyzing the data relating to several of the experiments described in Chapter 5.

I would like to thank my friends, and in particular Iliya Tsekov, for their support during these years. I thank my wife, Rene Chen, for always being there for me, reminding me to exercise and eat right (which I never do) and for her invaluable help with the scientific illustrations which appear in almost all chapters of my thesis and all of my papers. Lastly, I thank my family: my parents and my brother for giving me the opportunity to develop into the person that I am today.

CHAPTER 1 – INTRODUCTION AND MOTIVATION

Although the nervous system has an exceedingly rich repertoire of functions and abilities, its primary purpose is to produce movement as physical movement is essentially the only way an organism can interact with its environment. Movements give us the freedom to explore our environment and the power to affect our surroundings by interacting with those around including the ability to communicate. Correspondingly, among the most debilitating neurologic conditions are those which affect our ability to move, as they can limit communication and render patients unable to care for themselves.

Reflex loops, the processing of sensory information, and even higher-order abilities such as thought and reasoning likely exist only to improve the planning and execution of physical movements. One key feature of movement is that it is highly adaptable. Several different types of motor learning have been identified and the knowledge of the molecular, cellular, and genetic basis of motor learning is rapidly expanding. However, we do not yet understand the mechanisms for motor learning at an algorithmic level. Understanding these mechanisms would increase not only our basic knowledge about the function of the nervous system but also holds the promise of pointing towards improved rehabilitation strategies for people with debilitating motor deficits.

1.1 MEMORY FORMATION

Visually guided reaching is one of the earliest movement abilities that develop in young children (Halverson, 1931; Hofsten and Lindhagen, 1979; White et al, 1964). In fact, infants are able to accurately reach towards either stationary (Halverson, 1931; White et al, 1964) or moving (Hofsten and Lindhagen, 1979) visual targets by the time they are 4-months old. Soon after, the ability to adapt previously learned motor memories becomes essential for maintaining accurate performance in the face of changing biomechanical properties (e.g. using a tool) or operating in a new environment.

This dissertation focuses on the mechanisms for the formation of memories associated with the learning of visually-guided reaching arm movements and postural control of the arm. In particular, we examined the key features encoded in these memories, the coordinate system in which these memories are represented, and how they generalize to novel movements.

Here we focus on error-dependent learning in humans during visually guided movements (Mazzoni and Krakauer, 2006; Smith et al 2006; Thoroughman and Shadmehr, 2000) as a model system for understanding motor memory. In this type of learning the motor system relies on a real-time error signal, the difference between a desired and actual outcome, to drive memory formation.

1.2 ERROR-BASED LEARNING

Although it is likely that multiple learning algorithms contribute to motor learning (Diedrichsen et al., 2010; Huang et al., 2011; Izawa and Shadmehr, 2011; Wolpert et al., 2011) a form of error-based learning known as motor adaptation has been widely studied during visually guided reaching arm movements (Shadmehr and Mussa-Ivaldi, 1994; Ghahramani et al., 1996; Conditt et al., 1997; Conditt and Mussa-Ivaldi, 1999; Krakauer et al., 2000; Shadmehr and Moussavi, 2000; Morton et al., 2001; Baraduc and Wolpert, 2002; Malfait et al., 2002; Morton and Bastian, 2004; Smith and Shadmehr, 2005; Bays and Wolpert, 2006; Hwang et al., 2006; Ghez et al., 2007; Mattar and Ostry, 2007; Wagner and Smith, 2008; Haswell et al., 2009; Mattar and Ostry, 2010; Quaia et al., 2010; Gonzalez Castro et al., 2011; Joiner et al., 2011). Specifically, when errors occur during a movement, motor learning based on that error acts to reduce the chance of similar error in the future. For example, if a reaching movement overshoots a target, error-based learning will attempt to reduce the movement extent of the subsequent movement. Thus, when error

information is available, error-based learning provides a robust approach for achieving accurate movements in novel environments.

Two tasks, both of which appear in this dissertation, have been commonly used when studying error-based learning: force-field adaptation and visuomotor transformation learning. Force-field adaptation is a paradigm in which a novel dynamic environment can be constructed for subjects to learn by using a robotic manipulandum programmed to produce force as a function of motion state (Thoroughman and Shadmehr, 2000; Smith et al., 2006; Sing et al., 2009; Shadmehr and Mussa-Ivaldi, 1994; Scheidt et al., 2000; Bays et al., 2005). In this task, subjects grasp a robotic manipulandum and make visually guided reaching arm movements while external forces are applied to the subject's hand, leading at first to unexpected preturbations.

A second paradigm for studying motor adaptation is visuomotor transformation learning during voluntary reaching (Mazzoni and Krakauer, 2006; Krakauer et al, 2006; Krakauer, 2009; Krakauer et al., 2000; Krakauer et al., 1999; Kagerer et al., 1997; Huang et al., 2011; Ghez et al., 2007). In this task, direct vision of the hand is obstructed while a cursor representing hand position is shown on a screen. In one version of this task, visuomotor rotation learning, a visual perturbation is imposed by rotating the cursor around a fixed location so that it no longer accurately reflects hand position. In order to successfully maneuver the cursor to the target in a straight line, subjects need to adapt by moving their hand at a deviated angle relative to the visual target. Interestingly, since the imposed perturbation is purely visual in nature, the visual error signal conflicts with the unaltered proprioceptive information. Despite this conflict, subjects robustly recalibrate their movements to adapt to these visual perturbations.

1.3 SCOPE OF THIS WORK

In this dissertation we look at error-based learning for novel dynamic environments and visuomotor transformations.

In Chapter 2 we present evidence regarding the estimation of weight in the motor system when handling novel objects to improve postural stability. In particular, we demonstrate the ability of the motor system to integrate sensory information in a statistically-optimal fashion when estimating the weight of a novel object. Remarkably, the weight estimate generated by the motor system displays an opposite bias to the perceptual weight estimate for the same object, demonstrating the existence of two divergent modes for information integration within the CNS.

In Chapter 3 we investigate existing claims that movement dynamics are learned exclusively as a function of motion state. We provide evidence showing that while motion states (position, velocity, and acceleration) are important factors, the movement geometry and continuity just as important.

In Chapter 4 we investigate the reference frames used by the motor system in the internal representation of motor memories for movement kinematics. We provide evidence refuting previous claims that these memories are represented in purely extrinsic (world-based) coordinate and conclusively show that these memories are instead represented by a gain-field combination of intrinsic and extrinsic coordinates.

In Chapter 5 we examine how broadly motor memory generalizes across untrained conditions and demonstrate that the memories associated with visuomotor transformation learning are based on two distinct processes: One process learns quickly and generalizes broadly, whereas the other learns more slowly and generalizes locally. We draw a parallel to similar phenomena previously observed in sensory learning. These findings may provide the basis for the formation of a unified theory for procedural learning, bridging theories from sensory and motor learning.

CHAPTER 2: BAYESIAN AND "ANTI-BAYESIAN" BIASES IN SENSORY INTEGRATION FOR ACTION AND PERCEPTION IN THE SIZE-WEIGHT ILLUSION

2.1 SUMMARY

Which is heavier: a pound of lead or a pound of feathers? This classic trick question belies a simple but surprising truth: when lifted, the pound of lead feels heavier – a phenomenon known as the size-weight illusion. To estimate the weight of an object, our central nervous system combines two imperfect sources of information: a prior expectation, based on the object's appearance, and direct sensory information from lifting it. Bayes' Law defines the statistically-optimal way to combine multiple information sources for maximally accurate estimation. Here we asked whether the mechanisms for combining these information sources produce statistically-optimal weight estimates for both perceptions and actions.

We first studied the ability of subjects to hold one hand steady when the other removed an object from it, under conditions in which sensory information about the object's weight sometimes conflicted with prior expectations based on its size. Since the ability to steady the supporting hand depends on the generation of a motor command that accounts for lift timing and object weight, hand motion can be used to gauge biases in weight estimation by the motor system. We found that these motor system weight estimates reflected the integration of prior expectations with real-time proprioceptive information in a Bayesian, statistically-optimal fashion that discounted unexpected sensory information. This produces a motor size-weight-illusion that consistently biases weight estimates *toward* prior expectations. In contrast, when subjects compared the weights of two objects, their perceptions defied Bayes' Law, exaggerating the value of unexpected sensory information. This produces a perceptual size-weight-illusion that biases weight perceptions *away* from prior expectations. We term this effect "anti-Bayesian" because the bias is opposite that seen in Bayesian integration. Our findings suggest that two fundamentally different strategies for the integration of prior expectations with sensory information co-exist in the nervous system for weight estimation.

2.2 INTRODUCTION

Early work on the classic (perceptual) size-weight illusion (SWI) suggested that this illusion is due to the difference between anticipated and required motor output for lifting two objects of the same mass but different sizes (Charpentier 1891; Müller and Schumann 1889). The argument has traditionally been that, because people expect larger objects to be heavier (Cross and Rotkin 1975; Flanagan and Beltzner 2000), more force is generated when lifting a larger object, resulting in the perception that it is easier to lift (Davis and Roberts 1976; Müller and Schumann 1889). However, the SWI exists in the absence of motor activation. When objects of different heights but identical mass and cross-sectional area are passively placed on subjects' hands, which are supported from below, the shorter object feels heavier (Usnadze 1931). Furthermore, when two objects that elicit the SWI are alternately lifted, the load forces and grip forces applied to the objects become accurate after just 4-7 lift pairs (Flanagan and Beltzner 2000; Grandy and Westwood 2006) , although the SWI persists unmitigated for at least 20, indicating that mismatched motor output is not required for the illusion.

There is accumulating evidence that the size-weight illusion instead results from a discrepancy between prior expectations and sensory information about object weight. Similar weight perception illusions are seen when objects are expected to weigh different amounts for reasons other than size. For example, in the material-weight illusion (Ellis and Lederman 1999; Harshfield and DeHardt 1970), people perceive cubes that appear to be made of denser materials like steel or brass to be lighter than equal-weight, equal-sized cubes that appear to be made of less dense materials like wood. Similarly, non-golfers find no difference between the perceived weight of real golf balls and practice balls modified to have the same mass. However, experienced golfers consistently perceive the modified, usually lighter, practice balls to be

heavier than the real ones (Ellis and Lederman 1998). These results suggest that experience-dependent expectations about object weight, based on a variety of different object features, drive several weight perception illusions including the SWI (Ellis and Lederman 1998; Jones 1986; Koseleff 1957; Ross 1966). Furthermore, when prior expectations about the relationship between the size and weight of objects are experimentally altered by repeated lifting of unusual small-heavy and large-light objects for thousands of trials over several days, the size-weight-illusion reverses (Flanagan et al. 2008). This suggests that, like the weight expectations which guide motor actions, perceptual expectations can also adapt. However, the rate of this adaptation is much slower, suggesting the maintenance of distinct weight expectations for action and perception.

In the context of the SWI, subjects can combine the expectation that the smaller of two objects will be lighter (Cross and Rotkin 1975; Flanagan and Beltzner 2000) with unbiased but imperfect proprioceptive sensory information about the actual weight of each object when forming weight perceptions. Filtering noisy sensory information through prior expectations can yield more accurate estimates than when this information is used alone. Bayes' Law can be used to determine optimally-accurate estimates that minimize errors in judgment given noisy sensory measurements and prior expectations, and recent studies have suggested that Bayes' law explains several key features of perceptions and motor actions, including certain perceptual illusions (Ernst and Banks 2002; Gregory 2006; Körding et al. 2004; Körding and Wolpert 2004; Norris and Kinoshita 2008; Sato et al. 2007; Stocker and Simoncelli 2006a; Weiss et al. 2002). Therefore, Bayes' Law may provide a framework for understanding illusory weight perceptions driven by prior expectations.

However, it has been noted that the perceptual biases characterizing the SWI cannot be explained by Bayes' law (Ernst 2009; Flanagan et al. 2006), suggesting that weight estimation, in general,

may not be Bayesian. While previous work has shown that prior expectations about object weight can be processed differently for perception and action (Flanagan and Beltzner 2000), it is unclear whether the mechanisms which govern how these prior expectations can influence the interpretation of sensory information are similar or different. In particular, the dorsal and ventral visual streams may process information separately for actions and perceptions (Goodale and Milner 1992; Milner and Goodale 1993). However, it is not known whether these pathways process visually-based prior expectations in fundamentally different ways. Here we contrast the integration of prior expectations with sensory information for weight estimation in perception and involuntary motor action. We show why Bayesian estimation would produce weight and force estimation biases *opposite* to those seen in a variety of perceptual judgments, including the SWI and the attenuated perception of self-generated tactile sensations and force (Bays et al. 2005; Shergill et al. 2003; Weiskrantz et al. 1971), but consistent with motor output biases in a novel motor analog of the SWI.

2.3 METHODS

2.3.1 Participants

Forty healthy human subjects (14 male, 26 female, mean age = 21.4 yrs) with no known neurological deficits participated in this study. All participants gave informed consent and the experimental protocols were approved by the Harvard University Committee on Human Subjects Research.

2.3.2 Experiment 2.1: Motor Analog of the Size-Weight Illusion

In the first experimental task, subjects were presented with 2 cubes of 300 g mass but different sizes (26 mm & 52 mm). The cubes were covered with duct tape to make them look and feel like they might be made of the same material. Two square pieces (1 cm x 1 cm) of 120 grit sandpaper were glued to two opposite sides of the cubes, indicating the proper gripping locations and providing increased friction between the subject's fingers and the cubes. Subjects wore a right-handed glove, instrumented for data collection. On the palm side of the glove, we mounted two circular platforms made from acrylic (76.2 mm in diameter) with a 25 N load cell sandwiched between them. The load cell registered the placement and lifting of cubes on and off the acrylic platform. The platform ensured that the weight of both cubes was distributed over the same area in order to match the proprioceptive response from each one. On the back side of the glove, we mounted a six-axis position sensor and a three axis accelerometer to measure the position and motion of the subject's hand in space with a resolution of 38 μm and 0.1°.

While seated in a chair, each subject placed her right elbow on the table and kept the palm of her gloved right hand horizontal and facing up. Each subject was then asked to grip a cube between the thumb and index finger of her left hand and quickly place it on the platform on her right palm as shown in Figure 2.2a. Subjects maintained a fixed posture with the cube on their palms for 1-2

seconds and then quickly lifted the cube off using the same thumb-index finger grip. Data were continuously recorded at a sampling frequency of 60 Hz. In Experiment 2.1, 20 subjects performed 50 training lifts of the large cube followed by 8 "novel" lifts of the small cube, whereas the other 20 subjects performed 50 training lifts of the small cube, followed by 8 novel lifts of the large cube. After a 1-2 minute break, subjects performed two additional blocks of lifting trials (training followed by novel lifts), in which the number of training lifts was reduced from 50 to 25, but the number of novel cube lifts remained at 8.

2.3.3 Experiment 2.2: Anticipatory postural adjustments generated during a controlled mis-estimation of weight

In the second experimental task, subjects were presented with a stack of two identically-sized, identical-looking cubes, built the same way as the large cubes in the first experiment. We constructed 6 blocks total, 1 each of 150 g, 225 g, 300 g, 300 g, 375 g, and 450 g mass and stacked them together to make 3 stacks of 600 g mass (150 g / 450 g, 225 g / 375 g, 300 g / 300 g) which were indistinguishable from each other.

Subjects placed the stack on the palm of their right hands while maintaining the same fixed arm posture as in Experiment 2.1 (they transported the cubes by holding only the bottom one so that the individual weights could not be easily determined). Subjects then performed a rapid lift of only the top cube from the stack, as shown in Figure 2.4a. After each lifting trial, subjects returned the top cube to the stack on their palm and then picked up the stack by holding the bottom cube and returned it to the table. We then took the stack from them, placed it behind an opaque wall, and then placed another stack in front of them. We repeated these lifting trials 100 times (in 4 sets of 25) with 5 different pair combinations: 150 g / 450 g, 225 g / 375 g, 300 g / 300 g, 375 g / 225 g, and 450 g / 150 g. 76 lifts were with the "control" pair (300 g / 300 g) and 24

”surprise” lifts – 6 with each of the other 4 pairs, randomly interspersed after the 15th trial. The first 15 trials of the first set were all done with the control pair and served as initial training.

2.3.4 Experiment 2.3: Replication of the classic Size-Weight Illusion

In the third experiment we replicated a version of the classic size-weight illusion with the same objects (cubes) as in Experiment 2.1. Prior to this experiment, subjects removed the data collection glove used in Experiments 2.1 and 2.2. We used the small cube (26 mm) from Experiment 2.1 and 9 large cubes (52 mm), all covered in duct tape to look and feel as if they were made of the same material. The small cube had a mass of 300 g and the large cube masses spanned the range of 200 g to 600 g in increments of 50 g. We prepared 3 sequences of the large cubes, ordered by their weight: an increasing (I), a decreasing (D), and a pseudo-random (R). Each sequence contained all 9 large cubes and no cube appeared twice. For every subject a random arrangement of these three sequences was chosen (e.g. while one subject might get I-D-R, another might get D-I-R, etc…) and this determined the order in which the large cubes would be presented. In 27 consecutive trials, subjects were presented with the small cube and a large cube from this arrangement. Subjects were asked whether the small cube felt heavier after lifting both of them off the table, one at a time. Subjects who performed Experiment 2.1 with a small “novel” 300 g cube were asked to lift the large cube first and the small one second before they decided if the small one felt heavier, while the other subjects (who used a large “novel” 300 g cube) were asked to lift the small one first and the large one second.

2.3.5 Data Analyses: motor data

Using the data from the load cell, individual lifting trials from the data collected in Experiments 2.1 and 2.2 were aligned to the time at which the load on the platform decreased by 100g (approximately 1/3 of the linear portion of the unloading force profile, see Figure 2.2b). For

Experiment 2.1 we compared vertical motion of the right hand during the first novel cube lift to the average vertical motion during the previous 10 training cube lifts. We focused our analysis on the first novel cube lift for each subject in order to avoid the effects of motor adaptation. Significance was computed using paired t-tests. The results from the surprise lifts in Experiment 2.2 were used to estimate the sensitivity of the relationship between weight mis-estimation and hand displacement using a simple linear regression as shown in Figure 2.4c. We then used this sensitivity estimate to determine the weight estimation bias associated with the hand displacements obtained in Experiment 2.1 for each subject. The mean across subjects of these weight estimates is plotted in Figure 2.4d with its associated variance. The measurement-variance apropos to Bayesian estimation (the performance noise experienced by a particular subject) can generally be estimated by finding the within-subject, trial-to-trial variability and averaging this quantity across subjects. However, since we based our analysis (and the mean estimate of the weight bias in the motor task) on the first novel lift, the within-subject variability was not available. We did, however, have an estimate of each subject's trial-to-trial variability for the baseline lifts, which one could reasonably expect to be relatively similar to the novel cube lift trial-to-trial variability. To try and further improve the accuracy of our estimate of the associated variance, we scaled it by the ratio of overall variance in the novel cube lift (across subjects) to the overall variance in a single cube baseline lift (across subjects). Note, however, that this scaling had only a modest effect since this ratio was 1.16. This estimate removes the effect to subject-to-subject variability, but still includes the effects of motor output noise and experimental measurement noise, and thus likely overestimates the average variance associated with weight estimation in our sample of subjects slightly.

To estimate the sensitivity of the relationship between weight mis-estimation and hand displacement in Experiment 2.2, we averaged the vertical hand profiles for each stack

configuration: 150 g / 450 g, 225 g / 375g, 300 g / 300 g, 375 g / 225 g, and 450 g / 150 g after excluding the 15 training trials, and performed a simple linear regression.

2.3.6 Data Analyses: perceptual data from Experiment 2.3

For each individual large cube, we calculated the probability that each subject would perceive it to be heavier than the small 300 g cube. We then averaged those probabilities across subjects and fit this psychometric data with the standard logistic function shown in Equation 2.1 (R^2=99.6%). The dark purple curve in Figure 2.1c was obtained by differentiating this logistic function, fitting a Gaussian pdf to it (R^2=94.6%) and dividing the associated variance by a factor of 2. Since the variance in these data comes from independent estimates of the weights of the small and the large cube on each trial, we attributed half of the total variance to the weight estimate for the small cube.

$$S = \frac{1}{1 + e^{-\frac{x-\alpha}{\beta}}} \quad (eq.\ 2.1)$$

2.4 RESULTS AND DISCUSSION

2.4.1 A Bayesian perspective on the size-weight illusion

According to Bayes' Law (Equation 2.2), the likelihood associated with an object's weight can be expressed as a normalized product of the prior expectation (based on visual and/or haptic information about the object) and proprioceptive sensory input when holding the object.

$$\underbrace{P\left(\text{True Weight} \mid \text{Sensation}\right)}_{\substack{\text{Net estimate} \\ (\textit{Posterior})}} = \frac{\overbrace{P\left(\text{Sensation} \mid \text{True Weight}\right)}^{\text{Noisy but unbiased sensory input}} \cdot \overbrace{P\left(\text{True Weight}\right)}^{\text{Prior expectation}}}{\underbrace{P\left(\text{Sensation}\right)}_{\text{Normalization Factor}}} \quad \left(eq.\ 2.2\right)$$

To help understand how Bayesian integration applies to the SWI, Bayes Law can be re-written to explicitly include the effect of object size. We do this by parsing the overall "sensation" of the true weight (TW) referenced in Equation 2.2 into two components: proprioceptive sensation (PS) of object weight, acquired from holding the object, and the visual sensation of object size (Size), acquired from viewing the object (Equation 2.3).

$$\underbrace{P\left(\text{TW} \mid \text{PS},\text{Size}\right)}_{\substack{\text{Net estimate} \\ (\textit{Posterior})}} = \frac{\overbrace{P\left(\text{PS} \mid \text{TW},\text{Size}\right)}^{\substack{\text{Noisy but unbiased} \\ \text{sensory input}}} \cdot \overbrace{P\left(\text{TW},\text{Size}\right)}^{\text{Prior expectation}}}{\underbrace{P\left(\text{PS},\text{Size}\right)}_{\text{Normalization Factor}}} \quad \left(eq.\ 2.3\right)$$

For any given object size, Equation 2.3 can be simplified by applying the definition of conditional probability and noting that raw proprioceptive sensation of weight should not depend on object size.

$$\underbrace{P\left(\mathrm{TW}\mid \mathrm{PS},\mathrm{Size}\right)}_{\substack{\text{Net estimate}\\(\textit{Posterior})}} = \frac{\overbrace{P\left(\mathrm{PS}\mid \mathrm{TW},\mathrm{Size}\right)}^{\substack{\text{Noisy but unbiased}\\\text{sensory input}}}\cdot\overbrace{P\left(\mathrm{TW}\mid\mathrm{Size}\right)\cdot P\left(\mathrm{Size}\right)}^{\text{Prior expectation}}}{\underbrace{P\left(\mathrm{PS}\mid\mathrm{Size}\right)\cdot P\left(\mathrm{Size}\right)}_{\text{Normalization Factor}}} = \frac{\overbrace{P\left(\mathrm{PS}\mid \mathrm{TW}\right)}^{\substack{\text{Noisy but unbiased}\\\text{sensory input}}}\cdot\overbrace{P\left(\mathrm{TW}\mid\mathrm{Size}\right)}^{\text{Prior expectation}}}{\underbrace{P\left(\mathrm{PS}\right)}_{\text{Normalization Factor}}} \left(eq.\ 2.4\right)$$

In Equations 2.2-2.4, $P\left(x\right)$ refers to the unconditional probability of an event x occurring, while $P\left(x\mid A\right)$ signifies the conditional probability of an event x occurring given the occurrence of an event A. Similarly, $P\left(x\mid A,B\right)$ refers to the probability of x given the simultaneous occurrence of both events A and B.

In the SWI, direct **sensory input** from proprioceptive force sensors in the arm is unbiased but noisy. We define s_K to be the level of this sensory input on trial k, and we presume (1) that the distribution of s_K can be approximated by a Gaussian probability density function (pdf), $N\left(\mu_s,\sigma_s^2\right)$, and (2) that the **prior expectation** of the object weight has a pdf that can be approximated by $N\left(\mu_E,\sigma_E^2\right)$. For a small unexpectedly dense object, the distribution of effective sensory input should be centered around its true weight, while the distribution of expectations should be biased towards underestimating the true weight of the object (Cross and Rotkin 1975; Flanagan and Beltzner 2000), as shown in red in Figure 2.1a.

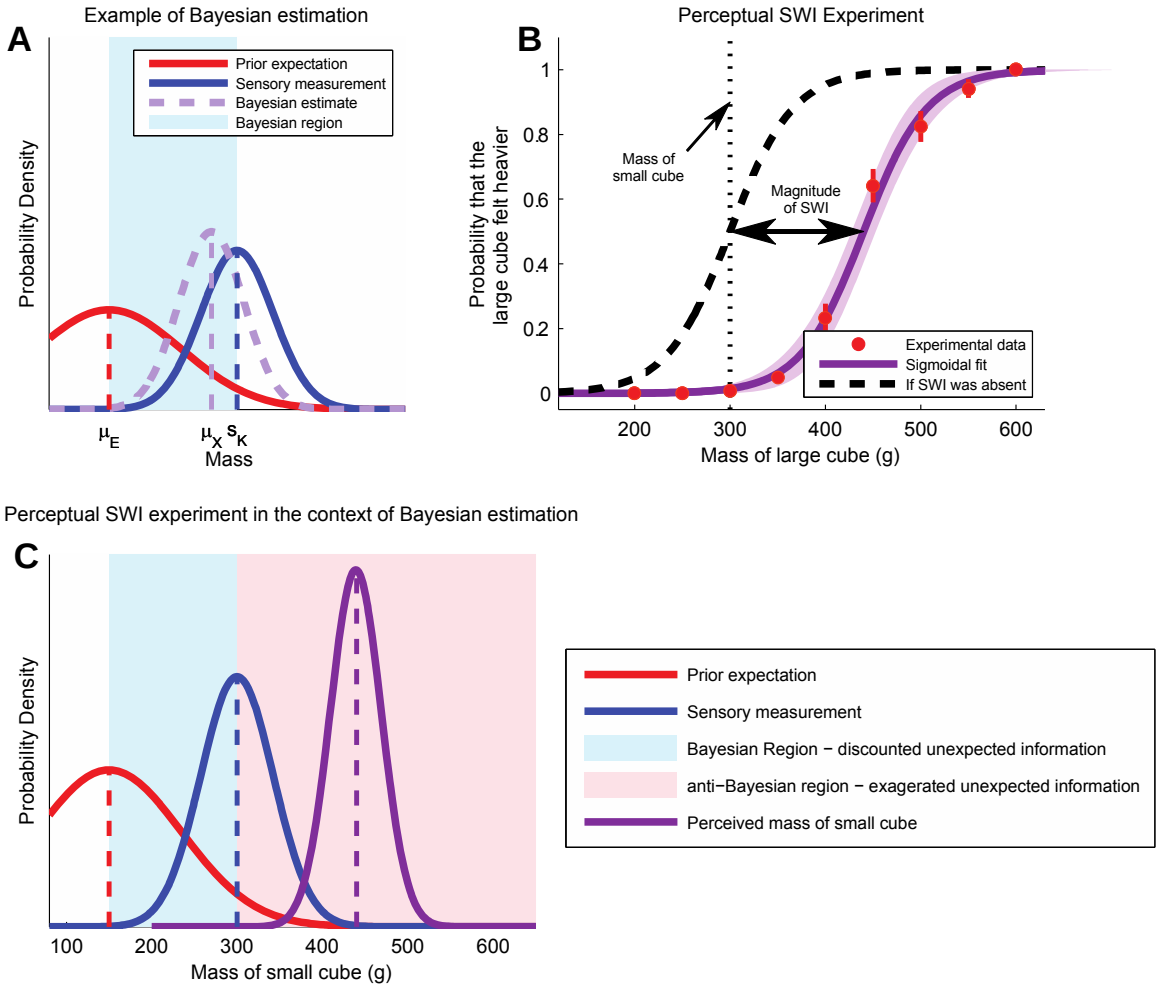

Figure 2.1 | The size-weight illusion and Bayesian estimation. A, Example of optimal estimation for the weight of a small, heavy object. The red curve represents the likelihood of the prior expectation of weight from seeing the object (μ_E is the mean of this likelihood), the blue Gaussian represents the distribution of noisy sensory information from feeling it (centered around s_k), and the light purple Gaussian is the posterior pdf for the weight, given the prior expectation and sensory information. The mean of this posterior pdf (μ_X) corresponds to the optimal (Bayesian) weight estimate. The shaded light blue region shows the range of values for which an estimate could be consistent with Bayes' Law depending on the variances associated with prior expectations and sensory measurements. **B,** Replication of the SWI. Red dots indicate the probability that a large cube of each mass is perceived to be heavier than a 300 g small cube. Error bars indicate SEM. The dark purple sigmoid is a fit through the data. The black curve is a shift of the dark purple sigmoid to a point with no illusion. **C,** Results from the SWI experiment presented as pdfs. The blue Gaussian curve represents the sensory estimates of the mass of the small object; the red Gaussian signifies a hypothetical prior expectation of this mass. The light blue area of the figure indicates the region in which the two sources of information would be integrated according to Bayes' Law given that the prior expectation is known to be smaller than 300 g. The pink area is the region where the integration would be anti-Bayesian. The dark purple Gaussian-like curve is the derivative of the dark purple sigmoid from panel B of this figure.

Application of Bayes' Law to a single lift gives the probability distribution for the true weight, x, shown in Equation 2.5. This distribution is the normalized product of $N\left(\mu_E, \sigma_E^2\right)$ and $N\left(s_K, \sigma_S^2\right)$, and will be Gaussian, $N\left(\mu_X, \sigma_X^2\right)$. Note that the peak of this distribution (which in this Gaussian case is the same as its mean) is an optimal estimate, $\hat{x}$, of the true weight. As shown in Equation 2.6, $\hat{x}$ is a weighted average of μ_E and s_K; therefore, based on Bayes' Law, it must fall between μ_E and s_K within the light blue colored Bayesian region in Figure 2.1a. If independent Bayesian estimates of the true weight are gathered from different subjects, the mean of these estimates would be a weighted average of μ_E and μ_S, as shown in Equation 2.7.

$$p\left(x \mid s_K\right) = N(\mu_x, \sigma_x^2) = \frac{N(\mu_E, \sigma_E^2) \cdot N(s_K, \sigma_S^2)}{\text{Normalization Factor}} \qquad (eq.\ 2.5)$$

$$\hat{x} = \mu_x = E\left[x \mid s_K\right] = \left(\frac{\sigma_S^2}{\sigma_E^2 + \sigma_S^2}\right)\mu_E + \left(\frac{\sigma_E^2}{\sigma_E^2 + \sigma_S^2}\right)s_K \quad (eq.\ 2.6)$$

$$\left\langle \hat{x} \right\rangle = \left\langle \mu_x \right\rangle = \left(\frac{\sigma_S^2}{\sigma_E^2 + \sigma_S^2}\right)\mu_E + \left(\frac{\sigma_E^2}{\sigma_E^2 + \sigma_S^2}\right)\mu_S \qquad (eq.\ 2.7)$$

2.4.2 Bayesian estimation viewed as a discount on unexpected information

If we define ε as the unexpected part of the sensory input averaged across samples - the difference between expected and actual sensations (Equation 2.8) – it becomes apparent that the average Bayes-optimal weight estimate is simply the sum of the expected weight and a fraction of the unexpected sensory input, as shown in Equation 2.9. Note that this fraction (K) is a gain on unexpected sensory input (ε) which must be between zero and one, indicating that Bayes-optimal estimates will always discount unexpected information. Note that this gain (K) is analogous to the gain of a Kalman filter. A gain greater than one would correspond to an exaggeration (rather than a discounting) of unexpected information and would thus reflect an "anti-Bayesian" estimate.

$$\varepsilon = \mu_S - \mu_E \Leftrightarrow \mu_S = \mu_E + \varepsilon \quad (eq.\ 2.8)$$

$$\langle \hat{x} \rangle = \left(\frac{\sigma_S^2}{\sigma_E^2 + \sigma_S^2} \right) \mu_E + \left(\frac{\sigma_E^2}{\sigma_E^2 + \sigma_S^2} \right) (\mu_E + \varepsilon) = \mu_E + \left(\frac{\sigma_E^2}{\sigma_E^2 + \sigma_S^2} \right) \varepsilon = \mu_E + K\varepsilon \quad (eq.\ 2.9)$$

2.4.3 Perceptual illusion

We designed experiments to quantify both perceptual and motor estimates of weight in the context of the same SWI in order to understand whether the neural systems underlying these estimates integrate prior expectations and unexpected sensory information in similar (or different) ways. While the perceptual effects of the SWI have been demonstrated in a wide variety of circumstances (Jones 1986; Koseleff 1957), we wanted to evaluate the magnitude of perceptual and motor biases associated with the SWI using the same objects. We constructed a set of 14 large cubes (52 mm side) with masses between 200 g and 600 g that we tested against a single small cube (26 mm side) with a 300 g mass. Subjects were presented with pairs of cubes (the small one and a randomly chosen large one) and asked to lift the two cubes one at a time and indicate which felt heavier. The results from this experiment were used to generate the dark purple psychometric curve displayed in Figure 2.1b. This curve shows the probability that the small 300 g cube felt lighter than each large cube. These data show that, on average, subjects perceived the small 300 g cube to feel as heavy as a large cube of 440 g (47% overestimate) +/- 13 g (95% confidence intervals). Differentiating this psychometric curve gives an estimate of the pdf of the perceived weight of the small cube – shown in Figure 2.1c. Since the difference between the perceived weight and the expected weight is greater than the difference between the raw sensory information and the expected weight, the gain on unexpected information is greater than one. This means that the perceived weight of the small cube exaggerates the unexpected component of the sensed weight rather than discounting it, indicating that the SWI generates an anti-Bayesian weight estimate.

Interestingly, the SWI is not the only percept that appears to display anti-Bayesian processing of unexpected information. It is well-known that predictable self-generated sensations are substantially attenuated compared to sensations arising from unpredictable external stimuli (Bays et al. 2005; Blakemore et al. 2000; Sperry 1950; Weiskrantz et al. 1971). For example, when tapping one finger against another, subjects perceive the taps as weaker than unpredictable externally-generated taps of the same force magnitude (Bays et al. 2005). This same effect explains why one cannot tickle himself (Blakemore et al. 2000; Weiskrantz et al. 1971) and leads to the escalation of force when subjects attempt to match blows with one another (Shergill et al. 2003). It is believed that an attenuation in the sensation of predictable, self-generated forces leads to an increase in the salience of sensations from external stimuli (Bays et al. 2005; Blakemore et al. 2000; Sperry 1950). However, this *attenuated* perception of self-generated, predictable sensations relative to externally-generated, unpredictable sensations is fully equivalent to the *exaggeration* of unexpected sensation relative to expected sensation. When a fixed-magnitude external stimulus is applied to a stationary target, the raw sensory information generated by it is the same regardless of whether it is expected or not. This proprioceptive information is primarily from Golgi tendon organs and as long as the targeted sensory area remains stationary (i.e. its muscle fibers' lengths remain unchanged), there should be little muscle spindle afferent activity.

If this stimulus is self-generated, the expected sensation should be accurate, especially after repeated exposure. In contrast, if the same stimulus is completely unexpected (i.e. the expected sensation is zero) then the unexpected stimulus will be perceived to be stronger than the expected one, only if the unexpected sensation is exaggerated. As such, it also amounts to an anti-Bayesian estimation, analogous to that displayed in the SWI, because Bayesian estimation always discounts unexpected information by some amount. Therefore, the observations about the perceptions of

force, pressure, and weight based on proprioceptive and tactile sensory information represent anti-Bayesian integration of sensory information with prior expectations which exaggerates unexpected sensory information in a variety of circumstances.

However, over the past decade several studies have shown that Bayesian-like processing can underlie both sensory percepts and motor actions when prior expectations are combined with sensory inputs and when different sensory inputs are combined with one another (Ernst and Banks 2002; Körding et al. 2004; Körding and Wolpert 2004; Stocker and Simoncelli 2006a; Weiss et al. 2002; Wolpert et al. 1995) and several perceptual illusions have been explained on the basis of Bayes' Law (Gregory 2006; Sato et al. 2007; Stocker and Simoncelli 2006a; Weiss et al. 2002). For example, visual uncertainty biases the perception of speed in a manner consistent with Bayes' Law. The prior expectation that most objects are stationary causes subjects to perceive moving objects in a low visibility situation (characterized by highly uncertain sensory information) as slower than the same objects in a high visibility situation (Weiss et al. 2002). Furthermore, it has been shown that visual and haptic sensory information are combined in a statistically-optimal fashion that modulates the influence of each in a Bayesian manner when perceiving the length of an object (Ernst and Banks 2002). In the motor system, Bayes' Law explains how the magnitudes of responses to visual (Körding and Wolpert 2004) and force pulse (Körding et al. 2004) perturbations are influenced by prior expectations, suggesting that the motor system's estimates of distance and force are formed by Bayesian integration.

2.4.4 Motor Illusion

Although the perception of weight and force is apparently anti-Bayesian, the motor system's estimate of force has been shown to be Bayesian on a task that does not involve the SWI (Körding et al. 2004). Therefore we sought to determine whether, in the context of this illusion,

the motor system is also fooled by the SWI (anti-Bayesian), unbiased, or Bayesian when estimating weight. To do this, we designed an involuntary motor task sensitive to weight estimation. We studied the generation of anticipatory postural adjustments (APAs) based on the motor system's weight estimate. APAs, which are involuntary muscle actions preceding a voluntary movement, have been shown to assist in minimizing postural changes when subjects raise their arms (Bouisset and Zattara 1981), catch a falling object (Shiratori and Latash 2001), or pull on a fixed handle (Brown and Frank 1987; Cordo and Nashner 1982) by activating muscles not directly involved with the performed action. The magnitude of APAs has been shown to correlate with the size of the expected perturbation (Horak et al. 1989), indicating that they are sensitive to weight estimation (Diedrichsen et al. 2007; Horak et al. 1989; Wing et al. 1997). Furthermore, APAs cannot be voluntarily modulated or initiated (Diedrichsen et al. 2003; Dufossae et al. 1985; Lum et al. 1992), making them unlikely to be directly influenced by perceptual estimates.

A waiter in a restaurant relies on APAs to keep a tray full of drinks steady if he holds the tray with one hand while removing a glass with the other. When lifting a glass from the tray, the weight of the tray is reduced by the weight of the glass; consequently, the force used to support the tray must be instantly reduced by this weight if the tray is to be held steady to prevent the remaining drinks from spilling. If the waiter fails to compensate for the weight change of the tray, it will shift upwards. In fact, any mismatch between the required and actual supporting forces would cause a corresponding acceleration of the tray. If the waiter *underestimates* the weight of the glass he picks up – effectively overestimating the weight of the tray remaining in his hand – the supporting force he produces after the lift will be greater than required to support the tray and the tray will be pushed up. If he *overestimates* the weight of the glass, the tray will move down.

We designed a motor analog of the size-weight illusion based on a version of this waiter task – diagrammed in Figure 2.2a. We asked subjects to maintain a fixed arm posture, elbow placed on the table, while supporting the weight of an object placed on the palm of their right hand approximately 6 inches off the table. For this experiment we used 2 cubes of 300 g mass: a small one (26 mm side) and a large one (52 mm side). In one group, 20 subjects were first given the large 300 g cube and asked to lift it with their left hand and place it on the palm of their right hand. They were instructed to hold their right arms steady while rapidly lifting the cube using their left hands. After each lift, subjects placed the large cube back on the palm of their right hand. Each subject performed 50 rapid lifting trials (training lifts) of this large 300g cube, while we recorded the vertical motion of their right hands associated with the left-hand lifts. Subsequently, subjects were given a small 300 g cube, which all subjects judged to be heavier, and were asked to repeat the same lifting task with it 8 times (novel lifts). The cubes were placed on the same circular platform, resting on the palm of the right hand and were fitted with identical grip surfaces in order to match the proprioceptive information associated with each one.

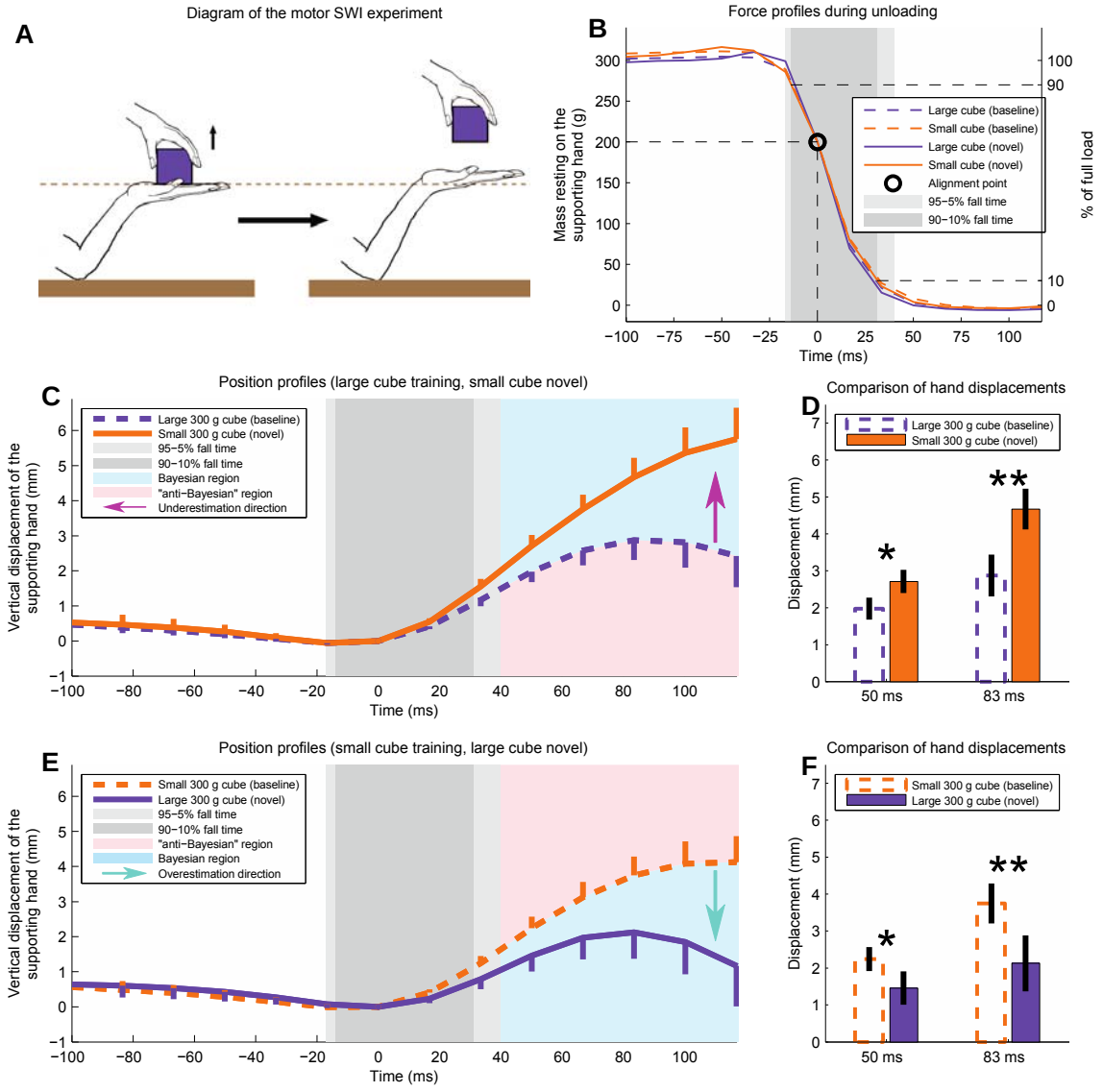

Figure 2.2 | Motor analog of the size-weight illusion. A, Diagram of the experiment. First, the subject maintains a fixed posture with his right hand while supporting a single cube on his palm. Then he reaches from the top and grabs the cube with his left hand, quickly lifting it up. Without an appropriate APA, the supporting hand would move far up after the lift. Even with a normal compensatory APA, the palm of the supporting hand moves up some amount after the cube has been lifted. An accurate estimate of the weight being unloaded helps reduce hand displacement. **B,** Force profiles during unloading. The dashed lines are the average profiles during the last 10 of the 50 baseline lifts. Solid lines show the corresponding profile during the first novel cube lift. Purple lines are the profiles for the large 300 g cube; orange lines are the profiles for the small 300 g cube. All profiles are aligned to the point in time (zero) when the load is reduced to 200g. The shaded gray regions represent the 10-90% and 5-95% of the fall time. **C & E,** Position profiles of the supporting hand during the motor analog of the SWI experiment. Line styles and colors are consistent with 2B. Error bars represent SEM across subjects. Bayesian (light blue) and anti-Bayesian (pink) regions are consistent with Figure 2.1c. **D & F,** Displacement at two instances: 50 and 83 ms after the lift onset.

Another group of 20 subjects performed the same task in reversed order: 50 training lifts with a small cube followed by 8 lifts of a novel large cube. The results from these experiments are shown in Figures 2.2c and 2.2e. Here the dashed traces show the vertical position profile of the supporting (right) hand during the last 10 of the 50 baseline cube lifts, while the solid traces show the corresponding position profiles during the first lift of each novel cube. Line colors indicate cube size. Both traces represent the mean across 20 subjects, with error bars indicating SEM. We found a 35% increase in post-lift displacement for the supporting hand when a novel small cube was lifted as shown in Figures 2.2c and 2.2d (2.7 mm versus 2.0 mm, $p<0.01$, 50 ms after the lift onset, see Figure 2.2d). In contrast, the first novel large cube lift showed a 32% decrease in post-lift displacement for the supporting hand compared to baseline as shown in Figures 2.2e and 2.2f (1.5 mm versus 2.2 mm, $p<0.01$, 50 ms after the lift onset, see Figure 2.2f). The increased vertical displacement observed in the novel small cube lifts corresponds to an underestimation of its weight, while the decreased displacement observed in the novel large cube lifts corresponds to an overestimation of its weight. Both of these results are consistent with Bayes Law and inconsistent with the anti-Bayesian perceptual weight estimate seen in the classic SWI.

2.4.5 Anticipatory behavior of the motor system

Since we are interested in the anticipatory (feed-forward) behavior of the motor system, we studied lifting profiles as close to the lift onset as possible to avoid contamination of our findings by feedback-driven responses. However, we wanted to examine motion profiles after the load had been fully removed from the supporting hand. Therefore, we instructed subjects to lift as rapidly as possible, to minimize the time between lift-force onset and lift-off for the cube. This resulted in the completion of more than 95% of all the lifts in our task by 50 ms after the lift-force onset (see Figure 2.2b), and so we decided to analyze our data at the 50 ms and 83 ms time points. Because error correction in response to proprioceptive perturbations associated with arm

movements typically lags velocity errors by at least 90 milliseconds (Cordo 1990), hand position measured 50-83 ms after lift onset is likely to reflect anticipatory feed-forward control of the supporting hand rather than feedback responses to hand displacements. While EMG signals from short-latency tendon-jerk reflexes can have latencies as short as 15-20 ms (Jones 1986; Marsden et al. 1976) for human biceps muscle, noticeable changes in position due to these EMG changes can be further delayed by 60-70 ms (Rothwell et al. 1980). However, these short latency reflexes generally have very small magnitudes unless high-acceleration perturbations are employed, and these responses do not vary across task conditions (Marsden et al. 1976). In contrast, long-latency responses are larger in magnitude and can be modulated by task-specific variables (Rothwell et al. 1980). However, EMG latencies associated with these responses display latencies of 50-60 ms (Marsden et al. 1976; Rothwell et al. 1980), corresponding to position change latencies of 110 ms or more (Rothwell et al. 1980), making it highly unlikely for long-latency reflexes to affect our results 50 or 83 ms after the movement onset. Furthermore, if we repeat the same data analysis at 33ms after force-onset (before lift-off in most trials), we see still see significant separation between the baseline and novel profiles in both subject groups ($p<0.05$ at 33 ms in both cases).

Another possible explanation for the difference in profiles between the baseline and novel cube lifts might be the existence of increased arm stiffness associated with object novelty. Increased arm stiffness would reduce motor errors in the face of uncertainty about object weight in novel cube lifts. However, increased arm stiffness would predict reduced displacements compared to baseline in both types of novel cube lifts, whereas our data show decreased displacement for the large novel cube but increased displacement for the small novel cube, consistent with a discounting of unexpected sensory information when the motor action is planned. Moreover, these opposite displacements are nearly symmetric (0.7 mm in both cases), suggesting that the

effects of any stiffness changes are much smaller than the effects associated with changes in anticipatory motor output that reflect the discounting of unexpected sensory information.

Note that in the former data analysis, we used only the first lifting trial of the novel object to avoid any effects of motor adaptation. In fact, subjects performed 8 consecutive lifting trials with each novel object after the initial 50-trial training period with the familiar object. Following this 8-trial block, subjects were administered two 25-trial re-training periods with the familiar object, each followed by an additional 8-trial novel cube lifting block. We show that the motor adaptation over the course of the first 8 novel cube lifts can be approximated by a decaying exponential having a time constant of 2 trials ($r=0.65$, $F(2,13)=4.65$, $p<0.03$, Figures 2.3a and 2.3c) or a line with a slope of -0.056 mm/trial ($r=0.55$, $F(1,14)=5.99$, $p<0.03$). Furthermore, when we compare the first novel lifts from each of the three consecutive lifting blocks (those lifts are separated by 25 lifting trials with the baseline object and 7 trials with the novel object) as shown in Figures 2.3b and 2.3d, we see that the novelty effect is reduced to practically 0 by the end of the experiment at a rate of -0.35 mm/block ($r=0.92$, $F(1,4)=21.7$, $p<0.01$). These results indicate rapid adaptation of the motor system's prior expectation about object weight both within and across blocks despite the persistence of a perceptual bias caused by the Size-Weight Illusion, consistent with previous work (Flanagan and Beltzner 2000; Grandy and Westwood 2006).

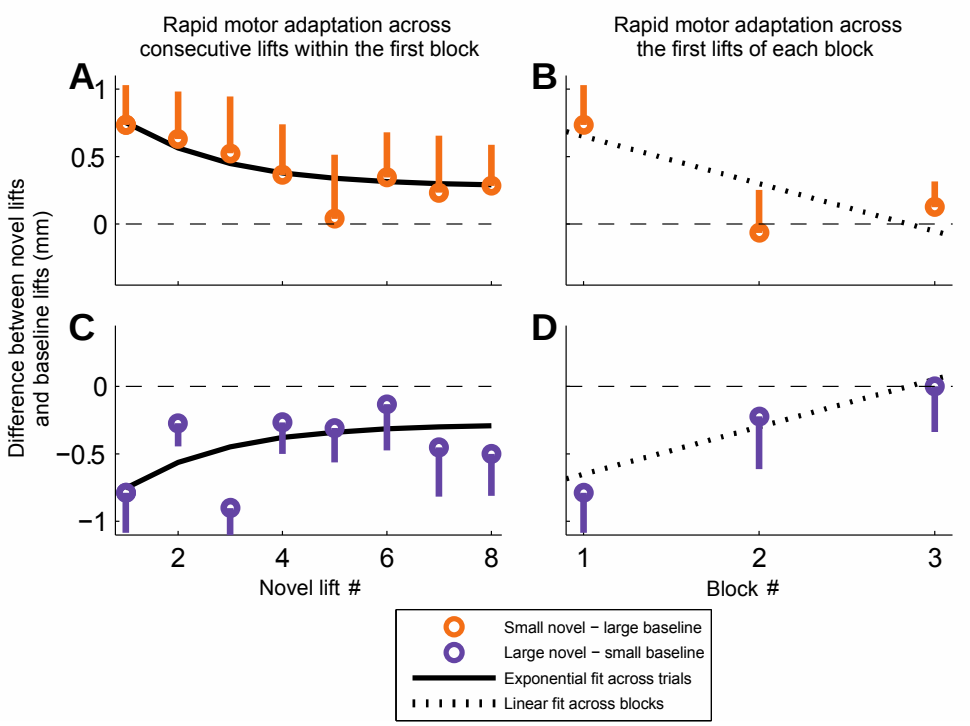

Figure 2.3 | Rapid adaptation in the motor analog of the size-weight illusion. Whereas the data in Figure 2.2 show the biases in motor output displayed in the very first novel cube lift, here we show how these biases change within a block of 8 repeated lifts of the novel cube and across 3 such blocks of novel cube lifts**.** Differences in position profiles of the supporting hand between the novel and baseline lifts 50 ms after the lift onset are shown. Each point represents an average difference across subjects and error bars represent SEM. For each subject we computed the difference between a particular "novel" lift and the mean of the last 10 baseline trials. The orange points (**A & B**) are the differences between small cube novel and large cube baseline lifts, and the purple points (**C & D**) are the differences between large cube novel and small cube baseline lifts. **A & C,** The data for the 8 novel cube lifts in the first block. The fit is a decaying exponential with a time constant of just 2 trials ($r=0.65$, $F(2,13)=4.65$, $p<0.03$). These data could also be fitted by a line with a slope of -0.056 mm/trial ($r=0.55$, $F(1,14)=5.99$, $p<0.03$). **B & D**, The first novel cube lift in each of the 3 blocks. The data show a decay at a rate of -0.35 mm/block ($r=0.92$, $F(1,4)=21.7$, $p<0.01$).

2.4.6 Quantifying weight estimates in the motor illusion

In order to assess the amount of weight estimation bias in the motor system responsible for the changes in hand displacement we observed, we designed a control experiment in which we asked each subject to place a stack of two identically-sized, identical-looking cubes on the palm of his or her right hand while maintaining the same fixed arm posture as in the previous experiment (subjects transported the cubes by holding only the bottom one so that the individual weights could not be easily determined). Subjects then performed a rapid lift of only the top cube from the stack, as shown in Figure 2.4a. We repeated these trials 100 times with 5 pairs of identical looking objects all with a total mass of 600 g: 150-450, 225-375, 300-300, 375-225, and 450-150. 76 out of 100 lifts were with the "control" pair (300-300) and 24 "surprise" lifts were randomly interspersed – 6 with each of the other pairs. We used the results from these surprise lifts to determine the relationship between the amount of weight estimation bias and post-lift displacement of the right hand. We found a simple linear relationship between the amount of weight mis-estimation and the post-lift displacement of the right hand (R^2=98.6%, $p<0.001$) at 50 ms post-lift, which we used as a calibration function. This calibration reveals that the 0.7 mm increase in displacement we found in the motor analog of the SWI experiments at 50 ms post-lift corresponds to a 65 g (22%) underestimation as shown in Figure 2.4c, indicating that the motor system estimates the small cube mass to be 235g rather than 300g on the novel-object lift.

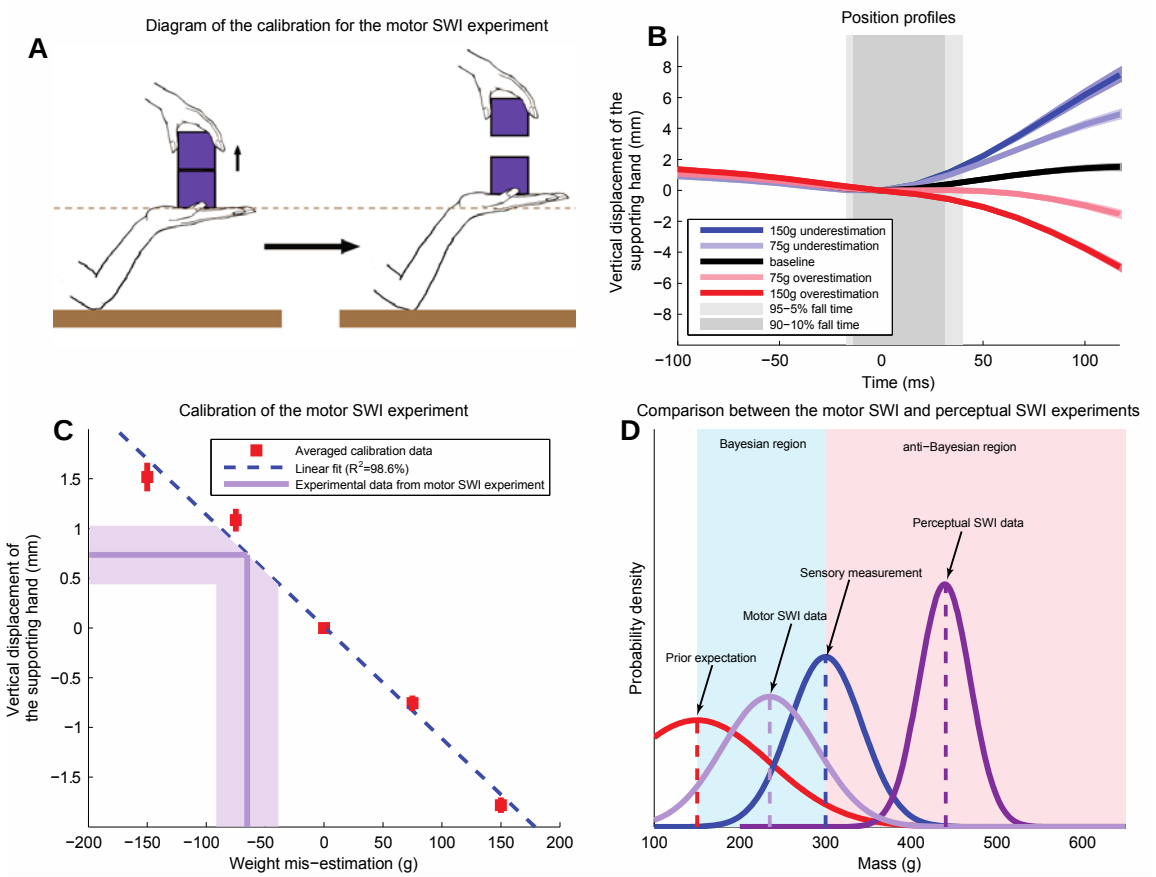

Figure 2.4 | Motor calibration experiment. A, Diagram of the experiment used to determine relationship between hand displacement and weight mis-estimation. The task is the same as before, except the subject places two cubes on his hand and then rapidly lifts the top cube of variable and unknown mass. The subject trains with a pair of equal mass cubes and is then asked to perform the same task with identical looking cube pairs that may differ from one another in mass but average 300g - the mass of the training cubes. If one underestimates the mass of the object he lifts, his supporting hand goes up, while overestimation causes the supporting hand to go down compared to baseline. **B,** Position profiles of the supporting hand during the control experiment. The black curve is the profile generated by the training pair (300g/300g), the red curves are generated after lifting lighter weights: 225g (light red) or 150g (darker red), and the blue curves are generated after lifting heavier weights: 375g (light blue) and 450g (darker blue). **C,** Calibration of the motor size-weight illusion. The red squares are experimental data from the calibration experiment at 50 ms, the blue line is a linear fit to these data, the horizontal light purple line indicates the displacement (0.7 mm) associated with weight under-estimation for the small cube in the motor analog of the SWI shown in Figure 2.2c and 2D and the vertical light purple line shows that the mass of the small cube is underestimated by 65 ± 26 g. The shaded light purple region indicates SEM in the data. **D,** Comparison of the classic SWI and motor SWI results to Bayesian integration. Just as in Figure 2.1c, we show the sensory estimation, the prior expectations, the Bayesian and anti-Bayesian regions, and the perceptual SWI curve. The light purple Gaussian, represents the distribution of weight estimates corresponding to the distribution of hand displacements shown in Figure 2.2. Note that the light purple Gaussian represents the mean and SD (not SEM) of the data.

2.4.7 Bayesian versus anti-Bayesian integration

If the APAs in our task were scaled solely based on the prior expectation of the weight of the small cube, we should see an APA corresponding to an 87.5% underestimate, since the volume of the small cube is 1/8 that of the large one. Alternatively, if these APAs were based on proprioceptive sensory input alone, there should be no difference in the lifting profiles for the two cubes. The 22% underestimation we see for the small cube is consistent with a gain on unexpected information of 0.75 as defined in Equation 2.9 – corresponding to a 25% discount on unexpected sensory information. While our results suggest that the gain on unexpected information is less than one, consistent with Bayesian estimation, we lack the data necessary to show that this gain corresponds to the ratio of variances shown in Equation 2.9, because the certainty of the prior is difficult to estimate. Thus, we demonstrate opposite biases for the motor and perceptual weight estimates, and show that perceptual biases are oppositely directed from the biases that would be generated by Bayesian integration. However, although the direction of the motor illusion is consistent with Bayesian integration, we cannot assess whether its magnitude matches that predicted by Bayes' Law. Overall, our findings indicate that while the perceptual system estimates the small cube to be 47% heavier than a comparable large cube, the motor system estimates this small cube to be 22% lighter, as shown in Figure 2.4d.

These results suggest that the motor system combines prior expectation and real-time sensory information to generate a Bayesian-like weight estimate, discounting the value of unexpected sensory information, whereas the perceptual system combines these information sources in an anti-Bayesian manner, exaggerating the value of unexpected sensory information. This gives rise to oppositely-biased weight estimates for perception and action. We believe that this is the first demonstration of opposite illusions (i.e. opposite biases) for perception and action in the context

of the same task. These results suggest that the nervous system uses two entirely different mechanisms to integrate prior expectations with current sensory information about object weight.

2.4.8 Different priors for action and perception

Previous studies of lifting dynamics during the SWI have suggested that the motor system and the perceptual system may form prior expectations independently (Flanagan and Beltzner 2000; Grandy and Westwood 2006). Because these studies focused on forces applied to objects suddenly lifted from a table top, direct sensory information was not available during the planning of these lifts, and thus could not be integrated with prior expectations. Therefore the initial pattern of grip force applied when a person lifts an object from a table top reflects the motor system's expectation of that object's weight, rather than the integration of sensory information about object weight (Flanagan et al. 2003). Studies of initial grip force show that the motor system adapts this expectation about object weight in just 3-5 trials in the context of the SWI (Flanagan and Beltzner 2000; Grandy and Westwood 2006), whereas the perceptual system requires hundreds or thousands of trials to adapt its expectations (Flanagan et al. 2008). The striking difference between adaptation rates for these expectations suggests that the neural bases for the weight expectations levied by the motor system and the perceptual system are indeed separate. Thus these studies provide clear evidence for the maintenance of separate expectations of object weight for perception and action; however, they do not provide an opportunity to assess how prior expectations are combined with direct sensory information when both are available. In the current work, we studied how the nervous system processes the integration of prior expectations and sensory information for action and perception and found oppositely-biased weight estimates for perception and action, reflecting divergent mechanisms for the processing of unexpected information.

2.4.9 Perception versus action in the central nervous system

The idea that the nervous system may process sensory information differently for perceptual and motor tasks is not new. For example, visual information is processed in two pathways – the dorsal and ventral streams (Mishkin and Ungerleider 1982; Ungerleider and Mishkin 1982). It has been hypothesized that the dorsal stream primarily carries spatial information for action, and the ventral stream primarily carries information about object identity for perception (Goodale and Milner 1992; Milner and Goodale 1993). However, while there is clear physiologic evidence for separate streams in the neural processing of visual information, the evidence that a particular visual quality, such as the size of an object, is processed differently for perception and action is still highly controversial. (de Grave et al. 2005; Franz 2001; Smeets and Brenner 2006). Much of this controversy stems from a series of studies (Aglioti et al. 1995; Haffenden et al. 2001) which contends that the effects of visual illusions on the perception of object size do not carry over to motor actions. However, the data from these studies and several others (de Grave et al. 2005; Franz 2001) show that motor actions can also be substantially affected by perceptual illusions, often to similar extents, leading several authors (de Grave et al. 2005; Franz 2001; Smeets and Brenner 2006) to suggest that these visual illusions have similar effects on perception and action. In addition, several aspects of the methodology used in these studies have been called into question, in particular the specificity of the measures used to assess the effect of the illusion on perception and action (Franz 2001; Smeets and Brenner 2006). For example, grip aperture has been widely used to assess the effects of visual size illusions on action (Aglioti et al. 1995; Franz 2001; Haffenden et al. 2001). However, it has been shown that grip aperture is planned based on the position of each grasp point rather that the distance between them (Brenner and Smeets 1996; Jackson and Shaw 2000; Smeets and Brenner 2008; 1999). Because visual size illusions generally have little effect on the perceived position of individual points within the illusory

figure, the finding that grip aperture is somewhat resistant to a size illusion, may reflect a dichotomy between the processing of visual information for size and position, rather than between perception and action (Brenner and Smeets 1996; Jackson and Shaw 2000; Smeets and Brenner 2008).

2.4.10 Information streams for action

Anticipatory postural adjustments, which are believed to be resistant to voluntary modulation (Diedrichsen et al. 2003; Dufossae et al. 1985; Lum et al. 1992), are modulated by the primary motor cortex (M1) (Chouinard et al. 2005; Gahery and Nieoullon 1978; Massion 1992), the cerebellum (Diedrichsen et al. 2005; Massion 1992; Rabe et al. 2009; Rispal-Padel et al. 1982), the supplementary motor area (SMA) (Massion 1992; Sakreida et al. 2005), and the dorsal premotor area (PMd) (Byblow et al. 2007; Chouinard et al. 2005; Massion 1992; Sakreida et al. 2005). Transcranial magnetic stimulation of M1 disrupts the trial-to-trial adaptation of APAs, while the same stimulation applied over PMd disrupts the ability to use visual cues to form prior expectations about object weight (Chouinard et al. 2005). Interestingly, TMS stimulation over PMd has been shown to enhance the ability of motion of one limb to facilitate activation of another limb, which is required for APA formation, while PMv stimulation does not (Byblow et al. 2007). Patients with cerebellar damage can produce appropriate APAs in common tasks (Diedrichsen et al. 2005; Massion 1992); however, degeneration of the cerebellum, which is strongly connected to structures in the dorsal visual stream, interferes with the formation of novel APAs and the adaptation of preexisting ones (Diedrichsen et al. 2005; Horak and Diener 1994) but not the adaptation of grip forces (Rabe et al. 2009).

These findings suggest a dissociation between the control of APAs and grasping. Two areas of premotor cortex, PMd and PMv, which receive largely distinct inputs, may mediate this

dissociation. The motor commands associated with APAs may be primarily driven by sensory input from the dorsal stream, whereas sensory input from the ventral visual stream may be most important for the control of grasping. Correspondingly, the inputs to PMd are from structures generally associated with the dorsal stream of visual processing (Hoshi and Tanji 2007; Kaas 2004; Rizzolatti and Luppino 2001), while PMv is substantially connected to ventral stream structures (Lu et al. 1994; Rizzolatti and Luppino 2001; Webster et al. 1994). In general, PMv is believed to exert more control over distal movements, like the shaping of fingers during precision grip (Davare et al. 2006; Fogassi et al. 2001; Hoshi and Tanji 2007), whereas PMd is closely associated with movement of more proximal joints including the shoulder and the elbow (Cisek et al. 2003; Davare et al. 2006; Hoshi and Tanji 2006), which are generally associated with APAs. Correspondingly, PMv and PMd activity are specifically activated by biological motion associated with proximal and distal joints, respectively (Sakreida et al. 2005). This is in line with previous ideas about the control of the fingers during grasping (Hoshi and Tanji 2007; Rizzolatti and Luppino 2001) including studies which have shown that PMd-sparing inactivation of PMv knocks out grasping movements while leaving reaching movements intact (Davare et al. 2006; Fogassi et al. 2001).

These findings are compatible with the idea that PMd is more involved with complex sensorimotor integration like that involved in the formation of APAs, whereas PMv supports the coding of actions in a way that is more directly based on sensory information about object properties (Hoshi and Tanji 2007; Rizzolatti and Luppino 2001), like the control of grasp aperture. The idea that ventral stream information feeds PMv, which controls grasp, may explain why previous work focused on grasp aperture has generally found somewhat incomplete dissociations between perception and action (Aglioti et al. 1995; Haffenden et al. 2001), and were often difficult to reproduce (de Grave et al. 2005; Franz 2001), whereas the current study, which

focused on the control of arm posture, demonstrates diametrically opposed illusions for perception and action.

A recent imaging study (Chouinard et al. 2009) supports the idea of a close relationship between the control of grasping actions by PMv and the illusory perception of weight. The authors found no changes in neural activity in PMd, M1 or cerebellum that correlated with the illusory perception of weight while gripping and lifting an object. Instead, the only illusion-related activity observed was registered in an area of PMv, which displayed density-related, but not size-related activity. Combined with the idea that PMv activity controls grasping behavior when reaching for objects (Hoshi and Tanji 2007; Rizzolatti and Luppino 2001) whereas PMd activity correlates with the mismatch between expected and actual grip forces (Schmitz et al. 2005), these findings suggest both a close connection between the control of grasp and the (illusory) perception of weight and also a dissociation between the production of force and the perception of weight.

2.4.11 Rapid adaptation of the motor system can obscure illusory effects

A key issue for the identification for motor illusions is the effect of motor adaptation. If feedback about motor performance is available, errors that occur on one trial can be used to correct future actions. Because the error-dependent adaptation of motor expectations can be exceedingly rapid, motor output can go from clearly biased to nearly unbiased in just 3-5 trials (Chang et al. 2008; Flanagan and Beltzner 2000; Grandy and Westwood 2006). Therefore studies which average the results of many (5-18) trials (Aglioti et al. 1995; Chang et al. 2008; Haffenden et al. 2001) may fail to detect motor illusions, even if they are initially present. For this reason we focused on the first instance in which subjects interacted with a novel cube (whether it be the small or large one) to minimize the possible effects of motor adaptation. This allowed us to show that the initial

weight estimate of the motor system is not only immune to the perceptual illusion, but is instead biased in the opposite direction to the perceptual estimate. Examination of the data from subsequent lifts in our study reveals that errors associated with the motor illusion we demonstrate are rapidly attenuated over the course of just 2-4 trials (see Figure 2.3), consistent with previous work on motor adaptation (Krakauer 2009; Krakauer et al. 2000; Scheidt et al. 2001; Scheidt et al. 2000; Smith et al. 2006; Thoroughman and Shadmehr 2000).

In a recent study, the grip force and load force profiles associated with using one hand to lift objects from the other showed that the lifting hand produced more appropriate motor output when lifting an object from the other hand than from a table top (Chang et al. 2008), indicating that sensory information from one hand can be used to modulate the actions of the other. In both the table-top and bimanual conditions, rapid motor adaptation led to the application of appropriate lift and grip forces after just a few trials. However, examination of the force profiles from the initial trial on which an object was lifted from the other hand reveals two interesting features. First, the required grip force is overestimated for both objects compared to subsequent trials although the load force is not, and second, both lift and grip forces were generally greater for the large object than the small one. Although the first of these effects was not specifically analyzed and the second was not statistically significant ($p>0.1$ for all relevant statistical tests), the first suggests that grip force but not load force is substantially modulated not only by the expected weight of an object but also by the uncertainty about this weight, and the second would be predicted by Bayesian integration, consistent with our current findings.

2.4.12 Opposite illusions versus opposite behavior

A few previous studies have documented oppositely-directed perceptions and actions that do not arise from opposite illusions, but rather the choice of conditions for comparison (Ganel et al.

2008; Grandy and Westwood 2006). In one such study (Grandy and Westwood 2006), grip forces associated with alternate rapid lifting of a small, lighter object (2.7N) and a large, heavier one (3.2N) from a table were measured. After several trials, motor adaptation led to the application of appropriate grip forces for both objects, although the SWI persisted – consistent with previous results (Flanagan and Beltzner 2000). Because the large object was chosen to be heavier than the small object and the SWI was sufficiently powerful to overcome the weight difference between them, the larger object was perceived as lighter (i.e. illusory underestimation) while grip forces associated with it were appropriately greater (i.e. accurate estimation). This resulted in oppositely-directed perceptions and actions without the presence of opposite illusions, i.e. the motor system's behavior was accurate, while the perceptual estimate was biased by the SWI. In contrast, our findings show illusions which oppose one another and generate opposite biases in the motor and perceptual systems. The current illusions depend on the integration of prior expectations with sensory information, unlike the grip force patterns previously studied which reflect only prior expectations about object weight (Flanagan and Beltzner 2000; Flanagan et al. 2001) rather than the integration of both sensory information with these expectations.

2.4.13 Contrast enhancement and efficient coding

Because the integration of prior expectation and raw sensory information by the perceptual system exaggerates unexpected sensory information (rather than discounting it) in the SWI, it cannot be optimal (i.e. minimize the variance) for producing accurate weight estimates in the presence of sensory noise. However, the exaggeration of unexpected sensory information in this anti-Bayesian weight estimation can be viewed as a type of contrast enhancement – an information processing mechanism that is pervasive throughout early sensorineural processing of auditory, somatosensory, and visual information (Barlow 2001). Contrast enhancement can be especially useful for the detection of object features to aid in classification. For example, in the

visual system, contrast enhancement can improve the ability to detect the edges of objects and thus identify their shapes at the cost of reduced ability to identify raw luminance levels or to accurately compare luminance in two different regions of the same visual scene (Albers 1975). A light object placed on a dark background appears lighter than it is. If we apply a simplistic Bayesian framework to this example, where the background color represents the prior expectation and the light object is the raw sensory information, we see that contrast enhancement produces a posterior in which the difference between the prior and the sensory information is exaggerated – hence forming an anti-Bayesian estimate.

Another apparently anti-Bayesian phenomenon that has been extensively studied is the tilt aftereffect (Campbell and Maffei 1971; Gibson 1937). After staring at a vertical grating for a period of time (30 seconds to a few minutes), a grating with similar orientation appears to be tilted further away from vertical than it is. Looking at this phenomenon from a Bayesian perspective, we would expect that prolonged exposure to a vertical grating will help form a prior expectation that the grating is most likely to be vertical (at 90°). Subsequent presentation of a rotated grating (e.g. 80°) would be combined with this prior expectation and we would expect the net estimate of the tilt to be between 80° and 90°, consistent with a discount on unexpected information. Note that the tilt aftereffect instead shows a repulsive, contrast-enhancing bias such that the perceived angle in this case is close to 75° (Campbell and Maffei 1971). This corresponds to an exaggeration of unexpected sensory information and an anti-Bayesian estimate.

It has been suggested that the repulsive bias seen in the tilt aftereffect might be compatible with Bayesian estimation if the adaptation was interpreted to affect the likelihood function rather than the prior (Simoncelli 2009; Stocker and Simoncelli 2006b). However, this explanation is somewhat difficult to defend because prior expectations must be derived from previous experience (Ellis and Lederman 1998; Flanagan et al. 2008; Körding and Wolpert 2004).

Additionally, the tilt illusion, which has essentially the same sensory consequences as the tilt aftereffect (Campbell and Maffei 1971; Gibson 1937; Wainwright 1999), is believed to arise from the same mechanisms (Schwartz et al. 2007) but cannot reasonably be explained by an adapted likelihood function because no adaptation occurs. Furthermore, the classic SWI in which two equal-mass but different-sized objects are compared cannot be explained by differences in adapted likelihood functions because (1) the SWI is present on the first lift, before adaptation could occur and (2) these likelihood functions would apply to raw sensory information about weight, which is the same for both objects.

Repulsive, contrast-enhancing biases are thought to be compatible with the efficient coding hypothesis. This hypothesis suggests that neural representations of information maximize the efficiency of information transmission. A key mechanism for accomplishing this is the reduction of redundancy in information transmission (Barlow 1990). Consequently, efficient coding schemes remove correlations between transmitted perceptual variables because correlations between these variables would lead to redundant information transmission with sub-optimal efficiency (Barlow 2001; Wainwright 1999). In these schemes, correlations between variables are generally removed by increasing mutual inhibition (Barlow 1990). Because prior expectations generally represent correlations between variables (e.g. the expectation driving the SWI is that object size and weight are positively correlated) and Bayesian integration biases sensory estimates towards these expectations, inhibitory decorrelation which increases the independence between variables produces biases that are opposite to Bayesian integration biases.

On the face of it, it would seem that optimal estimation (via Bayesian integration) and efficient coding for optimal transmission of information should produce similar, if not the same, effects. However, as discussed above, the biases produced are generally opposite of one another. How can this be? The answer is that these information processing schemes are optimal for different

things. In particular, efficient coding schemes dictate how sensory signals should be encoded in order to maximize the information carried during transmission (Wainwright 1999). This produces an adaptive encoding which must be decoded after transmission for the original sensory signals to be recovered without distortion. However, these efficient coding schemes do not specify how the original sensory signal should be decoded. The theories of efficient coding generally attempt to explain perceptual biases as a result of a "coding catastrophe" (Schwartz et al. 2007) – i.e. downstream decoding mechanisms do not provide any compensation for upstream adaptive encoding. Thus, according to this theory, the encoding is adaptive but the decoding is not, resulting in a mismatch between the two that accounts for perceptual biases. This mismatch occurs because efficient coding schemes are not concerned with how information from these sensory signals should be used after transmission. On the other hand, optimal estimation is only concerned with how sensory signals are decoded – here the computational goal is to provide decoded estimates, based on sensory information, which are maximally accurate.

This suggests that while certain perceptions might not be optimally accurate (consistent with Bayesian integration), they might reflect optimal information encoding, transmission, or storage. Alternatively, contrast-enhancement in the perception of weight may help to identify or classify objects that are lighter or heavier than expected so that appropriate behavioral strategies might be triggered, such as altering the posture used to grasp an object. In fact, while our motor actions generally benefit from maximally accurate estimates, the cognitive decisions informed by our perceptions may be better served by the ability to determine and remember when objects are different than expected even at the expense of accurate estimation. Further study is required to determine whether the perceptual biases observed in the classical SWI reflect efficient coding or task-dependent contrast enhancement or an entirely different mechanism for sensory integration.

Although we may not fully understand why anti-Bayesian perceptual estimates occur, it is clear that these estimates are oppositely biased from Bayesian estimates, suggesting the existence of multiple mechanisms for integration of prior expectations with raw sensory information. Widespread experimental evidence of Bayesian integration has accumulated over the last few decades (Ernst and Banks 2002; Körding et al. 2004; Körding and Wolpert 2004; Sato et al. 2007; Stocker and Simoncelli 2006a; Weiss et al. 2002). However, the current work makes it clear that Bayesian integration is not universal, as it does not always occur – even under conditions in which it could apply – when prior expectations and raw sensory information are known to influence final estimates.

CHAPTER 3: GENERALIZATION OF MOTOR ADAPTATION: EXAMINATION OF STATE AND CONTEXT DEPENDENCE

3.1 SUMMARY

In the healthy central nervous system, motor learning ability can account for changes in the environmental dynamics (Smith et al., 2006; Sing et al., 2009) or kinematics (Krakauer et al., 2000). Unfortunately, this ability can be impaired by neurological degeneration or traumatic brain injury, and thus uncovering the factors, which contribute to the formation and generalization of motor memories could be key in the development of more appropriate rehabilitation programs. Here we studied the formation of new motor memories during motor learning in human subjects following the exposure to a novel environmental dynamics in order to understand the internal representation of these memories by rigorously studying the manner in which this learning generalizes to several types of contextually different movements. In four experiments, subjects learned how to make straight point-to-point arm reaching movements while compensating for an externally applied velocity-dependent curl force-field. After an initial training period, we probed the transfer of motor memory to a variety of different movements, looking at the effects of several different mis-matched features between the trained and test movements. In particular, we examined the effects of three components of the state vector (position, velocity, acceleration) as well as two contextual variables (movement continuity and movement geometry).

We discovered that, although position and acceleration play a small role in the generalization of velocity-dependent force-field adaptation, movement geometry and continuity are responsible for over half of the adaptation that generalizes to other movements. Our findings provide a foundation for the development of better rehabilitation techniques, by illuminating the features most important to match between training and target movements during practice to improve target performance.

3.2 INTRODUCTION

It has been previously shown that motor adaptation to environmental force disturbances is learned as a function of motion state (i.e. position or velocity) rather than as a function of time (Conditt et al., 1997; Conditt and Mussa-Ivaldi, 1999; Shadmehr and Missa-Ivaldi, 1994). While past studies have demonstrated that adaptation to a velocity-dependent force-field transferred from straight point-to-point movements to circular and figure-8-shaped trajectories, the amount of this transfer has not been quantified. Here we quantified the amount of transfer for velocity-dependent force-field adaptation from straight to circular, semicircular, and S-shaped movements by directly measuring motor output changes associated with this learning using error-clamp trials.

When we attempted to reproduce previous findings (Conditt et al., 1997), we found that although the generalization from straight to circular movements was statistically significant, the amount of generalization was less that 50% - in fact, only about 20%. The substantial fall off in generalization from straight to circular movements suggests that although the adaptation to velocity-dependent dynamics depends on velocity, it also depends heavily on other factors. In particular, the geometry and continuity of movement differed between these two types of movements, as well as the position, acceleration at the point of matched velocity where we examined generalization.

We systematically investigated these factors by first examining the effect of position as a context for adaptation to viscous dynamics in experiment 3.2, and then looked at the effects of acceleration and geometry by studying semicircular vs. S-shaped discrete movements in experiment 3.3. In the middle of the semicircular movements, position and velocity were matched to the straight training movements, but the acceleration vector was orthogonal. Interestingly, we found very little fall off in generalization when only position was varied, and almost identical generalization from straight to both semicircular and S-shaped movements.

The results suggest that neither position nor acceleration serve as critical contexts for learning viscous dynamics. However, the amount of generalization from straight to semicircular and S-shaped movements was only 45-50%, suggesting that movement geometry serves as a key context for motor adaptation such that when this geometry is altered only, a substantial fall off in the amount generalization occurs.

3.3 METHODS

3.3.1 Participants

All participants gave informed consent for the experimental procedures, which were approved by Harvard's Committee on the Use of Human Subjects. In total, we recruited 68 healthy, neurologically intact people to participate in the 4 experiments in this chapter. 24 subjects participated in experiment 3.1, 12 in experiment 3.2, 20 in experiment 3.3, and 12 in experiment 3.4.

3.3.2 General procedures

For all experiments in this chapter, we used a motor adaptation task, force-field learning, which has been extensively used to study error-based learning (Gonzalez-Castro et al., 2011; Scheidt et al., 2000; Shadmehr and Mussa-Ivaldi, 1994; Sing et al., 2009; Sing and Smith, 2010; Smith et al., 2006). During these force-field experiments, subjects grasped a handle attached to a lightweight two-joint robotic manipulandum and were instructed to make point-to-point reaching arm movements. Subjects sat facing a monitor and made rapid (300+ mm/s peak velocity) 10 cm movements toward the torso using the arm configuration displayed in Figure 3.1A while viewing a screen cursor that represented real-time hand position. Subjects were instructed to make a fast, direct movement toward each target that appeared on the monitor, and after each trial subjects moved their hands back to the starting location. Positive auditory feedback was provided on trials with peak velocity between 300 and 350 mm/s. Movement onset was defined based on a speed threshold of 30 mm/s and movement offset was defined as the first time that the movement speed decreased below 30 mm/s and remained there for 200 ms consecutively. Experiments consisted of three different types of trials (Figure 3.1B-D): null field trials during which no active forces were applied to the subject's arm (Figure 3.1B), error-clamp trials to measure the lateral forces

produced on a given movement (Figure 3.1D), and force-field perturbation trials during which forces were applied to the arm during the movement based on the instantaneous position and/or velocity of the hand (Figure 3.1C). The position and velocity of the hand as well as the forces generated by the arm were recorded at a sampling rate of 200 Hz.

In addition, in experiments 3.1, 3.3 and 3.4 subjects were asked to perform movements that traced a shape displayed on the screen. In experiment 3.1 a fraction of the trials required subjects to trace a circular shape (see Figure 3.3 for details), whereas in experiments 3.3 and 3.4 subjects were asked to trace a semi-circular and S- shape (see Figure 3.7 for details). Importantly, in all of these shapes the velocity requirement necessary for positive auditory feedback was maintained the same as in the straight movements.

The adaptation measure we used in these experiments was calculated by comparing the measured compensatory force output at the peak speed point of a given movement with the ideal compensatory force at the same time point, averaged over a 100 ms window, as illustrated in Figure 3.2.

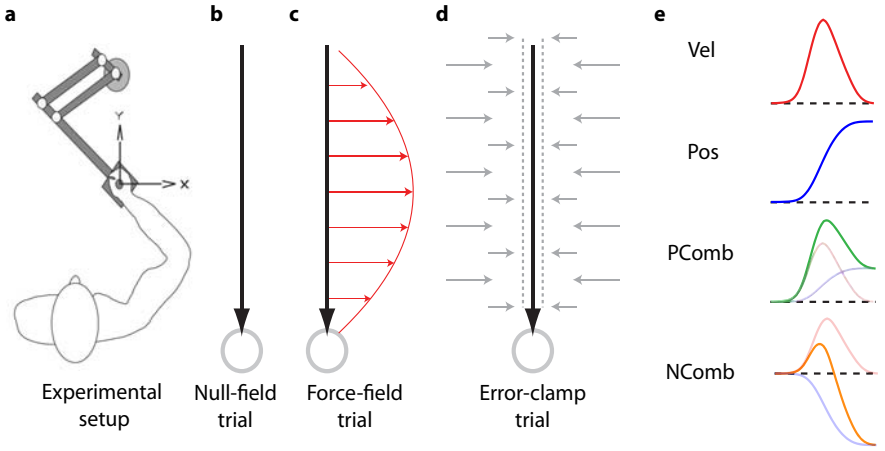

Figure 3.1: Basic experimental protocol for force-field adaptation experiments. (A) Illustration of the arm configuration subjects had when grasping the robotic arm. **(B)** Example of a Null-field trial. No forces are applied to the subject's hand and the movement is not restricted in any way. The majority of these movements were straight to the target. Not shown here are also shaped null-field movements (see Fig. 3.3 and 3.7) where subject had to trace a shape drawn on the screen. **(C)** Example of a force field trial. As subjects made a straight movement to the target, the force field exerted a force proportional to their velocity perpendicular to their movement direction. **(D)** Example of an error clamp trial. The robotic manipulandum constrained the movement in a straight line by counteracting any lateral forces subjects produced. This allowed for the measurement of lateral forces during a straight point-to-point movement.

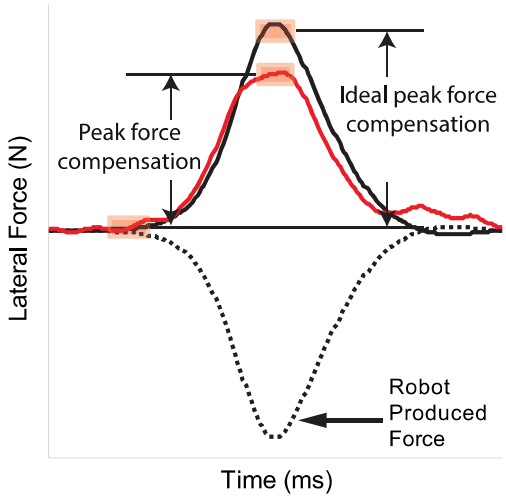

Figure 3.2: Learning metric. During an arm reaching movement the robot produces a velocity dependent force (dashed line) which pushes the subject's hand of course. If the subject were to execute a straight movement he or she would need to produce a force profile which is equal in magnitude and opposite in direction to the robot produced force (black line). In reality, subjects produce force profiles which are not 100% identical to the ideal force profile, but rather resemble in shape. Here we define the adaptation metric as the ratio between the actual force exerted by the subject at the peak speed point of the movement to the ideal force that would be required at the same point in time to completely compensate for the robot produced force. This ratio is calculated by averaging the data for the actual force and ideal force across a 100 ms window around the peak speed point, subtracting the average force during a 100 ms window prior to the beginning of the movement and then dividing the two. The learning metric calculated in the shaped movement in experiments 3.1, 3.3 and 3.4 is calculated in an analogous fashion.

3.3.3 Specific procedures

3.3.3.1 Experiment 3.1

In experiment 3.1 subjects were asked to perform straight point-to-point movements from a single starting location to an array of 24 targets spanning -180° to 180° as well as circular movements originating at the same starting location. The straight movements were 10 cm in length and the circular movement was along the circumference of a circle with a radius of 6 cm.

The experiment began with an extended baseline period during which subjects practiced straight and circular movements and without error clamps. This baseline period was followed by 120 straight movement training trials. After training was complete, subjects were asked to perform either three sets of straight movements towards 24 different directions followed by 20 circular movements or vice-versa, all of those in an error clamp, followed by another set of 60 straight training trials. After retraining, the order of testing between straight and circular movements was reversed, as diagrammed in Figure 3.3C.

3.3.3.2 Experiment 3.2

In experiment 3.2 subjects were asked to perform straight point-to-point movements from five different starting locations, as illustrated in Figure 3.5A during the baseline period subjects practiced movements from all five starting locations in a random order, making sure they have equal number of trials at each location. Movements from the lateral starting locations were not aligned parallel to the movements from the primary (training) location because we wanted to make sure that the joint excursions during those movements (the changes in elbow and shoulder angles) are the same as the joint excursions during the training movement. Movements from the anterior starting locations were co-linear with movements at the training location; however, they were shorter in length, once again making sure that joint excursions are maintained.

During the training period, subjects performed 160 trials at the training location only. In each of the five starting locations subjects performed seven test movements before and after training, as diagrammed in Figure 3.5B. For each location, the average of the seven trials during the baseline period served as a baseline and was subtracted from the average of the seven trials obtained after training.

After the first set of testing, an additional training set of 80 trials was performed with movements at the training location and a second set of tests was performed (seven trials in each of the five test locations).

3.3.3.3 Experiments 3.3 and 3.4

In these two experiments subjects performed three types of movements: straight, semicircular, and S-shaped. Both experiments began with an extended baseline training during which subjects performed a series of all three types of movements in both null field and error clamp trials.

In experiment 3.3 a training set of 160 straight movement trials was followed by a testing block of seven trials of each of the three types described above, followed by a retraining of 80 straight movement trials. The sequence of testing in retraining repeated three times to obtain a total of 21 measurement trials for each of the three movement types (straight, semicircular, and S-shaped).

In contrast, in experiment 2.4, there was no extended training. A single trial (straight, semicircular, or S-shaped movement) in an error clamp was followed by a single straight force field training trial, followed by another movement of the same type as the movement preceding the single force field training trial as diagrammed in Figure 3.7B. This triplet of movements allowed us to measure the adaptation in response to a single trial of force field learning.

3.3.4 Definition of the force-field environment and error-clamp trials

The force-fields used in the current experiments were velocity dependent (Figure 3.1C) with the form:

$$\begin{bmatrix} F_x \\ F_y \end{bmatrix} = B \cdot \vec{v} = \begin{bmatrix} 0 & -b \\ b & 0 \end{bmatrix} \cdot \begin{bmatrix} \dot{x} \\ \dot{y} \end{bmatrix} \quad \text{(eq. 3.1)}$$

Here, $\dot{x}$ and $\dot{y}$ denote the x and y velocities with y-axes as illustrated in Figure 3.1A. The force-field shown in Figure 3.1C had a value of b=15 Ns/m; the values of B used in all four experiments were b=±15 Ns/m, corresponding to clockwise and counterclockwise force-fields. To account for biases from biomechanical effects, clockwise and counter-clockwise versions of force-fields were balanced in all experiments, with half the subjects learning each and the data was then averaged across both conditions.

The error-clamp trials (Figure 3.1D) were designed to measure the feed-forward motor output produced during a reaching movement. Actions made during reaching movements result from feed-forward motor output and online feedback error correction. Error-clamp trials (Scheidt et al., 2000; Sing et al., 2009; Smith et al., 2006) restricted the lateral deviations during movement below 1 mm, effectively eliminating the lateral error signal and corresponding feedback responses, thus allowing for isolation of feed-forward motor output. We restricted these deviations by applying a very stiff, damped elastic force (K=6000 N/m, B=250 Ns/m) to counteract lateral forces produced by subjects, while essentially clamping movements into a straight line path. Since we were able to counteract the lateral deviations of the subject's arm with a robot generated force, we estimated the lateral force produced by the subject as the opposite of the robot generated clamping force at each time-point. All force data were smoothed

with a second order Butterworth filter with a cutoff frequency of 10 Hz to remove high frequency noise generated by force sensors and motor actuators.

In experiment 3.1 during error clamp trials in which subjects were supposed to move in a circle the error clamp was defined according to equation 3.2:

$$\begin{bmatrix} x \\ y \end{bmatrix} = \begin{bmatrix} \sin(t) \\ \cos(t) \end{bmatrix} \quad \text{(eq. 3.2)}$$

where x and y define the locus of points along the circle and t varies in the range 0 to 2π. In this error clamp trial subjects movement was restricted along the circle in the same manner as in the straight movements described above. Similarly, in experiments 3.3 and 3.4 in error clamp trials in which the subject was required to move along a semicircle the error clamp was defined analogously to equation 3.2, except for a semicircle T varied in the range 0 to π. In these experiments when an error clamp trial along an S-shape was called for, it was defined according to equation 3.3:

$$\begin{bmatrix} x \\ y \end{bmatrix} = \begin{bmatrix} \sin(2t) - 2 \cdot \cos(t) \\ \sin(2t) + 2 \cdot \cos(t) \end{bmatrix} \quad \text{(eq. 3.3)}$$

for t in the range 0 to 2π. Essentially, the error clamp movements were such that subjects were only allowed to move along the desired shape and any lateral forces, which would have otherwise caused lateral deviations, could be measured.

3.4 RESULTS

In order to determine the internal representations of motor memory associated with motor adaptation, we studied at the transfer of learned adaptation across different geometric shapes. In a series of classic studies, Conditt et al (1997; 1999) demonstrated that these memories generalize from straight point-to-point movements to circular and figure-8-shaped movements as a function of motion state. However, the evidence they presented was qualitative in nature, as it failed to quantify the amount of this generalization. Further work has corroborated this basic finding of state-dependent learning, showing that the primitives for motor adaptation are state-dependent – displaying a positive combination of position and velocity dependence (Sing et al., 2009) – and that motor adaptation can extrapolate to faster movements of the same geometry in a state-dependent manner (Goodbody and Wolpert, 1998; Joiner et al., 2011). However, the basic question of the extent to which learned dynamics generalize across different types of movements in a state-dependent fashion has not yet been answered.

3.4.1 Generalization from straight circular movements

In experiment 3.1, we replicated the basic paradigm used in these classic studies, but used an error-clamp technique developed in our lab (Smith et al., 2006; Sing et al., 2009, Gonzalez-Castro et al., 2011) to quantitatively characterize the generalization of learned force field dynamics. We accomplished this by comparing the generalization across movement directions for point-to-point arm reaching movements and circular movements.

The experiment began with a 964-trial baseline period, during which subjects made both straight and circular movements. The straight movements, in 24 different directions all originating at the same starting location, were randomly interspersed with the circular movements which originated from the same starting location. During the subsequent 120-trial training period, subjects made only straight point-to-point movements in a force field in which novel physical dynamics

perturbed them by pushing the hand off course. During the training period, subjects learned how to compensate for the force field and were eventually able to make movements, which were more or less straight to the target. After this training, we tested the generalization of learning to straight and circular movements introduced in the baseline. The 24 straight movements were spaced 15° apart, and the single circular movement spanned all directions. Figure 3.3A shows the workspace which was used for this experiment. If the same generalization pattern were to apply to straight point-to-point and circular movements then we could measure the whole generalization function using this single circular movement. This is the case because along the circumference of the circle the motion spans the whole range of possible directions, as illustrated in Figure 3.3B. Figure 3.3C shows a summary of the experimental protocol we used. Figure 3.4A shows the average learning curve of the 24 subjects, which took part in this experiment in the training period. By trial 120, subjects on average were able to compensate for approximately 70% of the imposed force field. This is consistent with previous findings reported in force field adaptation (Sing et al., 2011; Smith et al., 2006). Note that the shape of the learning curve shown here has a distinct rapid portion during the first 10 to 15 trials during which subjects reach approximately 60% of the final level of learning as well as a slower, more gradual part in the following 100 or so trials, as previously reported (Smith et al., 2006).

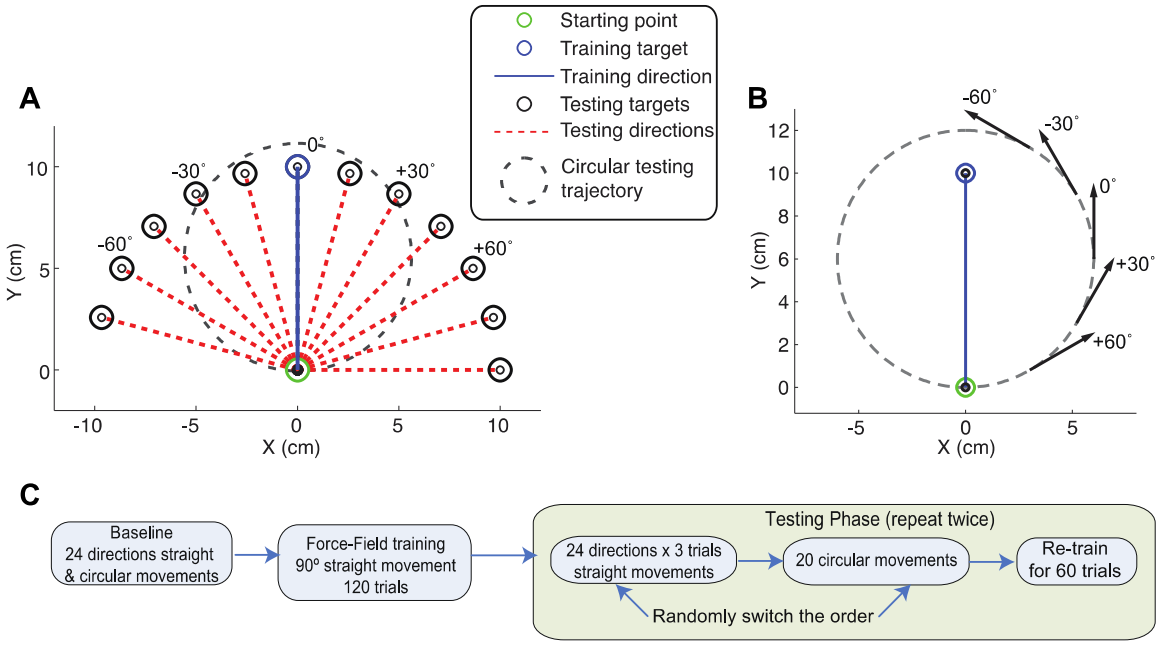

Figure 3.3: Experiment 3.1 diagram. **(A)** Schematic of the workspace of this experiment. All movements originated at the same starting point (green circle), the 10 cm trained movement was in the direction labeled as "0° direction", 10 cm test movements spanned the whole range of -180° to 180° (red dashed lines, not all shown), circular movement was along the circumference of a circle with radius 6 cm. **(B)** Diagram of different directions at which subjects were moving when performing a circular movement. Along the circumference of the circle subject effectively move in all possible directions. Note that in this experiment subjects were trained to move at the same velocity along the whole circumference of the circle and the velocity was equal to the peak velocity during a straight point-to-point movement. **(C)** Diagram of the experimental protocol for experiment 3.1. The force fields used in this experiment alternated between clockwise and counterclockwise and were balanced across subjects.

Surprisingly, as observed in Figure 3.4B, the generalization function obtained from the circular error clamp trials differed greatly from that obtained from the array of different movement directions. The key difference was that the generalization was smaller in the circular than the point-to-point movements. This reduction is most substantial near the trained direction, for example, when moving in a direction parallel to the trained direction (0°), the amount of adaptation transferred to the circular movement is approximately 20% of the adaptation observed for a straight movement in the same direction. Note that, in the circular error clamp, subjects were moving at a constant velocity, which was equal to the peak velocity they experienced in the training point-to-point movement trials, as shown in Figure 3.4B.

These results support the previous findings that velocity-dependent dynamics generalize in a state-dependent (velocity-dependent) manner (Conditt et al., 1997; 1999), however, we find that this generalization is far from complete. In fact, the 20% generalization we observe indicates that factors besides velocity, which were not matched in the current experiment, might account for most of the generalization (i.e. the remaining 80%). These factors include other components of the motion state (position and acceleration) as well as state-independent contexts, including movement geometry (i.e. shape) and continuity (discrete vs. continuous).

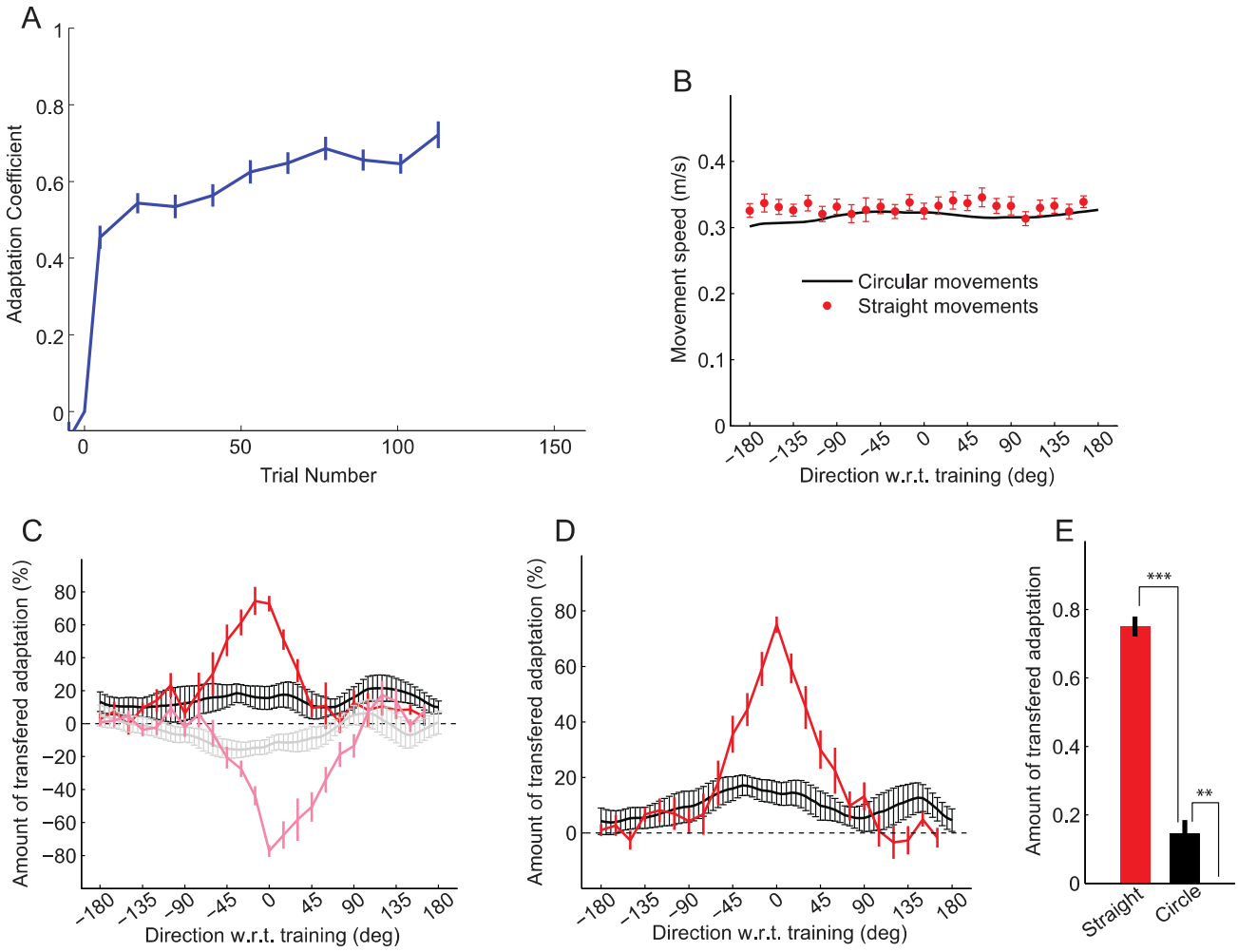

Figure 3.4: Results from experiment 3.1 showing distinct differences between the generalization to straight and circular movements. **(A)** Average learning curve across 24 subjects. Error bars show sem. Note the rapid initial learning over the first 15 or so trials in the distinct gradual learning over the last 100 or so trials. Subjects reach an asymptotic level of approximately 75% indicating that they learned roughly ¾ of the applied force field magnitude. **(B)** Average velocity along a circular movement (black line) and average peak velocity (with sem) in each of the 24 straight point-to-point movements (red). **(C)** Average generalization functions resulting from learning a clockwise (dark red and black) and counter-clockwise (right-red and gray) force field. Each trace here contains half of the subjects in the experiment. **(D)** Average generalization functions obtained in the two arms of the experiment. The traces here were produced by combining the traces in panel C. The traces corresponding to the counter-clockwise force field were reflected along the y=0 line and averaged together with the clockwise-based traces. Note that, the shapes of the generalization functions differ greatly between straight (red) and circular (black) movements. **(E)** At the trained direction (0°) approximately 75% of the adaptation was transferred towards a straight movement whereas only 15% (significantly less than 75% but significantly more than 0%, $p<0.01$) of the adaptation was transferred towards the circular movement in the same direction. (**, $p<0.005$ and ***, $p<10^{-10}$)

3.4.2 The effect of position on the generalization of a velocity-dependent motor adaptation

In experiment 3.2, we investigated the effect of position on the generalization of force field adaptation. In the experiment 3.1 we found only 20% generalization when we matched the velocity vectors (speed and heading direction) between straight and circular movements. However, we did not match the exact location (position in space) where the matched velocity and direction vectors occurred. In particular, point-to-point movements in the trained direction (0°) were offset 6 cm laterally compared to the portion of the circular test movement matched to this direction (see Fig.3.3A).

After learning a velocity-dependent force-field during point-to-point movements in one location, similar to experiment 3.1, we tested the generalization of this learning during a testing block with point-to-point movements at the trained location as well as 4 untrained locations each 10 or 20 cm away from the trained location. These four locations not only allowed us to look at generalization beyond the 6 cm lateral offset in experiment 3.1, but they also covered more than 75% of the reachable workspace in the left-lateral and anterior directions, as shown in Figure 3.5A. Here we matched joint excursions (intrinsic coordinate displacements) of the test movements to the training movement rather than the Cartesian excursions (extrinsic coordinate displacements), since it has been previously suggested that force-field learning generalizes in joint (intrinsic) coordinates (Shadmehr and Mussa-Ivaldi, 1994; Shadmehr and Moussavi, 2000; Malfait et al., 2002; Bays and Wolpert, 2006). Note that the two lateral test movements were therefore parallel to the trained movement in intrinsic rather than extrinsic coordinates, and the two forward test movements were the same length as the trained movement in intrinsic rather than extrinsic coordinates.

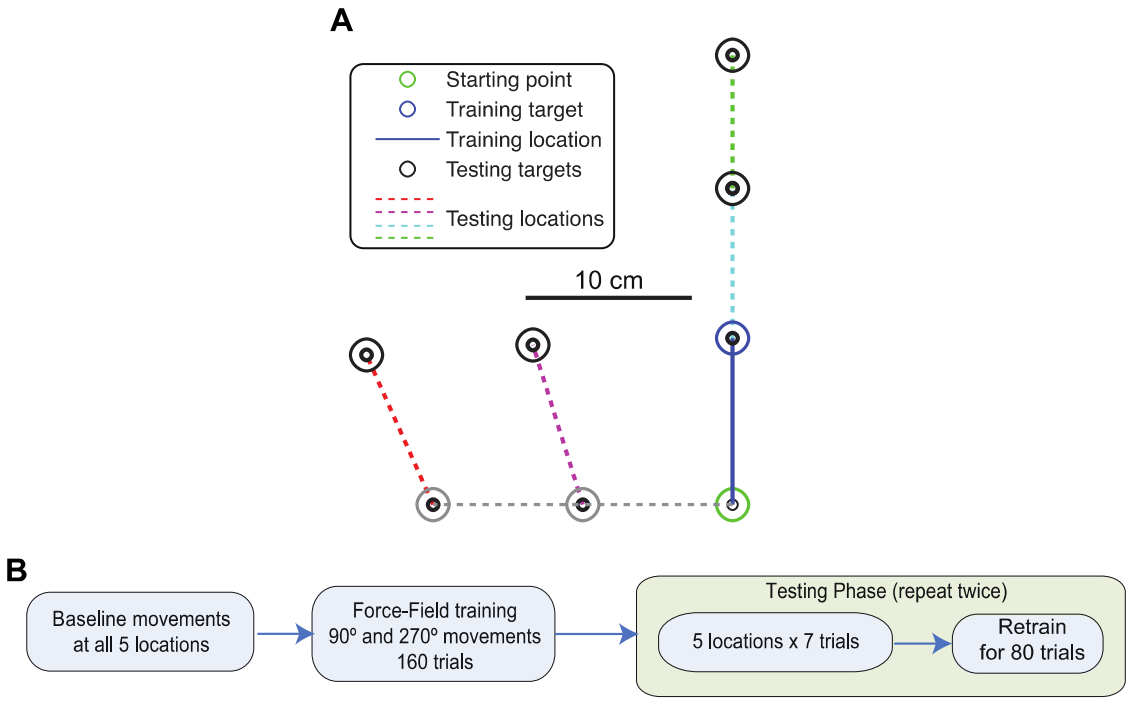

Figure 3.5: Experiment 3.2 diagram. (A) Diagram of the experimental workspace. The trained 10 cm movement (blue line) requires the same exact joint excursions (changes in elbow and shoulder angles) as the other four test movements. This results in a change in the angle for the movements which are left lateral to the trained movement (dashed purple and dashed red lines) and change in length for the movement who are anterior to the trained movement (dashed blue and dashed green lines). **(B)** Diagram of the experimental protocol for experiment 3.2. The force fields used in this experiment alternated between clockwise and counterclockwise and were balanced across subjects.

At the end of training about 70% of the learned of adaptation was retained at the trained location (Fig. 3.6A) similar to what we found in experiment 3.1. Interestingly, at locations 10 cm lateral or anterior to the trained location, the adaptation level was more than 60% of the initially learned adaptation and even at locations 20 cm away the level of adaptation was 55%. These results show that more than 80% of the adaptation which is retained and the trained location transfers across positions to locations within 75% of the reachable workspace, as shown in Figure 3.6B. These findings are in line with previous studies that reported minimal position-dependence on the generalization of the adaptation to velocity-dependent physical dynamics (Hwang et al., 2003; Hwang et al., 2006).

The results from experiment 3.2 suggest that the changes we observed in the generalization function observed in experiment 3.1 between the generalization to an array of different movement directions and the generalization to a circle is not due to position mismatch. In experiment 3.1 we observed a 3-fold decrease in generalization with a 6cm lateral mismatch in position, however in experiment 3.2, we found that lateral differences of 10 and 20cm result in only small 10-20% decreases in generalization in point-to-point movements equated for joint excursions which results in matched velocity, acceleration, movement geometry, and continuity. This suggests that the large generalization decrease of 60-70% observed in experiment 3.1 where, in addition to position, acceleration, movement geometry, and continuity were not matched was primarily due to these last three factors.

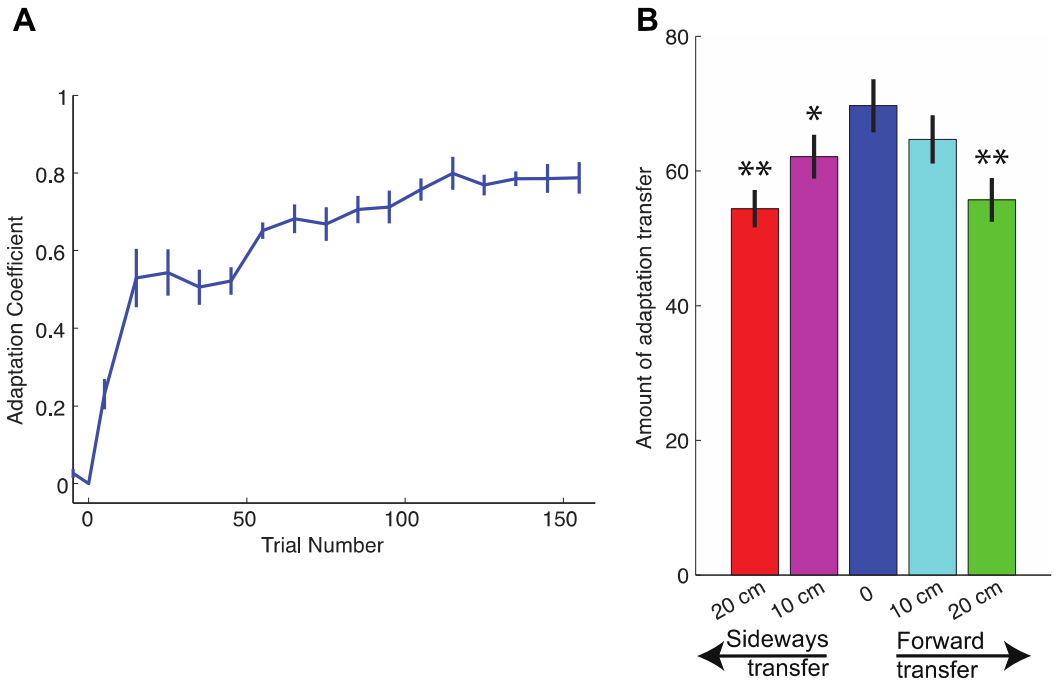

Figure 3.6: Experiment 3.2 results show minimal effect of position on the amount of adaptation transferred to untrained straight movements. (A) Average learning curve across 12 subjects. Error bars show sem. Subjects reach an asymptotic level of approximately 80%, consistent with the learning level reached in experiment 3.1. **(B)** Transfer of learned adaptation to the five test movements. The amount of adaptation transferred to the test movement located at the same location as the trained movement was approximately 70% of the asymptotic adaptation learned during training. The amount of transfer to movements 10 cm away in both lateral and anterior direction was above 60% of the asymptotic adaptation in even to movements which were 20 cm away the amount of transfer was above 55%. This suggests that the retention of learned adaptation falls off very gradually as a function of position and in fact 80% of the retention at the trained location is transferred to movements 20 cm away. (*, $p<0.05$ & **, $p<0.005$)

3.4.3 Matching the kinematic states does not lead to full transfer of adaptation

In experiment 3.3, we investigated the effects of the acceleration component of the state vector and the context that movement geometry or movement continuity provides on the generalization of motor adaptation. The velocity-dependent force-field studied in experiment 3.1 was matched for velocity but not position or acceleration across point-to-point and circular movements. In experiment 3.2 we found that the position mismatch of 6 cm that was present in experiment 3.1 could not account for the 80% transfer decrease we observed because a position mismatch of 10 cm only led to a 10% decrease in transfer.

To test the effects of acceleration, movement geometry, and movement continuity on the generalization of adaptation, we devised experiments 3.3 and 3.4 in which we compared the generalization across three differently shaped of point-to-point movements: straight movements, semicircular movements, and S-shaped movements. Note that, in straight and S-shaped movements, the acceleration vector in the middle of the movement will be near zero whereas in semi-circular (and circular) movements mid-movement acceleration will perpendicular to the movement trajectory and nonzero. As illustrated in Figure 3.7A, we designed the experiment so that all 3 movement types were matched at the mid-movement point in position and velocity. This resulted in matched position, velocity, acceleration and discreteness for the straight and S-shaped movements, and matched position, velocity, and discreteness for the straight and semicircular movements. Thus the straight and S-shaped movements differed at the midpoint only in movement geometry context, whereas the straight and semicircular movements differed in both the geometry context and the mid-movement acceleration.

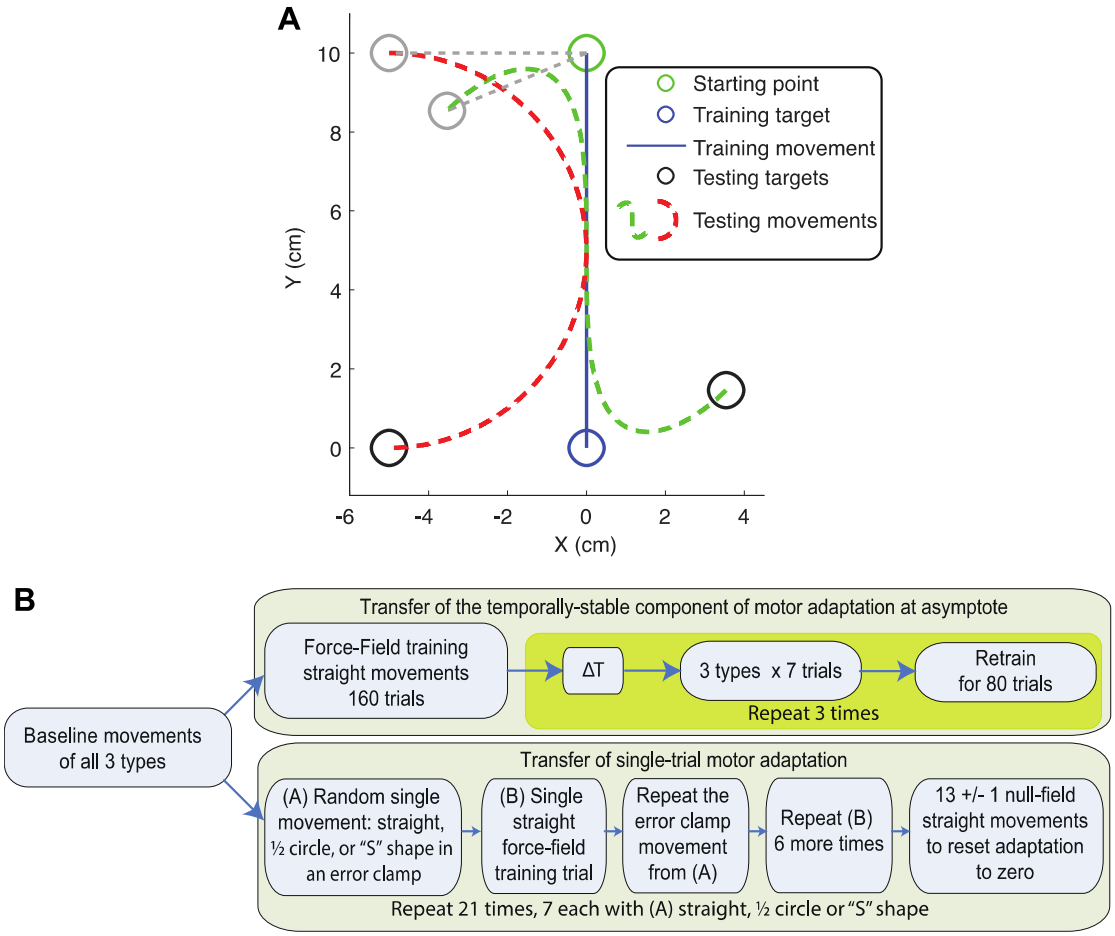

Figure 3.7: Experiments 3.3 and 3.4 diagram. **(A)** The three shapes studies in these experiments are shown exactly as they would appear on the screen. Note that subjects were only presented with one of these shapes at a time. The mid-points of all three movements coincide and subjects were trained to move at the same velocity at this point. In the straight and S-shaped movements, the acceleration at this point was also close to zero whereas, in the semicircular movement the acceleration at the midpoint was perpendicular to the movement trajectory and significantly greater than zero. **(B)** Diagram of the experimental protocol for experiment 3.3 (top branch) and 3.4 (bottom branch).

During the training period for experiment 3.3, subjects reached an adaptation level similar to what we observed in experiments 3.1 and 3.2 (75% vs. 70% or 75%, respectively) as shown in Figure 3.8A. We found that generalization to the S-shaped movements was only about 50% of that observed for the straight point-to-point movements. This indicates that movement geometry is a critical factor for determining the amount of generalization because the S-shaped movements were matched on all 3 components of the motion state vector (position, velocity, and acceleration) compared to the straight movements, and both types of movements were discrete – leaving movement geometry as sole unmatched factor responsible for the 50% decrement in generalization. Correspondingly, we found a similar amount of transfer to semicircular movements (45%), which were matched to the straight movements for position, velocity, and discreteness, but not acceleration or geometry. This corroborates the results for S-shape movements suggesting that movement geometry is a major determinant of generalization, and it further suggests that the acceleration component of the motion state vector has a relatively minor effect as generalization to semicircular movements further dropped by only 5% compared to the S-shaped movements ($p>0.1$).

In experiment 3.4, we compared the transfer of adaptation from straight to semicircular and S-shaped movements after only a single training trial. As shown in Figure 3.8C, we found approximately 20% adaptation in the straight movements but only 6-7% adaptation in the S-shaped and semicircular movements, corresponding to about 30% transfer of adaptation from straight to curved movements. Once again, we found no difference in the amount of generalization between S-shaped and semicircular movements ($p>0.5$), whereas we found a substantial decrease in generalization between straight and curved movements ($p<0.0001$).

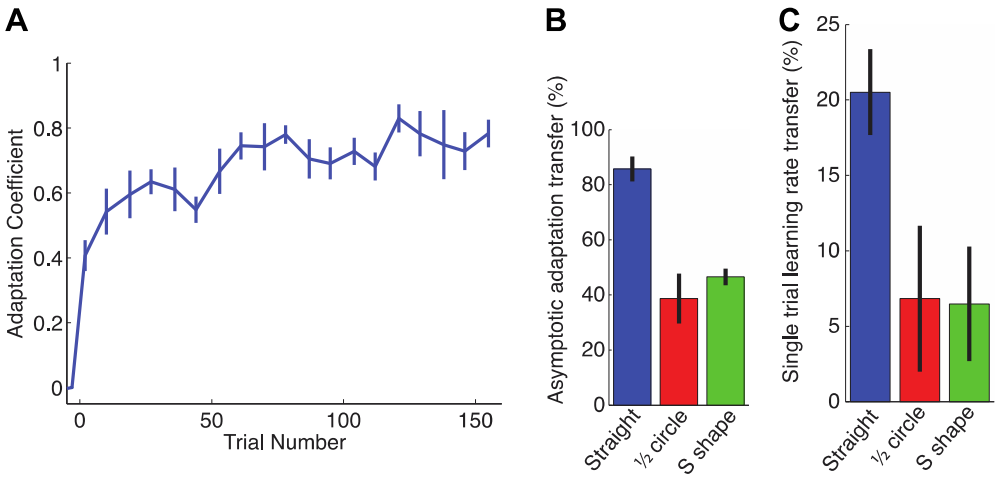

Figure 3.8: Experimental results from experiments 3.3 and 3.4 show that matching the three primary kinematics states only accounts for about half of the adaptation transfer. (A) Average learning curve for straight point-to-point movements during the training period across 20 subjects. Error bars show sem. Subjects reach an asymptotic level of approximately 80%, consistent with the learning level reached in experiments 3.1 and 3.2. **(B)** Transfer of asymptotic level of learned adaptation to straight (blue), semicircular (red), and S-shaped (green) movements. The transfer to a shape movement is approximately ½ of the transfer to the straight movement. **(C)** transfer of single trial learning to the three different types of movements. Note that only about one third of the adaptation which transfers to a straight movement transfers to a shape movement.

In order to carefully look at the effects of each individual factor, we combined the data from experiment 3.1-3.3 and presented them together in Figure 3.9. In each of these 3 experiments we tested the generalization to the trained movement as well as to other shaped or straight movements. In order to compare results across experiments, we normalized the observed adaptation in each subject by the adaptation level observed in that subject to the trained movement. This normalization effectively set the level of adaptation to the trained movement at 100%, allowing us to look at the differential effects of individual factors (position, velocity, acceleration, continuity, and geometry) across experimental conditions and across subjects. Our results suggest that positional mismatch of 10 cm leads to less than 10% decrease in adaptation (purple bars), geometry accounts for a 50% adaptation drop (green bar), acceleration has a 5-10% effect (cyan vs. green bar) and continuity accounts for an additional 20-30% (blue bar).

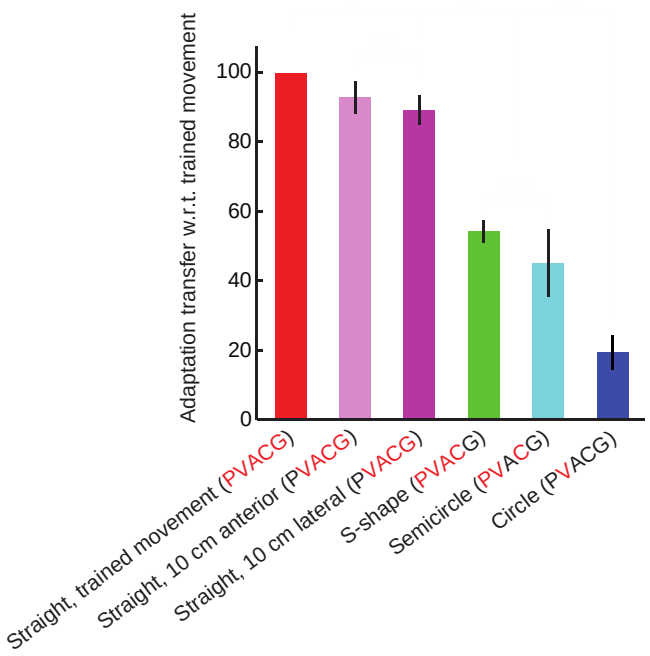

Figure 3.9: Factoring out motor generalization. When transferring adaptation to the trained movement (red) 5 factors that we considered were matched: position (P), velocity (V), acceleration (A), continuity (C), and geometry (G). The generalization to other movements in this plot was normalized to the amount of transfer to the trained movement measured in the same block. The movements in experiment 3.2 (purple) were matched for everything except P and displayed approximately 90% transfer, suggesting little effect of P. In experiment 3.3, the S-shaped movements were matched for all features but G, and the semicircular movements were matched for all features but G & A, both cases leading to approximately 50% transfer, suggesting a substantial dependence on movement geometry, but like P, little effect of A. In the circular movements in experiment 3.1 only velocity was matched, leading to only 20% generalization.

3.5 DISCUSSION

We studied the generalization of the adaptation to novel physical dynamics to different types of movements in an attempt to better understand its motion-state dependence. In four experiments, we investigated the effects of three different components of the motion state vector (position, velocity, acceleration), as well as the contextual effects that movement geometry (shape) and movement continuity (discrete vs. continuous) may provide. We showed that force-field adaptation transferred broadly across different positions in the workspace (experiment 3.2), and across different accelerations (comparison of S-shaped and semicircular movement results in experiments 3.3 and 3.4). However, when all three kinematic states (position, velocity, and acceleration) and movement continuity were matched, we found only 50% generalization from straight to curved movements. This indicates that, by itself, mismatched movement geometry can be responsible for a 50% decrement in generalization.

Our results are consistent with the pioneering work by Conditt et al (1997; 1999) demonstrating velocity-dependent generalization of learned dynamics from straight to curved movements, but whereas they demonstrate the existence of this generalization, we are in fact able to quantify the amount of generalization, and we find that it is far from complete. This underlines the importance of careful and quantitative analysis when studying the generalization of motor adaptation.

These results raise another important, practical issue, about the possible effectiveness and inherent value of rehabilitation exercises dissimilar from common practical actions in stroke survivors and other patients. Rehabilitation programs which use a robotic manipulandum in an attempt to help stroke patients regain their mobility may not be as effective as we would hope, if the motions are not designed to carefully mimic those that accompany activities of daily living. To fully address this, we would need to perform similar studies in a patient population and, given our current findings, we can now design these studies more efficiently.

CHAPTER 4: MOTOR MEMORY IS ENCODED AS A GAIN-FIELD COMBINATION OF INTRINSIC AND EXTRINSIC ACTION REPRESENTATIONS

4.1 SUMMARY

Actions can be planned in either an intrinsic (body-based) reference frame or an extrinsic (world-based) frame, and understanding how the internal representations associated with these frames contribute to the learning of motor actions is a key issue in motor control. We studied the internal representation of this learning in human subjects by analyzing generalization patterns across an array of different movement directions and workspaces after training a visuomotor rotation in a single movement direction in one workspace. This provided a dense sampling of the generalization function across intrinsic and extrinsic reference frames which allowed us to dissociate intrinsic and extrinsic representations and determine the manner in which they contributed to the motor memory for a trained action. A first experiment showed that the generalization pattern reflected a memory that was intermediate between intrinsic and extrinsic representations. A second experiment showed that this intermediate representation could not arise from separate intrinsic and extrinsic learning. Instead, we find that the representation of learning is based on a gain-field combination of local representations in intrinsic and extrinsic coordinates. This gain-field representation generalizes between actions by effectively computing similarity based on the (Mahalanobis) distance across intrinsic and extrinsic coordinates and is in line with neural recordings showing mixed intrinsic-extrinsic representations in motor and parietal cortices.

4.2 INTRODUCTION

During visually guided reaching, the sensorimotor system must estimate the spatial location of a target, the associated movement vector, and the motor output required to achieve it. The nature of the internal representation of this information is a key issue in understanding the mechanisms for sensorimotor control. The neural representation of the spatial information associated with the location of the target and the movement vector defines a coordinate system that determines the similarity with which the nervous system views different movements. In line with this idea, a series of studies have attempted to elucidate these representations by studying how learned changes in motor output generalize across spatial locations and motion states during reaching arm movements (Shadmehr and Mussa-Ivaldi, 1994; Ghahramani et al., 1996; Conditt et al., 1997; Conditt and Mussa-Ivaldi, 1999; Krakauer et al., 2000; Shadmehr and Moussavi, 2000; Morton et al., 2001; Baraduc and Wolpert, 2002; Malfait et al., 2002; Morton and Bastian, 2004; Smith and Shadmehr, 2005; Bays and Wolpert, 2006; Hwang et al., 2006; Ghez et al., 2007; Mattar and Ostry, 2007; Wagner and Smith, 2008; Haswell et al., 2009; Mattar and Ostry, 2010; Quaia et al., 2010; Gonzalez Castro et al., 2011; Joiner et al., 2011). As illustrated in Figure 4.1A, a change in the posture of the end effector allows for dissociation between intrinsic and extrinsic movement representations. Correspondingly, several studies have performed postural manipulations to explore the extent to which the neural coding of movement or the functional representations of motor memories are associated with coordinate systems intrinsic or extrinsic to the end effector. Studies in which novel physical dynamics were learned during reaching arm movements have generally found a representation for motor learning intrinsic to the end effector – in the joint coordinates of the arm (Shadmehr and Mussa-Ivaldi, 1994; Shadmehr and Moussavi, 2000; Malfait et al., 2002; Bays and Wolpert, 2006), whereas studies of visuomotor transformation

learning have often suggested that the coordinate frame is based on position or motion extrinsic to the end effector (Vetter et al., 1999; Ghez et al., 2000; Krakauer et al., 2000).

Much of this previous work has assumed that each type of motor memory is encoded in a single reference frame – either intrinsic or extrinsic (Shadmehr and Mussa-Ivaldi, 1994; Vindras and Viviani, 1998; Ghez et al., 2000; Krakauer et al., 2000; Shadmehr and Moussavi, 2000; Malfait et al., 2002) and thus these studies were not designed to carefully examine the possibility that multiple coordinate frames might contribute to the internal representation of motor memory. However, more recent evidence suggests that novel dynamics are learned with a representation that is not fully intrinsic. For example, studies of children with autism (Haswell et al., 2009) and tDCS stimulation of motor cortex (de Xivry et al., 2011) have found that disease or brain stimulation can lead to a significantly greater fraction of intrinsic generalization. However, this would not be possible if generalization were normally fully intrinsic. Another recent study looked at the coordinate frame used in the representation of dynamics in tasks with visualizations of different complexity and concluded that physical dynamics are represented in a coordinate frame intermediate between intrinsic and extrinsic (Ahmed et al., 2008).

Despite the accumulating evidence that intrinsic and extrinsic coordinate frames both contribute to motor memory, little is known about the manner in which their contributions are combined. A key issue with previous work is that the sparsity with which these studies sampled the generalization of learning throughout the workspace did not allow for this level of investigation. Here we address this issue by measuring the generalization of visuomotor learning across an array of different movement directions and arm configurations – amounting to more than 50 conditions in total, compared to the 1 or 2 untrained conditions examined in most previous studies. This dense sampling allows us to visualize the pattern of generalization across the combined intrinsic-extrinsic space, revealing a representation of motor memory that arises from a gain field

combination of intrinsic and extrinsic coordinate frames. Importantly, our data distinguishes this multiplicative gain field combination model from a previously assumed (Hikosaka et al., 2002; Cohen et al., 2005; Berniker and Kording, 2008; Berniker and Kording, 2011) additive combination model which corresponds to the idea of separate intrinsically-based and extrinsically-based learning. We show that this multiplicative gain field model is consistent with the presence of intrinsic, extrinsic, and jointly intrinsic-extrinsic representations within posterior parietal cortex (Andersen et al., 1985; Andersen et al., 1998; Andersen et al., 2004; Buneo and Andersen, 2006) and motor cortex (Kalaska et al., 1989; Kakei et al., 1999; Kalaska, 2009).

4.3 METHODS

4.3.1 Participants

Thirty two right-handed subjects (13 men, mean age 36.7 yrs) participated in this study. Twelve took part in experiment 4.1 and twenty in experiment 4.2. The subjects were naïve to the purpose of the experiments and all provided informed consent consistent with the policies of Harvard's Institutional Review Board. Each participant took part in only one of the two experiments we conducted.

4.3.2 Apparatus

The configuration of the experimental setup is shown in Figure 4.1A. Subjects sat in a chair facing a 120 Hz 23-inch LCD monitor, mounted horizontally in front of them at shoulder level, displaying the various visual cues during the experiment. Underneath the monitor, 8 inches below the face of the screen, a digitizing tablet (Wacom Intuos 3) was used to track and record the subjects' arm movements. Above the tablet, subjects held a handle containing a digitizing pen in their right hand, whose position was tracked by the tablet. The handle served two purposes: (1) it acted as a shell around the digitizing pen, increasing its diameter, making it more comfortable to grasp, (2) it provided a wider contact surface with the tablet, promoting a more consistent vertical orientation of the pen. The handle had a flat bottom covered with Teflon (PTFE) which lowered the contact friction, allowing it to glide smoothly on the tablet. The position data was recorded in real-time (sampled at 200 Hz) using the Psychophysics Toolbox (Brainard, 1997; Kleiner et al., 2007) in Matlab (MATLAB, 2010). The resolution of the position data in the plane of the tablet was 0.005 mm and the accuracy was 0.25 mm.

4.3.3 Experimental protocol

In this study subjects performed 9 cm point-to-point reaching arm movements from a single starting location to 19 different target locations, as illustrated in Figure 4.1A. The starting location was a circle with diameter of 5 mm and each target was a circle with diameter 10 mm. The cursor was also a circle with diameter of 2.5 mm. Subjects performed this task in two distinct workspaces, and we conducted two experiments, with different pairs of workspaces as illustrated in Figures 4.1 & 4.4, respectively.

Both experiments began with a block of trials in a first (training) workspace – workspace 1 (W1) and workspace 1* (W1*) for experiments 4.1 and 4.2, respectively. This block contained 114 movements - 6 trials to each of 19 target locations presented in a pseudo-random order. During these movements subjects were given veridical visual feedback during both the outward movements toward each target and the inward return movements toward the starting location. At the end of this block, subjects were given a 1 minute rest during which they were repositioned so that the same movements on the tablet constituted a second (novel) workspace with respect to the torso – workspace 2 (W2) and workspace 2* (W2*) for experiments 4.1 and 4.2, respectively – where they performed a second block of 114 movements, all with veridical visual feedback. Note that the repositioning of the subjects consisted of moving the chair they sat on, rather than moving the location of their hand or of the display, similar to Malfait et al 2002 and Shadmehr and Moussavi 2000. These two blocks constituted the "familiarization phase" of the experiment and allowed the subject to become comfortable with the reaching task. By the second half of these blocks the movements were mostly straight to the target with an average movement time of 267 ms (13 ms SEM) for each 9 cm movement.

The second phase of the experiments, the baseline phase, consisted of 342 movements in each workspace, divided into 3 blocks of 114 movements. We alternated the 6 blocks of movements

between the training and novel workspaces, allowing the subjects to rest for about 1 minute between blocks while we positioned them. In the baseline phase, veridical visual feedback of the cursor was present on ⅔ of the movements. Feedback was withheld and on the remaining movements (randomly chosen). During this block, a return movement had visual feedback if and only if the preceding outward reaching movement had visual feedback. On the no-visual-feedback trials, the cursor disappeared as soon as the subject began her movement (when movement velocity increased above 5 cm/s) towards the target. A movement was considered complete when the subject came to a stop (defined by hand velocity remaining below 5 cm/s for a period of 100 ms). The return-to-center movement following a no-visual-feedback movement was without visual feedback and subjects had to find the starting location without visual guidance. The cursor reappeared only after subject came within 7.6 mm of the starting location.

During the third phase of the experiment, the training phase, each subject was presented with a 30° rotation of the cursor (either clockwise or counterclockwise). As she reached towards a target positioned at 90° (the training target), the cursor location was rotated about the starting location by 30°. All return movements in the training phase were without visual feedback. The imposed rotation was clockwise for half the subjects and counterclockwise for the other half. In order for the cursor to move directly toward the target, hand motion would need to be directed 30° opposite to the direction of the cursor rotation as shown in the leftmost panel of Figure 4.1A. Subjects performed a single training block of 120 movements to the training target with 10% of the trials in this block without visual feedback. At the end of the training block, movements were generally straight, indicating that participants learned the imposed rotation. In the last 40 trials of this block, subjects' movements were rotated by 27.3° ± 2.7° on average, with 30° corresponding to full learning of the imposed rotation and the average movement time was 211 ± 10 ms (213 ms in movement with visual feedback, 183 in movement without visual feedback). There was no

significant difference in the asymptotic learning level between the subjects who learned clockwise rotation and those who learned counterclockwise rotation ($p>0.2$).

Following training, subjects were given a 1 minute break before we tested the generalization of the learned adaptation to 19 targets in both the training and novel workspaces with 3 trials towards each target location in each workspace, in random order, all without visual feedback. The return movements in this testing phase were also without visual feedback. As shown in Figure 4.1E, we counterbalanced the order of testing the two workspaces: for half the subjects, generalization was tested in the training workspace followed by the novel workspace, whereas for the other half the order was reversed. After generalization was tested in both workspaces, subjects performed an additional block of training (60 trials) followed by two additional testing blocks, one in each workspace. The order of testing in these blocks was reversed from that of the first two testing blocks. The second set of training and testing was performed in order to double the amount of data collected from each subject. The data from both testing sets was combined and is presented together throughout the manuscript.

4.3.3.1 Experiment-specific procedures

In experiment 4.1 (shown in Figure 4.1A), W1 was chosen such that the starting location was in front of the subject's torso. Subjects were positioned so that at the starting location the subject's elbow formed a 90° angle between the upper arm and the forearm and the shoulder formed a 45° angle between the upper arm and the left-right horizontal axis of the subject's torso, as shown in Figure 4.1A, middle. In this workspace the 19 target locations spanned the range of +225° to -45° (90° ± 135°) and were spaced 15° apart. In W2 the elbow angle was maintained at 90°, however, the shoulder angle was rotated such that the upper arm was parallel to the subject's left-right axis. As shown in Figure 4.1A, right, in this workspace the 19 targets spanned the range of +240° to -30° (120° ± 135°). This range was chosen so as to best capture the shape of the generalization

function based on a set of pilot data we collected. As illustrated in Figure 4.1A, W2 differed from W1 by a -45° (45° clockwise) shoulder rotation.

Experiment 4.2 aimed to distinguish between two multi-reference frame models that Experiment 4.1 could not distinguish. To accomplish this, we used a greater separation between the training and testing workspaces and increased the number of participants. As shown in Figure 4.4, the training workspace in experiment 4.2 (W1*) was the same as the untrained workspace in experiment 4.1 (W2), and the untrained workspace in experiment 4.2 (W2*) was chosen such that it differed from W1* by a +90° shoulder rotation. The testing targets in both workspaces were chosen such that they were 15° apart spanning 270° and centered at the target location trained in W1* or +45° away from it in W2*.

4.3.4 Defining the space for visualizing intrinsic and extrinsic directional similarity

One way to define a movement is by specifying its starting point and a movement vector. For a straight point-to-point movement, the movement vector in Cartesian space is simply the directed line segment connecting its start and end points. In Figure 4.1B we show the movement vectors in Cartesian space for all 38 targets in experiment 4.1 (19 in each workspace). The origin of this plot is located at the subject's right shoulder. We used the average upper arm length (31.8 cm) and forearm length (33.0 cm) from all 32 subjects and the postures diagrammed in Figure 4.1A to calculate the starting locations for W1 and W2. Given any two straight movements originating from the same starting point and ending at two different targets we can describe the relationship between them by the angle formed by their movement vectors in Cartesian space. The same two movements can also be presented in joint coordinates as a pair of joint-space movement vectors with a common origin and the difference between them can also be characterized by the joint-space angle formed by the two vectors. In Figure 4.1C we show the joint-space representations of the Cartesian movement vectors from Figure 4.1B. We calculated these joint-space trajectories

using the inverse kinematics equations for a two-link planar manipulator (Spong et al., 2006). Shoulder and elbow angles were defined with respect to an axis parallel to the subject's torso. Note that in joint coordinates the movement trajectories are no longer straight lines, but rather have slight curvatures, as illustrated in Figure 4.1C. In addition, these trajectories are not equally-spaced. These features stem from the combination of (a) unequal lengths of the forearm and the upper arm and (b) nonlinearity in the inverse kinematics equations. In contrast, the movement trajectories in extrinsic coordinates (Fig. 4.1B) are equally-spaced straight lines, resulting in uniform 15° spacing between targets in extrinsic coordinates in Figure 4.1D. In intrinsic coordinates (Fig. 4.1C) the trajectories are slightly curved, resulting in non-uniform intrinsic coordinate spacing between consecutive targets. This result in the slight curvatures observed in W1 and W2 in Figure 4.1D.

Using this framework we can parameterize each movement for which we can test generalization by two parameters: how far away from the trained movement it is in both intrinsic (I) and extrinsic (E) coordinates. These two parameters can be used as cardinal axes in a 2D plot, defining a 2D I-E space for illustrating the similarity between any arbitrary movement and the trained movement in terms of their intrinsic and extrinsic representations, as shown in Figure 4.1D. Note that the trained target in the training workspace is located at the origin (0°,0°). Also note that all targets in the trained workspace are located near the main diagonal (gray circles), since the angular separation between two targets in both intrinsic (joint-space) and extrinsic (Cartesian) coordinates is very similar (see Fig. 4.1B and 4.1C).

The change in posture introduced in experiment 4.1 which resulted in a 45° change in the shoulder angle between the posture in W1 and the posture in W2 resulted in a -45° lateral shift in the locus of target locations (Fig. 4.1D, red circles). This shift is such that the target in the direction corresponding to the trained movement direction in extrinsic space (orange) is located at

position (0°,45°), while the target in the direction of the trained movement direction in intrinsic space (blue) is located at position (-45°,0°). The four models examined in this manuscript are all based on this I-E space.

4.3.5 Models of motor adaptation

4.3.5.1 Single reference frame models of adaptation: the fully extrinsic and fully intrinsic models

Single reference frame models of adaptation postulate that adaptation depends on only one coordinate system (intrinsic or extrinsic) and not on the other. More specifically, the extrinsic adaption model (Eq. 4.1) postulates that the amount of generalization (z) to a given target direction (θ) depends only on the distance between this target direction and the trained target direction in extrinsic coordinates and does not depend on the distance in intrinsic coordinates:

$$z(\theta_E,\theta_I) = z(\theta_E) = k \cdot e^{-\frac{D_E^2}{2\sigma^2}} \quad \text{(eq. 4.1)}$$

where $D_E = \left|\theta_E - \theta_{E_0}\right|$ and $\theta_{E_0} = 0°$ is the extrinsic representation of the trained direction since the origin of I-E space is set to the trained target location. In this model, the generalization of adaptation falls off in a Gaussian-like manner with extrinsic distance from a peak at the trained direction. This model has two free parameters: a magnitude (k) – the amount of adaptation in the trained target direction – and a width (σ). Note that the level of generalization is invariant to changes in the intrinsic representation of the target.

Similarly, the intrinsic adaptation model (Eq. 4.2) is defined analogously to the extrinsic model, except that the overall level of adaptation depends on the intrinsic representation of the target and is invariant to the extrinsic representation:

$$z(\theta_E,\theta_I) = z(\theta_I) = k \cdot e^{-\frac{D_I^2}{2\sigma^2}} \text{ (eq. 4.2)}$$

where: $D_I = \left|\theta_I - \theta_{I_0}\right|$ and $\theta_{I_0} = 0°$ is the intrinsic representation of the trained direction. This model is characterized by two parameters as well: the magnitude (k) and the width (σ) of generalization.

4.3.5.2 Independent adaptation model

The independent adaptation model (Eq. 4.3) postulates that there are two distinct components of adaptation – one extrinsic and one intrinsic:

$$z\left(\theta_E, \theta_I\right) = k_E \cdot e^{-\frac{D_E^2}{2\sigma_E^2}} + k_I \cdot e^{-\frac{D_I^2}{2\sigma_I^2}} \quad \text{(eq. 4.3)}$$

where $D_E = \left|\theta_E - \theta_{E_0}\right|$ and $D_I = \left|\theta_I - \theta_{I_0}\right|$. The two components independently contribute to the learned adaptation. Since the components correspond to the two single reference frame models described above, the independent adaptation model acts as a linear combination of them with two gain parameters (k_E and k_I) and two width parameters (σ_E and σ_I). Note that, since we put the trained target location at the origin, $\theta_{I_0} = \theta_{E_0} = 0$.

To evaluate this model along a diagonal slice of the I-E space, which corresponds to generalization within a single workspace as illustrated in Figure 4.1D, we can make the substitution $\theta_I = \theta_E - \alpha$, where α is the offset between any given workspace and the training workspace to yield:

$$z\left(\theta_E\right) = k_E \cdot e^{-\frac{\theta_E^2}{2\sigma_E^2}} + k_I \cdot e^{-\frac{\left(\theta_E - \alpha\right)^2}{2\sigma_I^2}} \quad \text{(eq. 4.4)}$$

Inspection of Equation 4.4 reveals that along any diagonal slice the generalization pattern predicted by the independent adaptation model is the sum of two Gaussians: one centered at the trained target direction (0°) – corresponding to the extrinsic component – and one centered at a

direction α away (α = -45° for experiment 4.1 and α = +90° for experiment 4.2) – corresponding to the intrinsic component, when generalization (z) is viewed in terms of the extrinsic movement direction (θ_E). In the primary analysis, we assume that the widths of the two components are the same $\left(\sigma_I = \sigma_E = \sigma\right)$ since the shape of the generalization function in the trained workspace is extremely well approximated (R^2 = 94-98%) by a single Gaussian and therefore is unlikely to result from the sum of two Gaussians with very different widths. Note that we used the data from the training workspaces in each experiment (W1 and W1*) to determine σ so that there were only two free parameters (k_E and k_I) when fitting the data from the novel workspaces (W2 and W2*) in the primary analysis.

4.3.5.3 Composite adaptation model

The composite adaptation model (Eq. 4.5) postulates that generalization depends on the combined distance across I-E space from the trained direction $(\theta_{E_0}, \theta_{I_0})$:

$$z\left(\theta_E, \theta_I\right) = k \cdot e^{-\frac{D^2}{2\sigma^2}}, \text{ where: } D = \sqrt{s_E \cdot (\theta_E - \theta_{E_0})^2 + s_I \cdot (\theta_I - \theta_{I_0})^2} \quad \text{(eq. 4.5)}$$

In this model, the generalization (z) is a bivariate Gaussian function that depends on the combined distance (D) across I-E space from the trained direction. Note that this dimension-weighted distance corresponds to the Mahalanobis distance across I-E space. This expression is mathematically equivalent to a generalization function that effectively combines the single reference frame models in a multiplicative gain-field:

$$z\left(\theta_E, \theta_I\right) = k \cdot e^{-\frac{s_E (\theta_E - \theta_{E0})^2 + s_I (\theta_I - \theta_{I0})^2}{2\sigma^2}} = k \cdot e^{-\frac{(\theta_E - \theta_{E0})^2}{2\sigma_E^2}} \cdot e^{-\frac{(\theta_I - \theta_{I0})^2}{2\sigma_I^2}} \quad \text{(eq. 4.6)}$$

where $\sigma_E = \sigma / \sqrt{s_E}$ and $\sigma_I = \sigma / \sqrt{s_I}$. Note that the coefficients, s_E and s_I, are included to allow for differential weighting of the extrinsic and intrinsic components of the distance.

Evaluating the composite adaptation model along a diagonal slice of the I-E space, as illustrated in Figure 4.1D, with an offset between the training and testing workspace of α, allows us to substitute $\theta_I = \theta_E - \alpha$ into Equation 4.6. If we combine this with the fact that we put the trained target location at the origin ($\theta_{I_0} = \theta_{E_0} = 0$) we obtain:

$$z(\theta_E) = A \cdot e^{-\frac{(\theta_E - \theta_0^*)^2}{2(\sigma^*)^2}} \quad \text{(eq. 4.7)}$$

where $\sigma^* = \frac{\sigma}{\sqrt{s_E + s_I}}$, $\theta_0^* = \frac{s_I \cdot \alpha}{s_E + s_I}$, and $A = k \cdot e^{-\frac{(s_E/s_I)\cdot(\theta_0^*)^2}{2(\sigma^*)}}$. Thus the composite adaptation model predicts a single Gaussian generalization function in any given workspace that can be characterized by 3 parameters: a gain *A*, a center θ_0^*, and a width σ^*. None of these parameters depends on θ_I or θ_E, effectively making them constants within any particular workspace. Also note that σ^* does not change from one workspace to another because it does not depend on α. This corresponds to the fact that any two parallel slices through a two-dimensional Gaussian are one-dimensional Gaussians with the same width. In contrast, *A* and θ_0^* (the height and center position) do change from one workspace to another. Just as with the independent model, we used the data from the training workspace in each experiment (W1 and W1*) to constrain the width of generalization (σ^*). Thus there were only two free parameters when fitting the data from the novel workspaces (W2 and W2*) for this model.

4.3.6 Data analysis

All of the generalization function data presented in this manuscript were collected during no-visual-feedback outward movements during the testing phase. Return movements (toward the center location) were not analyzed. For each movement we calculated its heading direction, defined as the direction of the vector connecting the start and end points of the movement. The start point was operationally defined as the location of the hand on the tablet when the speed of the movement first exceeded 5 cm/s, and the end point was the location of the hand 100 ms after the velocity dropped below 5 cm/s. Note that movements typically had peak velocities between 40 and 60 cm/s.

For each of the 19 directions in each of the two workspaces we estimated the average heading direction per subject separately for the baseline and the testing phase (by averaging the 6 no-visual-feedback trials towards each target). As expected, the individual subject's heading directions to all targets were close to the ideal heading directions during baseline movements (none of the average deviations exceeded 3°). We subtracted these small baseline biases from the learning curve and the post-adaptation generalization data to compute the learning-related changes. Note that, because the baseline movements were almost straight to the targets in most cases, very similar results would be obtained if baseline subtraction was not used. For each subject we estimated generalization functions in W1 and W2 (or W1* and W2* for the participants in experiment 4.2). Individual subject data were then averaged across subjects and both generalization functions were normalized in amplitude by the average deviation across subjects towards the trained target in W1 (or W1*). Note that, in order to estimate the confidence intervals in the parameters of the fits to the average generalization functions, we performed a bootstrap analysis with 1000 iterations allowing us to estimate the variability of the parameter values associated with the mean data. On each iteration, we selected N subjects (N=12 for

experiment 4.1 and N=20 for experiment 4.2) with replacement from the respective subject pool and computed the generalization function and corresponding fits based to this selection. The confidence intervals were then estimated from the distribution of these fit parameters.

As local generalization of learning can be well described by Gaussian tuning functions (Poggio and Bizzi, 2004; Fine and Thoroughman, 2006; Tanaka et al., 2009), our models use this form as a working approximation of the generalization function:

$$z(\theta) = k \cdot e^{-\frac{(\theta-\theta_0)^2}{2\sigma^2}} \quad \text{(eq. 4.8)}$$

Here the generalization of learning, $z(\theta)$, is centered around the movement direction eliciting maximal adaptation, θ_0, has an amplitude of $k=z(\theta_0)$, and is local with an effective width characterized by σ. This type of generalization function can only account for local adaptation; therefore, all models we present in this manuscript have one extra constant parameter (not shown) which accounts for the global (uniform) portion of motor adaptation. For the analyses in Figures 4.2F and 4.5C, we estimated the centers of the generalization functions individually for each subject before averaging across subjects. We fitted a Gaussian function (see Eq. 4.6) to each individual subject's generalization data (19 data points per subject) in order to estimate the center of the generalization function (θ_0). We fixed the width (σ) for these individual fits based on the group average data (30.7° in experiment 4.1 and 32.3° in experiment 4.2). One subject in each experiment had a generalization pattern in the novel workspace which yielded a non-significant fit characterized by $R^2<31.3\%$, $F(2,16)<3.63$, $p>0.05$, and the results from these fits were not included in our analysis of individual subject data because the parameters estimated from non-significant fits are not reliable.

In order to statistically compare the goodness-of-fit between models to the individual subject data we computed the Akaike information criterion corrected for finite sample size (AICc) for each model (Akaike, 1981; Anderson et al., 1998; Burnham and Anderson, 2004). For the individual subject analysis in experiment 4.2 this generated 20 ΔAICc comparisons between models, each corresponding to the difference in goodness-of-fit between the two models being compared for each subject. We then performed a two-tailed t-test to test whether the ΔAICc values were significantly different than zero. Note that, measures based on ΔAICc allow for comparison between models with either the same or different number of parameters as well as nested and non-nested models. Also note that when comparing two models with the same number of parameters, a t-test on the ΔAICc values amounts to a t-test based on the R^2 values of the individual model fits – in particular, a paired t-test on $\log\left(1-R^2\right)$.

When comparing the goodness-of-fit of two particular models to the averaged data, we used the Vuong closeness test (Vuong, 1989) in addition to the AICc. Just as AICc, the Vuong test can be used to compare two non-nested models, but unlike ΔAICc, the Vuong test provides a p-value. Thus, whereas ΔAICc estimates if one model is better than the other based on the goodness-of-fit, the number of parameters, and the degrees of freedom in the data, the Vuong test calculates the probability that the observed improvement occurs randomly.

4.4 RESULTS

4.4.1 Computational framework for action generalization: visualizing the intrinsic-extrinsic space

We began by examining the natural interrelationships between intrinsic and extrinsic coordinate systems for representations of motor learning in order to build a computational framework for understanding how these coordinate frames might contribute to motor learning. Several different types of motor adaptation including saccade adaptation (Noto et al., 1999), force field learning (Gandolfo et al., 1996; Thoroughman and Shadmehr, 2000; Mattar and Ostry, 2007), and visuomotor rotation learning (Pine et al., 1996; Ghez et al., 2000; Krakauer et al., 2000) generalize locally around the trained movement direction, meaning that movements in directions far from an adapted movement show little effect of the adaptation. This indicates that movement direction similarity effectively determines the degree to which the adaptation associated with one movement will be expressed in another (Wang and Sainburg, 2005). We thus focused on how an adaptation is associated with movement directions across the combined space of intrinsic and extrinsic coordinates. Critically, we note that a movement direction θ could be represented in either intrinsic or extrinsic coordinates: We define the extrinsic movement direction θ_E in terms of x-y coordinates, and the intrinsic movement direction θ_I , analogously, in terms of shoulder-elbow coordinates:

$$\begin{vmatrix} \theta_E = \arctan\left(\frac{\Delta y}{\Delta x}\right) \\ \theta_I = \arctan\left(\frac{shoulder\ angle\ excursion}{elbow\ angle\ excursion}\right) \end{vmatrix} \quad \text{(eq. 4.9)}$$

Inspection of Figure 4.1D reveals that although the relationship between θ_E and θ_I is not perfectly linear (due to differences in the lengths of limb segments), these two variables vary in a highly-correlated, nearly one-to-one manner within any single workspace – i.e. any particular starting

posture. Thus movements in different target directions in the same workspace can be viewed as constituting a single diagonal slice through intrinsic-extrinsic (I-E) space, as illustrated in Figure 4.1D (the gray and red lines show two different workspaces). Intrinsic and extrinsic representations are highly correlated within a workspace because the fashion in which untrained movement directions (θ) differ from the trained movement direction θ_0 is similar in intrinsic and extrinsic coordinates. For example, within workspace 1 (W1), movement directions slightly clockwise of the trained direction (black arrow) contain more *x* and less *y* excursion in extrinsic space (Fig. 4.1B gray traces), and more elbow and less shoulder excursion in intrinsic (joint) space (Fig. 4.1C gray traces). However, the high correlation between θ_E and θ_I within the training workspace observed in Figure 4.1D indicates that within W1 there is essentially no ability to distinguish whether the observed pattern of generalization is based on intrinsic versus extrinsic representations. This is the case because extrinsic generalization around the training location (Figure 4.2A) would have essentially the same projection onto the training workspace (W1) as intrinsic generalization around the training location (Figure 4.2B).

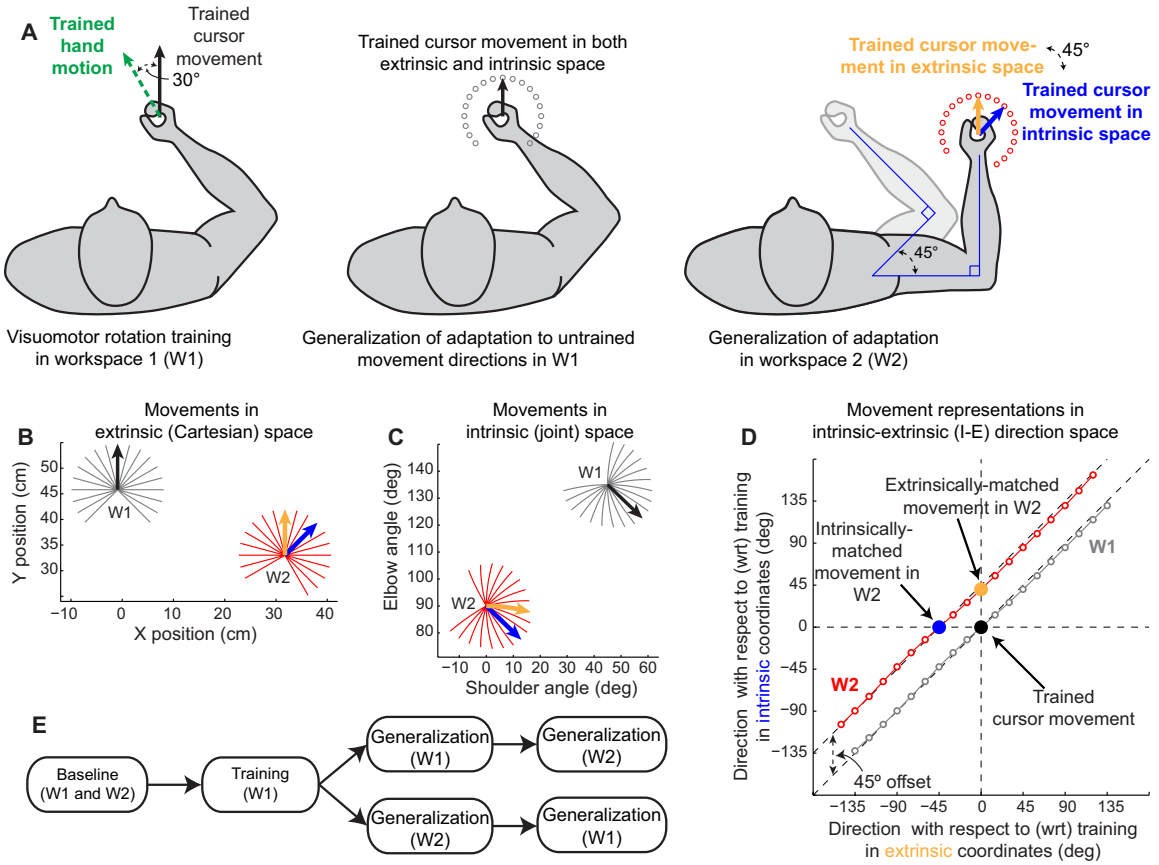

Figure 4.1: Experiment 4.1 diagram and theoretical framework. (**A)** Task illustration. Left panel: Subjects adapt to a 30° visuomotor rotation (VMR) while reaching to a single target positioned in the 90° direction (trained direction), 9 cm away from the starting point. To move the cursor straight to the trained target (Trained cursor movement, solid black line) subjects need to perform a movement in the 120° direction (Trained hand motion, dashed green line). Middle panel: After learning the rotation, subjects performed reaching arm movements to an array of 19 probe targets (hollow gray circles), spaced 15° apart, spanning a range of -135° to +135° with respect to the trained direction in workspace 1 (W1). Note that in W1 the target at the 90° direction is the trained target and therefore it corresponds to the trained target represented in both intrinsic and extrinsic space. Right panel: After learning the rotation, subjects also performed reaching arm movements to an array of probe targets (red circles) in workspace 2 (W2), also spaced 15° apart. In W2 the trained target's extrinsic representation is the target at 90° (yellow arrow), while the intrinsic representation of the trained target lies in the 45° direction (blue arrow). **(B)** & **(C)** Ideal cursor movements to all targets in both workspaces. In (B) movements are shown in extrinsic (Cartesian) coordinates and in (C) they are shown in intrinsic (joint) coordinates. In W1 (gray), the black arrow shows the trained cursor movement. In W2 (red), the yellow arrow shows the trained cursor movement in extrinsic space, whereas the blue arrow shows the trained cursor movement in joint space. Note that the black and yellow arrows are parallel in (B), indicating that in Cartesian coordinates these two movements require the same position changes, whereas the black and blue arrows are parallel in (C), showing that in joint coordinates those two movements require the same joint excursions. **(D)** Target representations in

Figure 4.1 (Continued)

I-E direction space. The x-value for each movement is calculated as the distance between that movement and the trained movement in extrinsic coordinates. Similarly, the y-value for each movement is calculated as the distance between that movement and the trained one in intrinsic coordinates. The intrinsic and extrinsic displacements from one target to the next are highly correlated within any particular workspace, yielding the nearly linear patterns for W1 and W2 shown in this panel (gray and red traces). **(E)** Experimental protocol. The order of testing in W1 and W2 is randomized such that half the subjects were tested in W1 first (top path) and half were tested in W2 first (bottom path).

Examining generalization in another workspace (workspace 2 – W2) with a different starting arm posture following training in W1 allows for the dissociation between intrinsic and extrinsic representations for motor learning. Comparison of Figure 4.1B and 1C shows that the movement in W2 that matches the direction of the training movement in extrinsic space (orange vector) is distinct from the movement in W2 which matches the direction of the training movement in intrinsic space (blue vector). Correspondingly, the orange (but not the blue) direction matches the black direction in 4.1B, whereas the blue (but not the orange) direction matches the black direction in 4.1C. Note that the intrinsic and extrinsic representations of these movement vectors can be simultaneously visualized in the I-E direction space shown in Figure 4.1D. Here intrinsically-matched movements (black & blue circles) correspond to points with the same vertical position, whereas extrinsically-matched movements (black & orange circles) correspond to points with the same horizontal position. In summary, W2 provides an additional diagonal slice through I-E space (red line in Figure 4.1D) in which movements that are extrinsically- versus intrinsically-matched to the training location are distinct.

This conception of I-E space provides a unified way of looking at a number of previous studies examining the coordinate system for motor memory formation. These studies have, in general, sampled a subset of the I-E space following adaptation to physical dynamics (Shadmehr and Mussa-Ivaldi, 1994; Shadmehr and Moussavi, 2000; Malfait et al., 2002) and visuomotor transformations (Ghez et al., 2000; Krakauer et al., 2000; Baraduc and Wolpert, 2002; Ahmed et al., 2008), and can be classified into two groups. In one group of studies (Ghez et al., 2000; Krakauer et al., 2000; Baraduc and Wolpert, 2002; Ahmed et al., 2008) a single action (i.e. a single point in I-E space) was trained before the generalization of the trained action was probed in a second workspace at one or two untrained locations. This amounts to a sparse sampling of the I-E space. For example, in the context of our framework, Krakauer et al. 2000 trained VMR at the

center of the workspace (Fig 1D, black circle) and tested the transfer to a single extrinsically-matched movement: a point with the same extrinsic coordinate as the trained movement, but 45° away in intrinsic space - Fig 1D, orange circle at (0°, 45°). Similarly, Malfait et al. 2002 trained a force field at the center and tested the generalization of adaptation to two points: the same joint coordinate, but 90° away in extrinsic coordinates (0°, 90°) and the same extrinsic coordinate, but 90° away in joint coordinates (90°, 0°).

In a second group of studies (Shadmehr and Mussa-Ivaldi, 1994; Shadmehr and Moussavi, 2000), adaptation was trained in multiple movement directions in one workspace before generalization was tested in the same movement directions in a second workspace. Although these studies provide denser sampling of generalization in I-E space, the fact that training occurs at multiple points in this space makes it difficult to unravel the relationship between the observed generalization data and the nature of the internal representation that gives rise to it, as has been previously pointed out (Malfait et al., 2002). In fact, some force-fields will yield identical generalization data in this paradigm, regardless of whether the internal representation of dynamics is fully intrinsic or fully extrinsic (Shadmehr and Moussavi, 2000).

4.4.2 Pure intrinsic and pure extrinsic generalization patterns in intrinsic-extrinsic space

Figure 4.2A illustrates the pattern of generalization that would arise from the extrinsic representation of visuomotor rotation learning. The generalization pattern predicted by the extrinsic representation model (Equation 4.1) is plotted as a colormap over the space of intrinsic and extrinsic coordinates for representing target direction. This generalization pattern has a maximum value at the trained target location (white dot) and gradually decreases away from it along the extrinsic coordinate axis (the x-axis). Note that in this model, generalization is invariant along the intrinsic coordinate axis (the y-axis) because the intrinsic direction is irrelevant for a

purely extrinsic model. This invariance results in a vertical stripe appearance in the colormap. In this illustration, the training workspace (W1, white solid line) is located along the main diagonal since for every target direction in that workspace the distance away from the trained direction in both intrinsic and extrinsic coordinates is approximately matched (as emphasized in Figure 4.1D). In contrast, W2 (white dashed line) is located along a diagonal above and parallel to W1. This corresponds to the locus of points in I-E space for which there is a -45° offset between intrinsic and extrinsic target directions. Note that the width of the extrinsic model was chosen to match the width of the local generalization observed in W1 which is depicted in Figure 4.2C.

According to the extrinsic representation model, maximal generalization in W2 would be at the coordinate (0°, 45°) in Figure 4.2A (orange dot in Fig. 4.1D) which corresponds to the same extrinsic direction as the trained target but a 45° difference in intrinsic direction compared to the trained target. This makes sense because if adaptation was represented in purely extrinsic manner, the intrinsic target direction would have no bearing on the amount of generalization.

Figure 4.2B illustrates the pattern of generalization that would arise from an intrinsic representation of visuomotor rotation learning, as described in Equation 4.2. This illustration is similar to Figure 4.2A except that the colormap has a horizontal, rather than vertical, stripe appearance reflecting a dependence on intrinsic rather than extrinsic coordinates. Here, the maximal generalization in W2 is at the coordinate (-45°, 0°) which corresponds to the same intrinsic direction as the trained target but a -45° difference in extrinsic direction compared to the trained target. Again, this makes sense because if adaptation was represented in purely intrinsic manner, the extrinsic target direction would have no bearing on the amount of generalization.

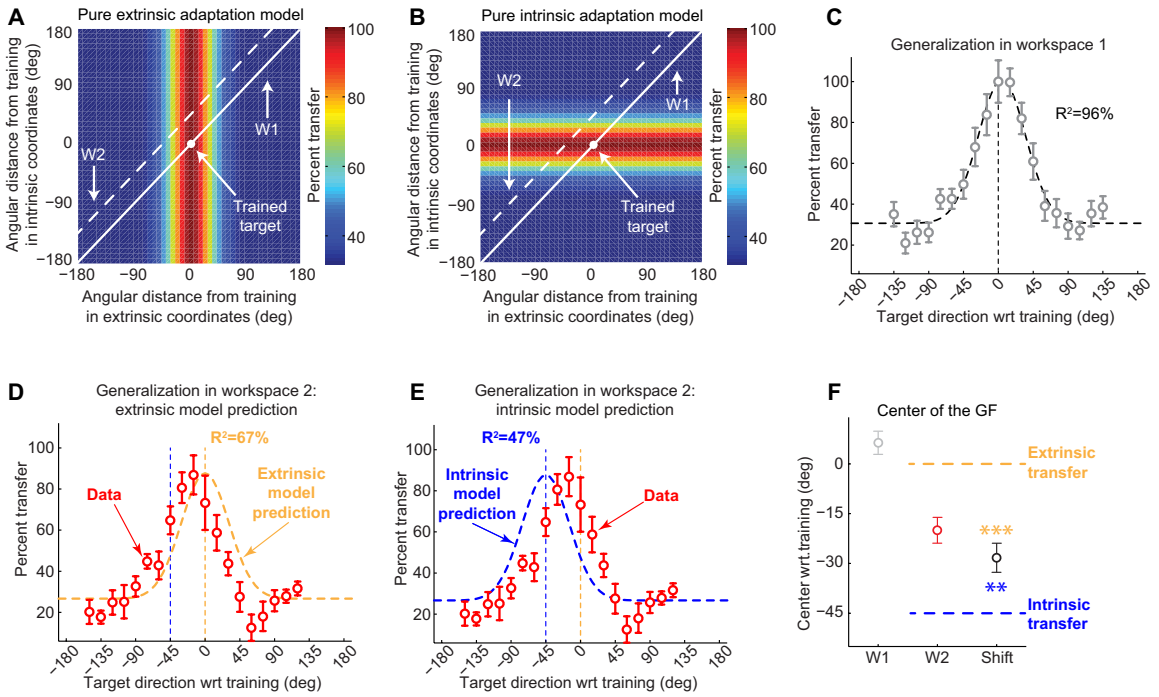

Figure 4.2: Single reference frame models. (**A) & (B)** Pure extrinsic and pure intrinsic adaptation models. The framework used here is the same as the one used in Figure 4.1D. The trained target is represented as a white dot at the origin (0°, 0°), and the corresponding motor adaptation is scaled to 100% (dark red). W1 and W2 are represented as solid and dashed lines, respectively, and their locations are consistent with Figure 4.1D. In the extrinsic model, generalization falls off along the extrinsic (x) axis but remains invariant along the intrinsic (y) axis. The intrinsic model (B) makes orthogonal predictions: the generalization is invariant along the extrinsic axis but variable along the intrinsic axis. **(C) - (E)**. Generalization data from W1 and W2. The data from W1 (panel C) is well-approximated by a Gaussian centered at 4.7° with a width (σ) of 30.7° (R^2=96.3%). The data from W2 is poorly approximated by the extrinsic model prediction (panel D, R^2=67.2%) or the intrinsic model prediction (panel E, R^2=47.4%). **(F)** Generalization function centers. In this plot all values are calculated by fitting Gaussians to individual subject data and averaging the center locations across subjects. In W1 the center is at 6.4°, not significantly different than zero ($p>0.1$), while the center in W2 is at -19.8°. The shift of the generalization function from W1 to W2 is -28.2° on average, significantly different from -45° and 0°. (**, $p<0.01$; ***, $p<0.001$)

4.4.3 Measuring generalization across an array of arm postures and movement directions

To understand the internal model that the motor system builds during visuomotor transformation learning, we studied how a motor adaptation learned in one arm configuration generalizes to different arm configurations. As discussed above, a number of previous studies have taken this basic approach. However in the current study we train adaptation in a single movement direction in one workspace and measure the generalization of this learning across a range of untrained conditions in both the initial and novel workspaces rather than one or two untrained conditions. This allows us to visualize the pattern of generalization across I-E space.

We recruited 12 subjects for the first experiment diagramed in Figure 4.1E. After a baseline period with no rotation in which subjects made twenty-four 9 cm movements each to 19 target locations in two different workspaces, subjects were trained for 120 trials with a 30° visuomotor rotation (VMR) from a fixed starting point to a single target location in W1 (Fig. 4.1A, left). Following this training period, we tested the generalization of VMR adaptation by probing all 19 target directions in both workspaces in an interleaved fashion with half the subjects tested first in W1 (Fig. 4.1A, middle) and the other half tested first in W2 (Fig. 4.1A, right). The interleaved generalization testing was designed to prevent any decay from the first to second testing blocks from systematically affecting the comparison between workspaces. However, examination of the generalization data revealed that there was no significant effect of whether generalization was tested on the first or second block – mean generalization across all 19 directions of 9.5±0.65° (SEM) vs. 9.6±0.9° for W1 when tested first vs. second ($p>0.5$, unpaired t-test), and 8.4±0.5° vs. 7.0±0.8° for W2 when tested first vs. second ($p>0.1$, unpaired t-test). Importantly, visual feedback of the cursor motion was withheld on all trials in these post-adaptation testing blocks to prevent re-learning during the testing period.

We found that by the end of the training block, subjects had learned 27.3±2.7° (mean ± SD) of the 30° VMR – a 91% compensation of the imposed rotation when moving in the trained direction. In fact, during the first 10 training trials subjects rapidly adapted to 24.5° (82% compensation) and during the following 110 trials their adaptation gradually increased. In the training workspace, we found local generalization around the trained target direction as shown in Figure 4.2C. A single Gaussian centered at the target direction with a width (σ) of 31.2° closely matched the shape of the subject-averaged generalization pattern we observed in W1 (R^2=94.6%). If we allow the center of this Gaussian to vary, the fit is only marginally improved (R^2=96.3%), with σ = 30.7° and a center at 4.7°. The 4.7° ± 3.5° center (mean ± SEM, based on bootstrap analysis of these data) is not significantly different than 0° - the trained direction ($p>0.1$). These findings indicate local generalization of adaptation around the trained target direction in W1, which is well characterized by a simple Gaussian fit with a width of about 31° and is in line with previous results (Pine et al., 1996; Ghez et al., 2000; Krakauer et al., 2000).

4.4.4 Single reference frame models cannot account for the internal representation of motor memory

We also found local generalization in W2. However, this generalization pattern did not resemble what would be predicted by projecting the generalization patterns associated with purely extrinsic (Fig. 4.2A) or intrinsic (Fig. 4.2B) representations of motor memory onto W2 in I-E space, as shown Figures 4.2D and 4.2E. Figure 4.2D shows a comparison between the generalization pattern in W2 predicted by the extrinsic adaptation model and the one that we observed experimentally. The extrinsic prediction (yellow dashed line) does not match the data (red) terribly well (R^2=67.2%) because the observed pattern of generalization appears to be shifted away from the trained target direction. Analogously, Figure 4.2E shows a comparison between the generalization pattern in W2 predicted by the intrinsic adaptation model and the one that we observed experimentally. Like the extrinsic prediction, the intrinsic model prediction (blue

dashed line) does not match the data (red) well (R^2=47.4%). Inspection of Figure 4.2E reveals that this mismatch occurs because the observed pattern of generalization is not fully shifted towards the intrinsic representation of the trained target direction which is centered at -45° from the trained target direction. Note that the x-axis of panels C, D and E in Figure 4.2 represent extrinsic target direction (as do the x-axes of all panels of Figures 4.3 and 4.5 on which we present generalization data). The poor correspondence between the generalization data in W2 and the predictions of either the extrinsic adaptation or intrinsic adaptation models suggests that adaptation we elicited is neither purely extrinsic nor purely intrinsic in nature.

Comparison of the generalization data in W1 and W2 (Fig. 4.2C vs. 4.2D) reveals that the W2 generalization function is similar in shape to that observed in W1 but shifted to the left. The model comparisons above reveal that the shift is large enough to create a mismatch between the data and the no-shift prediction of the extrinsic representation model. However, although in the appropriate direction, this shift is not sufficiently large to create a good match between the data and the -45° shift prediction of the intrinsic representation model. Figure 4.2F shows an analysis of the amount of shift we observed. We estimated the center of generalization in each workspace by fitting a Gaussian function with three free parameters (center location, amplitude, and vertical offset) to each individual subject's generalization data and then averaging across subjects. As expected, the center locations in W1 were near zero (6.4° ± 4.4° SEM). However, the generalization functions in W2 were centered at -19.8° ± 4.8° , corresponding to a -28.2° ± 5.6° shift. Note that our estimate of the mean shift is slightly different than the shift between the mean center locations because the fit to 1 of the 12 subjects in W2 was not significant (R^2=29.9%, $F(2,16)=3.41$, $p>0.05$) and this data was thus excluded from the estimate of the W2 center location and the mean shift (but not the W1 center location). Interestingly, the mean shift is about half-way between the -45° shift predicted by the intrinsic representation model and the zero-shift

predicted by the extrinsic representation model, and is significantly different from both model predictions ($p<0.01$ and $p<0.001$, respectively). This suggests that visuomotor rotation learning may be represented in a way that depends about equally on both intrinsic and extrinsic coordinates, rather than on either one alone.

4.4.5 Multi-reference frame models can account for the generalization data from experiment 4.1

The partial generalization function shift observed in experiment 4.1 suggests that the VMR adaptation is generalized in a way that depends on both intrinsic and extrinsic coordinates, rather than on extrinsic coordinates alone as previously suggested (Ghez et al., 2000; Krakauer et al., 2000). We examined two distinct ways in which intrinsic and extrinsic representations might be combined during visuomotor rotation learning. One possibility, defined in Equation 4.3 and diagramed as the "independent intrinsic and extrinsic adaptation model" in Figure 4.3A, is that adaptation occurs in parallel in both coordinate frames (Hikosaka et al., 2002; Cohen et al., 2005; Berniker and Kording, 2008; Berniker and Kording, 2011). Here, intrinsic and extrinsic representations of the task independently lead to motor adaptation in each of their respective coordinate systems and both types of adaptation would contribute in an additive manner to the overall adaptation. This independent adaptation scheme would predict some amount of intrinsic generalization and some amount of extrinsic generalization corresponding to the "plus sign" appearance of the generalization colormap illustrated in Figure 4.3B. Note that this plus sign shape corresponds to the locus of points that are near the trained target location in *either* extrinsic *or* intrinsic coordinates.

We found that the independent adaptation model (Equation 4.4) is able to fit the generalization data from W2 remarkably well (R^2=91.2%) with only 3 free parameters – the amplitudes of the intrinsic and extrinsic contributions (k_I and k_E) and a vertical offset. Note that the widths of the

Gaussian functions for each independent contribution were predetermined based on the generalization data from W1 (σ_E=σ_I=30.7°) and the center locations were set to 0° and -45° for the extrinsic and intrinsic contributions, respectively, according to Equation 4.4.

We next compared the independent adaptation model to the "composite intrinsic-extrinsic adaptation model", defined in Equation 4.5 and diagramed in Figure 4.3D, in which extrinsic and intrinsic representations of the task combined into a single composite representation. Here, the generalization is a multi-dimensional Gaussian function that is simultaneously local with respect to both intrinsic and extrinsic coordinates, resulting in a hump-shaped generalization pattern (see Methods). We refer to this model as high-dimensional because its generalization depends on a two-dimensional distance across I-E space, as shown in Equation 4.5.

Figure 4.3E illustrates this model for equal values of s_E and s_I, parameters which specify the widths of the extrinsic and intrinsic generalization, respectively (see Methods). This results in circular isogeneralization contours in the I-E direction space. Unequal values of s_E and s_I would result in elliptical contours for the local hump-shaped generalization pattern. This high-dimensional combined-distance model corresponds to a multi-dimensional Gaussian which is *mathematically equivalent* to a representation in which extrinsic and intrinsic generalization patterns are multiplicatively combined (see Equation 4.6). The multiplicative combination dictated by this model is a *gain-field* combination of intrinsic and extrinsic coordinate representations ("gain" referring to multiplication and "field" to the space over which each representation is defined). This is similar to the encoding observed in parietal cortex in the combined coding of eye position and retinal location (Andersen and Mountcastle, 1983; Andersen et al., 1985; Buneo and Andersen, 2006), where neurons' receptive fields are multiplied together to produce a planar gain field.

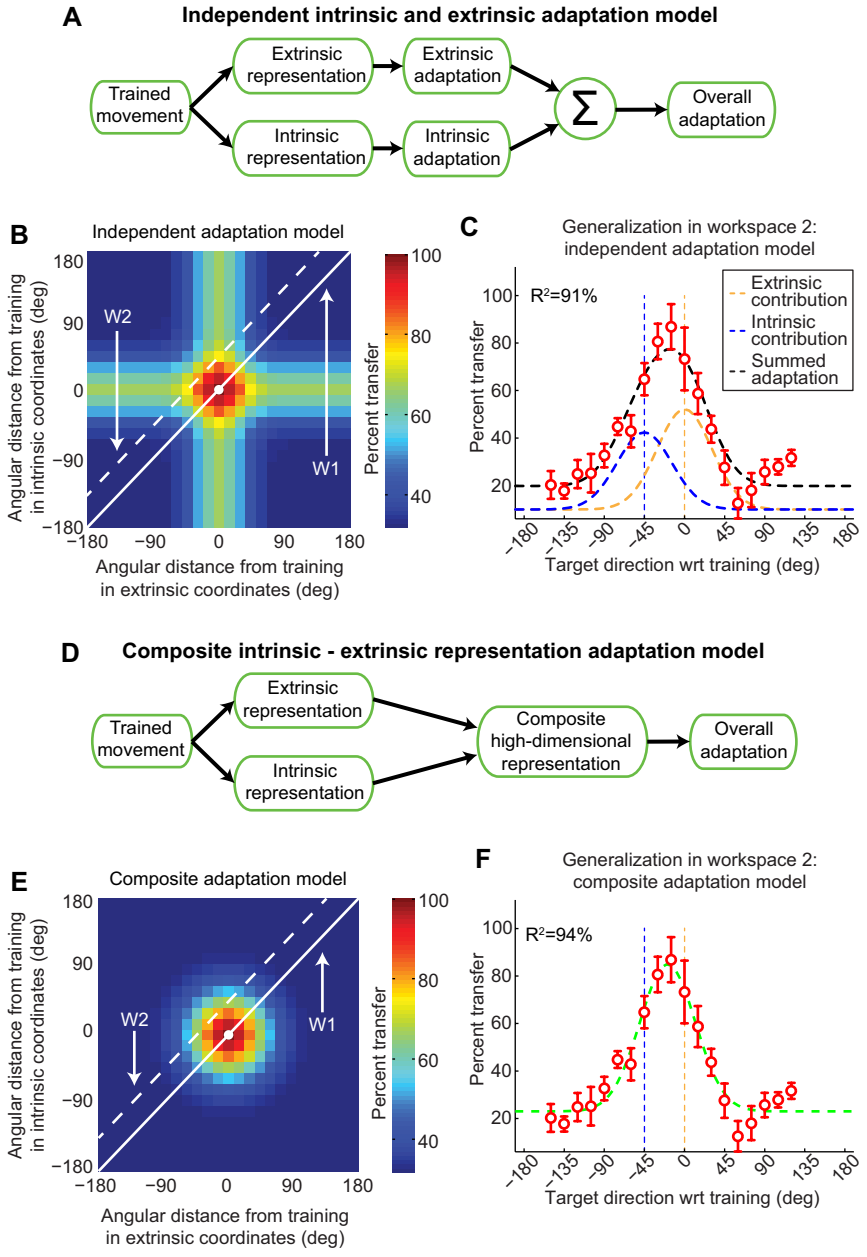

Figure 4.3: Comparison of two models for motor memory that combine intrinsic and extrinsic representations. **(A)** Diagram of the independent adaptation model. Two representations of the trained movement (intrinsic and extrinsic) adapt independently of each other and the overall adaptation is simply the sum of the two. **(B)** Predictions from the independent adaptation model in the same format as Figures 4.2A & 4.2B. As depicted by the "plus sign" generalization pattern, the trained adaptation retains a non-zero value along both the intrinsic and extrinsic axes. This is a result of the summation of the intrinsic and extrinsic generalization patterns shown in Figures 4.2A & 4.2B. **(C)** According to the independent adaptation model the generalization pattern in W2 (black) should be equal to a weighted sum of

Figure 4.3 (Continued)

intrinsic (blue) and extrinsic (orange) components each with a width identical to that observed in W1. This model explains 91.2% of the variance in the W2 data. (**D)** Diagram of the composite gain-field I-E adaptation model. (**E)** Predictions from the composite adaptation model in the same format as panel B. The generalization pattern has an "island" shape, indicative of a decrease in adaptation away from the trained movement. This arises from a bivariate Gaussian function centered at the origin. (**F)** According to the composite model the total adaptation (green) should be a single Gaussian with a width equal to that observed in W1 but shifted and scaled. This model explains 94.3% of the variance in the W2 data.

Our model, however, does not represent a *planar* gain field because both the extrinsic and intrinsic generalization functions are nonlinear. The prevalence of gain-field encoding in neural representations that combine different sources of spatial information would be compatible with the idea that motor memories that depend on multiple spatial contexts are encoded in the same way.

We found that the composite adaptation model (Eq. 4.7) is, like the independent adaptation model, able to fit the subject-averaged generalization data from W2 remarkably well (R^2=94.3% vs 91.2%) with just 3 free parameters – the amplitude (A) and center (θ_0^*) of the local adaptation and a vertical offset. As with the independent adaptation model, the width of the Gaussian function for the diagonal slice corresponding to W2 (σ=30.7°) was predetermined based on the generalization data from W1.

Since both multi-reference frame models can explain the generalization pattern we observed in W2 well, we cannot distinguish between them using the experiment 4.1 data set. In fact, a paired t-test on the R^2 values from individual subject's data fits to both models yields $p>0.6$. Note, however, that both multi-reference frame models fit the W2 data significantly better than either of the single reference frame models ($p<0.001$ in all cases). Thus we cannot determine whether the CNS adapts motor output based on an independent or a composite representation based on the data from experiment 4.1 alone. However, a closer look at the generalization colormaps in Figures 4.3B and 4.3E reveals that while the predictions from both models are similar for workspaces near the main diagonal, moving farther away would yield radically different predictions. The independent adaptation model predicts a unimodal generalization function when the peaks of the extrinsic and intrinsic representations are separated by less than $\sqrt{2}\sigma$. However, in a workspace in which the distance between the intrinsic and extrinsic representations is increased, the independent adaptation model would predict a bimodally-shaped generalization

function. In contrast, the composite adaptation model predicts that the shape of the generalization function would remain unimodal and maintain the same width regardless of the distance between the intrinsic and extrinsic reference frames. Thus an experiment in which the two workspaces are separated by substantially more than $\sqrt{2}\sigma$ should allow us to distinguish between the independent adaptation and joint adaptation models.

4.4.6 Generalization data from experiment 4.2 reveals a motor memory representation that is a gain-field combination of intrinsic and extrinsic coordinates

Since the data from experiment 4.1 can be explained by both the independent adaptation and the composite adaptation models, we conducted a second experiment in order to distinguish between them. In this second experiment, we also trained adaptation in one workspace and compared the pattern of generalization observed there with the pattern observed in a second workspace. However, we designed the experiment with a greater distance between the two workspaces. As illustrated in the left and center panels of Figure 4.4, the training workspace (workspace 1*, W1*) was positioned to the right of body midline, corresponding to shoulder extension, whereas the testing workspace (workspace 2*, W2*, Figure 4.4, right panel) was left of W1*, corresponding to 90° of shoulder flexion with respect to W1*. Aside from the workspace locations and the locations of the testing targets in W2*, the protocol for experiment 4.2 was identical to that for experiment 4.1.

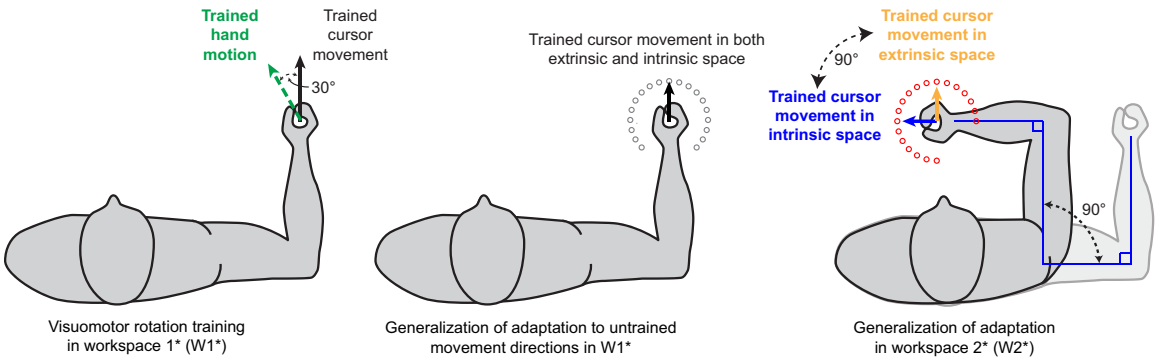

Figure 4.4: Experiment 4.2 diagram. Subjects adapted to a 30° rotation (left panel) before generalization was tested in 19 different movement directions in two distinct workspaces (center and right panels) as in experiment 4.1. Note that here the trained workspace (W1*) is the same as the novel workspace (W2) in experiment 4.1, and the novel workspace in experiment 4.2 (W2*) is separated from W1* by +90°, compared to the -45° separation in experiment 4.1.

Similarly to experiment 4.1, subjects learned the trained adaptation very well, displaying 28.3° ±0.7° (mean ± SEM) of rotation at asymptote during the training block (94% adaptation). The generalization function we observed in W1* (Fig. 4.5A) was very similar to what we found in the training workspace in experiment 4.1 (Fig. 4.2C), despite the difference in arm configurations (central in experiment 4.1 versus right in experiment 4.2 with respect to the center of the body). We found local generalization in W1* with a width (σ) of 32.3° and a center location of -0.3° ±2.7° relative to the direction of the trained target based on fitting Gaussian functions to the individual subject data. The mean data were fit extremely well by a single Gaussian function and a vertical offset (R^2=98.0%).

The 90° rotation of arm configurations in experiment 4.2 creates a +90° separation between the representation of the trained target in extrinsic and intrinsic coordinates in W2* as illustrated in right panel of Figure 4.4. The center of generalization shifted from W1* to W2* by 61.2° ± 4.2° (mean ± SEM). This corresponds to a 68% shift towards a pure intrinsic representation, similar to the 63% shift observed in experiment 4.1. As in experiment 4.1, this shift is intermediate between the pure extrinsic (0° or 0%) and pure intrinsic (90° or 100%) model predictions, but significantly

different from both ($p<0.001$ in both cases as shown in Figure 4.4F). Furthermore, 14 subjects (74%) of the 19 for whom we were able to estimate the centers in both workspaces displayed generalization pattern shifts which were within 15° of the mean shift (61.2°). In contrast, only 1 subject (5%) displayed a shift within 15° of 0° (the extrinsically-matched movement direction) and only 3 subjects (16%) were within 15° of 90° (the intrinsically-matched movement direction). Thus, the shifts we observe from individual subjects (Fig 5C) are consistent with the idea that individual subjects within the population display intermediate intrinsic-extrinsic representations in line with the gain-field model. These shifts are not consistent with the idea that the intermediate representation we observe for the group averaged W2* data might arise from two separate populations of subjects, one displaying extrinsic representations and one displaying intrinsic representations.

Based on the value of σ estimated from the W1* data, the large 90° workspace separation we employed in experiment 4.2 is 1.97 times greater than $\sqrt{2}\sigma$, which should be large enough to disambiguate between the independent and composite models. Correspondingly, the independent adaptation model predicts a bimodal generalization function in W2* with distinct peaks centered near 0° (the trained target direction in extrinsic coordinates) and +90° (the trained target direction in intrinsic coordinates), as illustrated in Figure 4.5D and 4.5E. In contrast, the composite adaptation model predicts a unimodal generalization function centered somewhere between 0° and +90°, as illustrated in Figure 4.5F and 4.5G.

The subject-averaged generalization data from W2* is shown in Figure 4.5B. Here the shape of the generalization function is unimodal with a peak about +60° away from the training direction. These data cannot be well explained by the independent adaptation model predicting bimodal generalization, as shown in Figure 4.5E (R^2=68.3%). However, the generalization data from W2* can be explained by the composite adaptation model remarkably well as shown in Figure 4.5G

(R^2=94.7%). This indicates that the mean squared error for the gain-field model (5.3% of the variance) is approximately 6-fold smaller than for the independent adaptation model (31.7% of the variance). Since the two models have the same number of parameters, we compared them using Vuong's closeness test (Vuong, 1989) which reveals that the gain-field model explains the subject-averaged data significantly better than the independent model ($p<0.001$). Relatedly, the R^2 value here for the independent adaptation model is substantially smaller than what we found for the same model in experiment 4.1 (91.2% vs. 68.3%, note this decrement in the R^2 value corresponds to a 3-fold increment in the mean squared error of the fit). In contrast, the R^2 value for the gain-field model is remarkably similar to what we found in Experiment 4.1 (94.3% vs. 94.7%). Moreover, fitting the independent and the gain-field adaptation models to individual subject generalization function data yielded a better fit for the gain-field model for 16 out of the 20 subjects ($p<0.001$, paired t-test on the AIC_C values for the model fits across subjects).

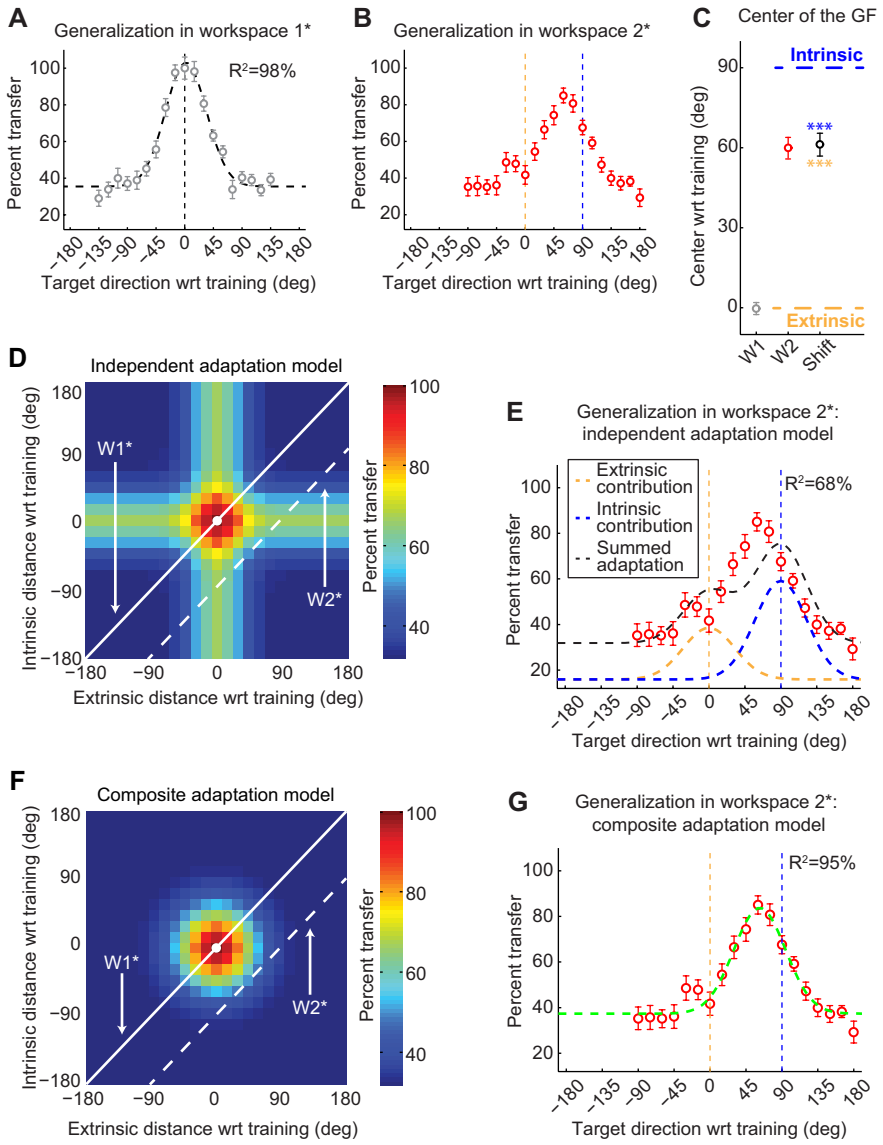

Figure 4.5: Results from the second experiment. (A) & (B) Raw generalization data from experiment 4.2 in the same format as Figures 4.2 C-E. The generalization data in W1* is well approximated (R^2=98.0%) by a Gaussian function centered at 2° with a width (σ) of 32.3°, similar to the W1 data from experiment 4.1. **(C)** Generalization function centers in the same format as Figure 4.2E. In W1* the center is at -0.3°, not significantly different than zero (p>0.2), whereas in W2* the center is at 59.9°. The shift of the generalization function from W1* to W2* is 61.2° on average. **(D) & (E)** Predictions from the independent adaptation model. Since the separation between W1* and W2* is greater that between W1 and W2, the model predicts a bimodal generalization function with two distinct peaks at 0° and 90° (white dashed line in panel D). The sum of intrinsic (blue) and extrinsic (yellow) components (black dashed line in panel E) is unable to capture the shape of the observed generalization pattern (R^2=68.3%). Note the substantial contrast between the model fits to the data here and in the first experiment (Fig. 4.3C), despite an equal number (two) of free parameters. **(F) & (G)**. Predictions from the composite gain-field

Figure 4.5 (Continued)

adaptation model. Regardless of the separation between W1* and W2*, the model predicts a unimodal generalization function (white dashed line in panel F). The prediction (green dashed line in panel G) from the composite model explains 94.7% of the variance in the data, very similar to this model's prediction for the W2 data in experiment 4.1 (94.3% as shown in Figure 4.3F) with the same number of parameters (two) as before. (***, $p<0.001$)

It is important to note that for both the subject-averaged and individual subject model analyses discussed above, we constrained the widths of the Gaussians to be equal to the best-fit σ from the W1* fits. However, if we ignore the W1* data in fitting the W2* with the independent adaptation model, allowing σ_I and σ_E to vary independently of the W1* σ and each other, effectively adding 2 additional parameters to the independent adaptation model, the ability of this model to explain the W2 data improves, but only to R^2=81.6%. If we compare this expanded independent model (with 5 parameters and R^2=81.7%) to the gain-field one (with 3 parameters and R^2=94.7%) we get $\Delta AIC_C < 0$, an indication that the gain-field model is still superior. Furthermore, comparing the two model fits using the Vuong test for non-nested models (Vuong, 1989) demonstrates that the gain-field model is significantly better ($p<10^{-6}$) than the independent model with σ_I and σ_E free. This result makes sense intuitively, as the mean-squared-error for the gain-field model with 3 parameters (5.3% of the variance) is almost 3.5 times smaller than the mean-squared-error for the expanded independent model with 5 parameters (18.3% of the variance). Note that while there appears to be a small "bump" at -30° and -15°, this feature is not predicted by either model and the difference between these data points and the tail of the generalization (the average of the data from -90° to -45°) is not statistically significant for either one of the points or for the average of the two (paired t-test, $p>0.05$ in all cases), indicating that it is most likely due to noise. These findings demonstrate that the CNS effectively maintains a representation of motor memory that is based on a gain-field combination of local intrinsic and extrinsic representations. This gain-field combination produces a hump-shaped generalization pattern across the two-dimensional I-E space that results in shifted generalization functions in different workspaces, as illustrated in Figure 4.5F and 4.5G.

4.5 DISCUSSION

We studied the internal representation of visuomotor rotation learning in an attempt to better understand the coordinate system used by the CNS for the planning of visually guided movement. We dissociated intrinsic and extrinsic movement representations by comparing the directional generalization of a learned motor adaptation over an array of 19 movement directions and 3 workspaces – amounting to 56 workspace locations in addition to the training workspace. This allowed us new insight into how intrinsic and extrinsic reference frames contribute to the internal representation for motor memory. The first experiment, in which the workspaces were separated by 45°, provided generalization function data which clearly showed that the trained adaptation did not transfer in either purely intrinsic or purely extrinsic coordinates as illustrated in Figure 4.2. Instead, the data were intermediate between intrinsic and extrinsic generalization patterns, suggesting a hybrid internal representation. However, based on these data we could not distinguish between (1) a hybrid representation composed of separate local intrinsic and extrinsic adaptive components which could learn and transfer independently as has been assumed by several models of multi-reference frame learning (Hikosaka et al., 2002; Cohen et al., 2005; Berniker and Kording, 2008; Berniker and Kording, 2011) and (2) a hybrid representation based on multiplicative gain-field combination of local intrinsic and extrinsic coordinate representations which would transfer depending on the combined distance across intrinsic-extrinsic space as illustrated in Figures 4.3 and 4.5. The generalization data from the second experiment, in which the workspace separation was increased to 90°, provided convincing evidence for a composite adaptation model based on multiplicative gain-field combination of local intrinsic and extrinsic representations, ruling out separate intrinsic and extrinsic representations for motor adaptation. While gain field coding has been extensively studied in the context of neural representations (Andersen et al., 1985; Snyder et al., 1998b; Pouget and Snyder, 2000; Andersen et al., 2004;

Buneo and Andersen, 2006; Pesaran et al., 2006; Chang et al., 2009), it has generally been associated with an intermediate step in the transformation between different coordinate frames for sensorimotor integration (Andersen et al., 1985; Pouget and Snyder, 2000). Our results suggest that gain-field combinations of intrinsic and extrinsic coordinate representations may also act as basis elements for storing motor memories. These memories are the substrate for adaptive changes in motor output and are locally tuned to the trained movement in both intrinsic and extrinsic coordinates. Our findings suggest a connection between the formation of motor memory and neural representations in posterior parietal cortex (Andersen et al., 1985; Snyder et al., 1998b; Andersen et al., 2004; Buneo and Andersen, 2006; Chang et al., 2009) and motor cortex (Kalaska et al., 1989; Kakei et al., 1999; Sergio et al., 2005; Pesaran et al., 2006; Kalaska, 2009).

4.5.1 Locally-tuned gain-fields for motor memory and their computational implications

Recently, Yokoi et al (Yokoi et al., 2011) demonstrated a different way in which a multiplicative gain field accounts for internal representations underlying motor memory. They did not dissociate intrinsic and extrinsic reference frames, but were able to uncover a different type of gain-field representation. In a force-field learning task with bimanual reaching arm movements, they found that a learned action generalized to untrained actions based on the movement directions of both arms. However, the memory for the learned bimanual action was not comprised of one component associated with the right arm's motion and another component associated with the left. Instead, the amount of generalization was well-characterized by a gain field combination of local tuning to the movement directions of both arms. In other words, they demonstrate that the motor memory associated with a complex movement can be formed as a gain field combination of its individual parts. This complements our finding that the motor

memory associated with a movement is formed as gain field combination of different reference frames in which it can be represented.

Importantly, this study used a dense sampling of the dominant–nondominant arm space in order to visualize the gain-field encoding across that space. Taken together, these findings suggest that the representation of motor memories formed during adaptation can be elucidated by dense sampling of generalization and is based on a gain field combination of local tuning to the relevant features of the learned action. These "features" can reflect either different reference frames for representing the learned action or different physical subcomponents of that action or perhaps other task-relevant variables.

If this is the case, we can, in a computational sense, represent the memory associated with a learned action by a function in a multidimensional feature space that defines how it generalizes across arbitrary combinations of an arbitrary number of features. If each of the individual locally generalizing features can be represented by a Gaussian function, the gain-field combination describing the overall generalization function will simply be a multidimensional Gaussian over the feature space (see Equation 4.6). In two dimensions, this corresponds to a generalization pattern resembling the bivariate Gaussian local generalization function plotted in Figure 4.3E and 4.5F. For a multi-dimensional Gaussian centered at the trained action, the amount of generalization to any point in this space corresponds to a dimension-weighted distance between the trained action and that point. The specific weighting is given by the Mahalanobis distance – a measure which effectively adds the normalized distances across different features, each normalized based on the width of its generalization. This conception provides a compact computational way to view how a memory formed from multiplicative combination of local tuning to different features would generalize to untrained conditions: The memory will simply generalize based on the similarity between the trained and untrained conditions, when this

similarity is characterized by the Mahalanobis distance between these conditions across feature space.

4.5.2 Neural substrates responsible for coordinate frame encoding

While the neural substrate for the visuomotor adaptation that we studied is unclear, there is evidence suggesting that cerebellum (Morton and Bastian, 2004; Rabe et al., 2009; Galea et al., 2011; Donchin et al., 2012), posterior parietal cortex (PPC) (Buneo and Andersen, 2006; Tanaka et al., 2009) and motor cortex (M1) (Galea et al., 2011) are involved. Gain-field encoding has been extensively studied in PPC as a way to combine coordinate representations. In area 7a of posterior parietal cortex (PPC) the spatial location of an object is represented with respect to the eyes and the external world in an extrinsic coordinate system, independent of limb posture and joint configurations (Andersen et al., 1985). But other parts of PPC, for example area 5a, maintain object representation in body-referenced (intrinsic) coordinates (Snyder et al., 1998a; Snyder et al., 1998b) as well. Recently, a mixed I-E object representation was found in the superficial layers of area 5 of PPC (Buneo and Andersen, 2006), indicating that within a single neuron multiple reference frames may be used to simultaneously represent a single object or action. It should be noted, however, that whereas eye-centered and hand-centered representations have clearly been dissociated, the limited workspaces used in these studies make it difficult to distinguish a Cartesian reference frame centered at the hand from a fully intrinsic coordinate system based on joint angles or muscle actions.

In contrast, several studies in M1 have rigorously dissociated Cartesian and fully-intrinsic coordinates. Although there is still a debate about whether M1 neurons encode movement direction primarily in intrinsic or extrinsic coordinates (Hatsopoulos, 2005; Kalaska, 2009), studies have generally found that most cells display activity that is intermediate between fully-intrinsic and fully-extrinsic representations of movement direction (Scott and Kalaska, 1997;

Kakei et al., 1999; Wu and Hatsopoulos, 2006; Kalaska, 2009). However, to date, studies of neural encoding in M1 have not investigated a gain-field combination of intrinsic and extrinsic coordinates. A key feature of our current work and the Yokoi et al. (2011) study was the dense sampling of the generalization function across combinations of two different features. Intriguingly, several studies of neural activity in M1 which have employed analogously dense sampling across combinations of different features appear to provide evidence for gain-field encoding across those features. One study (Kalaska et al., 1989) looked at tuning in M1 as a function of both movement direction and external load direction. The two-dimensional tuning curves were local, like the generalization functions we observe (see Figure 8 of their manuscript). Although the tuning was modeled as resulting from additive independent contributions of movement and load direction, inspection of parallel slices through their data (see Figure 13 of their manuscript) reveal that load direction clearly modulates the depth of movement direction tuning – which can be explained by a multiplicative, but not additive, combination of features. A second study (Sergio and Kalaska, 2003) reveals that the depth of the tuning to external force direction is systematically modulated by arm posture (see Figure 7 of their manuscript). And other studies (Kakei et al., 1999; Wu and Hatsopoulos, 2006) have shown that posture can strongly modulate the depth of tuning to movement direction, consistent with the prediction of gain-field tuning across these features (see Figures 3 and 4, respectively from these papers).

4.5.3 Previous work examining the coordinate system for motor adaptation

The idea of using different arm postures to investigate the coordinate system used for the adaptive control of movement is not new (Shadmehr and Mussa-Ivaldi, 1994; Kakei et al., 1999; Ghez et al., 2000; Krakauer et al., 2000; Shadmehr and Moussavi, 2000; Baraduc and Wolpert, 2002; Malfait et al., 2002; Ghez et al., 2007). Krakauer et al (2000) investigated this issue for visuomotor rotation learning as in the current paper by training a rotation in a single movement

direction in one arm configuration and testing the transfer of adaptation to a single extrinsically-matched movement in a different arm configuration (45° away). They found almost complete transfer of the learned rotation to the extrinsically-matched movement in the novel workspace and concluded that visuomotor rotations are learned in extrinsic coordinates. However, this experiment is equivalent to sampling only the 0° movement direction from the W2 generalization function shown in Figure 4.2D, and as our data from experiment 4.1 show (see Figure 4.2), generalization intermediate between fully-intrinsic and fully-extrinsic coordinates can lead to the near complete (86%) extrinsically-matched transfer that they observed alongside near complete (91%) intrinsically-matched transfer. Thus, our findings are consistent with their experimental results, although we demonstrate that the fully-extrinsic transfer they suggested is not present. This underscores the importance of measuring the entire generalization pattern in a second workspace if the coordinate system for the internal representation of motor memory is to be determined.

In view of our findings, similar questions arise about the force-field adaptation literature. The consensus is that movement dynamics are learned in purely intrinsic coordinates (Shadmehr and Mussa-Ivaldi, 1994; Shadmehr and Moussavi, 2000; Malfait et al., 2002). However, a closer look reveals that the evidence may not be definitive. In an elegant study, Malfait et al (2002) looked at the transfer of force field learning from one direction in one workspace to two directions in a second workspace. The two directions in the second workspace were aligned with the intrinsic and extrinsic representations of the trained movement in the first workspace – equivalent to sampling the 0° and 90° directions from the W2* generalization function shown in Figure 4.5B. They found nearly complete transfer to the intrinsically-aligned movement direction and minimal transfer to the extrinsically-aligned movement direction, and concluded that internal representations of physical dynamics were coded in intrinsic coordinates. However, the authors

did not consider the possibility of an intermediate reference frame for which the maximum transfer might be to an intermediate movement direction.

A pair of earlier studies also looked at the transfer of force-field adaptation across workspaces in order to determine the coordinate system for motor memory of physical dynamics (Shadmehr and Mussa-Ivaldi, 1994; Shadmehr and Moussavi, 2000). But unlike Krakauer et al. (2000) and Malfait et al. (2002), multiple movement directions were examined in the second workspace, like in the current study. However, adaptation was also trained in multiple directions in the first workspace, preventing a straightforward analysis of the specific effect of training any particular movement direction in W1 across movement directions in W2. In other words, the generalization in W2 associated with each trained movement in W1 could not be directly determined. Instead, the authors studied the differential effects of force-fields that would be specifically compatible with either intrinsic or extrinsic transfer. The results showed large, but incomplete, transfer of adaptation to an intrinsically-matched environment, with intrinsic transfer clearly stronger than extrinsically-matched transfer. While the authors concluded that the adaptation was represented in intrinsic coordinates, their results are again consistent with a gain-field combination of intrinsic and extrinsic frames, in line with our findings for visuomotor rotation. Moreover, inspection of our results (Figures 4.2F and 4.5C) reveals somewhat greater intrinsic than extrinsic contributions to the motor memory, in line with the finding of predominantly intrinsic transfer for learning physical dynamics. Taken together with the neurophysiologic evidence of mixed coordinate representations for reaching arm movements (Scott and Kalaska, 1997; Kakei et al., 1999, 2001; Buneo and Andersen, 2006; Kalaska, 2009), our findings suggest that a composite I-E coordinate system, resulting from a gain-field combination of intrinsic and extrinsic reference frames may underlie the motor memories for both internal models of dynamics and internal representations for trajectory planning.

CHAPTER 5: A UNIFORM ARCHITECTURE FOR PROCEDURAL LEARNING IN THE HUMAN NERVOUS SYSTEM

5.1 SUMMARY

The ability to transfer learning, i.e. to generalize, to untrained conditions is a fundamental feature of any neural system, and the footprint of this generalization provides a window into its internal structure (Shadmehr and Mussa-Ivaldi, 1994; Ghahramani et al., 1996; Ahissar and Hochstein, 1997; Shadmehr and Moussavi, 2000; Donchin et al., 2003; Morton and Bastian, 2004; Poggio and Bizzi, 2004; Mattar and Ostry, 2007; Haswell et al., 2009; Gonzalez Castro et al., 2011; Yokoi et al., 2011). An influential theory in perceptual learning, the reverse hierarchy theory (RHT), posits an intrinsic relationship between the amount of generalization and the rate of learning (Ahissar and Hochstein, 1997, 2004; Ahissar et al., 2009). This theory maintains that learning occurs at multiple levels of neural processing: high-level neural representations learn rapidly and generalize broadly to untrained conditions, whereas more specific lower-level representations learn more slowly. However, whether this applies to the motor system is not known because the relationship between motor learning rate and the specificity of generalization remains unclear. Here we examine learning during visually-guided movements in humans and demonstrate the existence of two distinct components of motor memory with different generalization footprints: One generalizes only locally, around the trained movement direction and with the trained end effector, whereas the other generalizes broadly across both. In line with the RHT, we demonstrate that broad generalization results from a rapidly-learning adaptive process, dominates on easier-to-learn tasks, and performs higher-level processing, producing adaptation vectors that integrate multiple sources of information. This high-level adaptive process evolves in parallel to a slower-learning, more specific low-level adaptation. Our findings explain how the generalization of motor adaptation varies between individuals and across tasks and provide an intriguing link between the structure of the neural systems for motor and perceptual learning, suggesting a unified architecture for procedural learning in the nervous system.

5.2 INTRODUCTION

A key issue in the study of neural learning systems is the manner and extent to which learning generalizes to untrained conditions. In both cases, the pattern of generalization provides a footprint that reflects the structure of the learning system.

Accurate motor output depends on a large number of continuously changing factors, including the geometry and motion of various body parts. As a result, the function relating a desired movement to the required neural activation is exceedingly high-dimensional, unlikely to be based on a look-up table with memories of learned actions. Instead, motor memories must generalize over a range of conditions to facilitate the application of learned actions in different contexts. This generalization determines the trade-off between contextual specificity and the flexibility of learning transfer.

Here we draw a parallel between the specificity of motor memories, which is poorly understood, and the specificity of perceptual learning, for which we have a well-formulated working theory (Ahissar and Hochstein, 1997, 2004; Ahissar et al., 2009). We hypothesized that a unified architecture underlies both types of procedural learning. First we uncovered two distinct processes responsible for the encoding of motor memories. Next, we were able to demonstrate a relationship between the rate of learning and the extent of generalization. More specifically, we demonstrated that the broadly-generalizing process learns faster than the locally-generalizing one. Finally, we concluded that the broadly-generalizing process integrates multiple sources of information and as such must be located in a higher brain area. Our findings provide a road map linking motor and perceptual memory formation, possibly serving as the basis for a unified theory of procedural learning.

5.3 METHODS

5.3.1 Participants

104 right-handed subjects participated in this study. Twenty took part in experiment 5.1, 18 in experiment 5.2, 24 in experiment 5.3, 22 in experiment 5.4, and 20 in experiment 5.5. The subjects were naïve to the purpose of the experiments and all provided informed consent consistent with the policies of Harvard's Institutional Review Board.

5.3.2 Apparatus

The configuration of the experimental setup is shown in Figure 5.1A. Subjects sat in a chair facing a 120 Hz 23-inch LCD monitor, mounted horizontally in front of them at shoulder level, displaying the various visual cues during the experiment. Underneath the monitor, 8 inches below the face of the screen, a digitizing tablet (Wacom Intuos 3) was used to track and record the subjects' arm movements. Above the tablet, subjects held a handle containing a digitizing pen in their right hand, whose position was tracked by the tablet. The handle served two purposes: (1) it acted as a shell around the digitizing pen, increasing its diameter, making it more comfortable to grasp, (2) it provided a wider contact surface with the tablet, promoting a more consistent vertical orientation of the pen. The handle had a flat bottom covered with Teflon (PTFE) which lowered the contact friction, allowing it to glide smoothly on the tablet. The position data was recorded in real-time (sampled at 200 Hz) using the Psychophysics Toolbox (Brainard, 1997; Kleiner et al., 2007) in Matlab (MATLAB, 2010). The resolution of the position data in the plane of the tablet was 0.005 mm and the accuracy was 0.25 mm.

5.3.3 General procedures

In this study subjects performed 9 cm point-to-point reaching arm movements from a single starting location to 19 different target locations, as illustrated in Figure 4.1A. The starting location was a circle with diameter of 5 mm and each target was a circle with diameter 10 mm. The cursor was also a circle with diameter of 2.5 mm.

Each experiment began with a block of trials containing 114 movements (with the exception of experiment 5.3 – see specific procedures for details) - 6 trials to each of 19 target locations presented in a pseudo-random order. During these movements subjects were given veridical visual feedback during both the outward movements toward each target and the inward return movements toward the starting location. This block constituted the "familiarization phase" of the experiment and allowed the subject to become comfortable with the reaching task.

The second phase of the experiments, the baseline phase, consisted of 342 movements, divided into 3 blocks of 114 movements (again, with the exception of experiment 5.3 – see specific procedures). In the baseline phase, veridical visual feedback of the cursor was present on ⅔ of the movements. Feedback was withheld on the remaining movements (randomly chosen). During this block, a return movement had visual feedback if and only if the preceding outward reaching movement had visual feedback. On the no-visual-feedback trials, the cursor disappeared as soon as the subject began her movement (when movement velocity increased above 5 cm/s) towards the target. A movement was considered complete when the subject came to a stop (defined by hand velocity remaining below 5 cm/s for a period of 100 ms). The return-to-center movement following a no-visual-feedback movement was without visual feedback and subjects had to find the starting location without visual guidance. The cursor reappeared only after the subject came within 7.6 mm of the starting location.

During the third phase of the experiment, the training phase, each subject was presented with a specific visuomotor transformation of the cursor. This phase was distinctly different in the 5 experiments presented here and details about it are presented in the "Specific procedures" section.

Following training, subjects were given a 1-minute break before we tested the generalization of the learned adaptation to the same 19 targets they reached to in the baseline period with 3 trials towards each target location in each workspace, in random order, all without visual feedback. The return movements in this testing phase were also without visual feedback. After generalization was tested, subjects performed at least one additional block of training followed by an additional testing block.

5.3.4 Specific procedures

5.3.4.1 Experiment 5.1

In experiment 5.1 we imposed a 30° rotation of the cursor (either clockwise or counterclockwise) for 120 consecutive trials. The onset of the rotation occurred suddenly at the beginning of the training phase. As a subject reached towards a target positioned at 90° (the training target), the cursor location was rotated about the starting location by 30°. All return movements in the training phase were without visual feedback. In each experiment, the imposed rotation was clockwise for half the subjects and counterclockwise for the other half. In order for the cursor to move directly toward the target, hand motion would need to be directed 30° opposite to the direction of the cursor rotation as shown in the leftmost panel of Figure 5.1B.

Subjects performed a single training block of 120 movements to the training target with 10% of the trials in this block without visual feedback. At the end of the training block, movements were generally straight, indicating that participants learned the imposed rotation. In this experiment

subject performed one additional training set (60 trials) and one additional testing set. The data from both testing sets were combined and is presented together throughout the manuscript.

5.3.4.2 Experiment 5.2

In experiment 5.2 we also imposed a 30° rotation of the cursor (either clockwise or counterclockwise) but only for 20 consecutive trials (18 with visual feedback and 2 without). The onset of the rotation occurred suddenly at the beginning of the training phase. After this short training block, generalization was tested and afterwards training resumed. The second training block had 100 trials (90 with visual feedback, 10 without) and afterwards we tested generalization again. The second testing block was followed by 600 additional training trials (540 with visual feedback, 60 without, split into 6 blocks) and generalization was tested for a third and final time. The data from all three testing sets were analyzed individually in this manuscript.

5.3.4.3 Experiments 5.3

In experiment 5.3 subjects performed the familiarization and baseline phases of the experiment with both hands prior to training. The 2 familiarization blocks (one with the right and one with the left hand, lasting 76 trials each) and 4 baseline blocks (2 with the right and 2 with the left, lasting 114 trials each) were alternating between the two hands. In the training block we once again imposed a 30° rotation of the cursor for 120 consecutive trials (108 with visual feedback and 12 without) and all movements were done with the right hand. Afterwards, generalization was tested in both the left and right hands in a testing block of 19 movement directions x 5 trials at each direction. A retraining block of 60 trials with the right hand was followed by a second testing block. To minimize the effect of testing order, half the subjects were tested with the left hand first and half with the right first.

5.3.4.4 Experiments 5.4

In experiment 5.4 we imposed a visuomotor gain transformation on the cursor, resulting in a 43% movement length change (balanced between positive or negative) for 120 consecutive trials. The onset of the gain transformation occurred suddenly at the beginning of the training phase. As a subject made a 9 cm reaching movement towards a target positioned at 90° (the training target), the cursor-displayed movement was extended or shrunk by 43% with respect to the starting location. Just as in experiment 5.1, training was followed by one testing block, followed by re-training (60 trials) with the same transformation, followed by a second testing block. The data from both testing sets were combined and is presented together throughout the manuscript.

5.3.4.5 Experiments 5.5

Experiment 5.5 was split into two arms: in the first "Abrupt" arm (10 subjects) followed the same exact paradigm as in experiment 5.1. In the second "Gradual" arm (10 subjects) we also introduced a 30° rotation of the cursor, but instead of instant introduction of this rotation, the rotation was gradually introduced to the subjects (starting at 0 rotation and increasing it at a rate of 0.17° per trials) over the course of 180 trials, after which the complete 30° rotation was maintained for an additional 120 training trials. Testing in this group was followed by a second set of gradual introduction of the rotation (starting at 18° rotation and increasing it at a rate of 0.17° per trials), followed by 60 trials at 30° rotation. Second testing block followed. The data from both testing sets were combined and is presented together throughout the manuscript.

5.3.5 Data analysis

All of the generalization function data presented in this manuscript were collected during no-visual-feedback outward movements during the testing phase. Return movements (toward the center location) were not analyzed. For each movement we calculated its heading direction and length, both components of the vector connecting the start and end points of the movement. The

start point was operationally defined as the location of the hand on the tablet when the speed of the movement first exceeded 5 cm/s, and the end point was the location of the hand 100 ms after the velocity dropped below 5 cm/s. Note that movements typically had peak velocities between 40 and 60 cm/s.

For each of the 19 directions tested in each condition we estimated the average heading direction per subject and condition separately for the baseline and the testing phase (by averaging the 6 no-visual-feedback trials towards each target). We subtracted the small baseline biases from the learning curve and the post-adaptation generalization data to compute the learning-related changes. Note that, because the baseline movements were almost straight to the targets in most cases, very similar results would be obtained if baseline subtraction were not used.

In order to estimate the confidence intervals in the parameters of the fits to the average generalization functions, we performed a bootstrap analysis with 10000 iterations allowing us to estimate the variability of the parameter values associated with the mean data. On each iteration, we selected N subjects (N was the number of participants in each experiment) with replacement from the respective subject pool and computed the generalization function and corresponding fits based to this selection. The confidence intervals were then estimated from the distribution of these fit parameters.

Throughout the manuscript, we used this form as a working approximation of the generalization function:

$$z(\theta) = k \cdot e^{-\frac{(\theta-\theta_0)^2}{2\sigma^2}} + k_0 \quad \text{(eq. 5.1)}$$

Here the generalization of learning, $z(\theta)$, is centered around the movement direction eliciting maximal adaptation, θ_0, has a local component with an amplitude of $k=z(\theta_0)$, and an effective width characterized by σ, and a global component k_0.

For each experiment we computed the characteristic width (σ) based on the group data as well as the bootstrap approach described above. Once we had an estimate for σ we used it to constrain the model and fit the other two parameters (k_0 and k) to each person's individual generalization curve. Using individual subject fits we calculated the relative contributions between the local and global components as well as the confidence intervals for them.

5.4 RESULTS

5.4.1 Distinct components of visuomotor memory

We began by measuring the generalization function for adaptation to a visuomotor rotation (VMR), a type of visuomotor learning in which the location of a hand-controlled cursor is systematically rotated about the center of the workspace during goal-directed reaching arm movements. We accomplished this by training a 30° rotation (either clockwise or counter-clockwise, balanced across subjects) in a single 9-cm movement for 120 trials, before probing how the resulting adaptation generalized to 9-cm movements in different directions, as illustrated in Figure 5.1C. This basic paradigm has been studied before (Pine et al., 1996; Krakauer et al., 2000; Brayanov 2012) but here we took an especially close look at the shape of the generalization function (GF) by measuring it in 20 participants, sampling 19 different movement directions with 6 probe trials per direction in each subject. This resulted in a precise estimate, revealing that the directional generalization function is composed of both local and global components, as shown in Figure 5.1D. Correspondingly, we found that a model (green) of the shape of the GF based on the sum of a local Gaussian component (blue) and a global offset component (yellow) explained 97% of its variance. The amplitude of the local component was roughly double that of the global component. However, both the local and global components were highly significant with lower residual errors for a model in which both components were combined (see Figure 5.1E), even when the effect of the additional parameters was taken into account ($F(1,17)=759.05$, $p=1.5\times10^{-15}$ and $F(1,17)=1041.50$, $p=1.1\times10^{-16}$, when comparing the combined model to the global-only and the local-only models, respectively). Moreover, examination of individual subject data revealed that 19 of 20 subjects displayed statistically significant local and global components of generalization (at $\alpha=0.01$). These results appear, at first, to be at odds with previous studies suggesting purely local generalization for VMR learning (Pine et al., 1996; Ghez et al., 2000;

Krakauer et al., 2000; Tanaka et al., 2009), however, close inspection of these studies reveals that the data, although noisier, are squarely in line with the existence of a global offset in addition to a larger local component of generalization. Moreover, the width of the local component in our data (σ=32.3±1.6° S.E.M.) appears to match the width of the local generalization previously observed.

5.4.2 The broadly-generalizing component adapts faster

We next examined whether these two memory components adapted at the same rate. The reverse hierarchy hypothesis (Ahissar and Hochstein, 1997; Hochstein and Ahissar, 2002; Ahissar and Hochstein, 2004; Ahissar et al., 2009) suggests that broadly-generalizing high-level perceptual learning evolves more rapidly than low-level learning that generalizes locally. Since locally-generalizing and broadly-generalizing learning coexist in our task, this idea, if extended to motor learning, would predict that the individuals with greater global generalization on our task would display faster adaptation. In an initial test of this prediction, we stratified the participants in experiment 5.1 based on the size of the global component of their GFs. We found that individuals with larger global generalization displayed learning curves that were significantly faster over the first 10 trials than individuals with smaller global generalization (p=0.019), despite reaching similar asymptotic learning levels by the end of the training period (p=0.44), as shown in Figure 5.2A. This suggests a key parallel between motor and perceptual skill acquisition: Globally-generalizing learning appears to proceed at a faster rate in both cases.

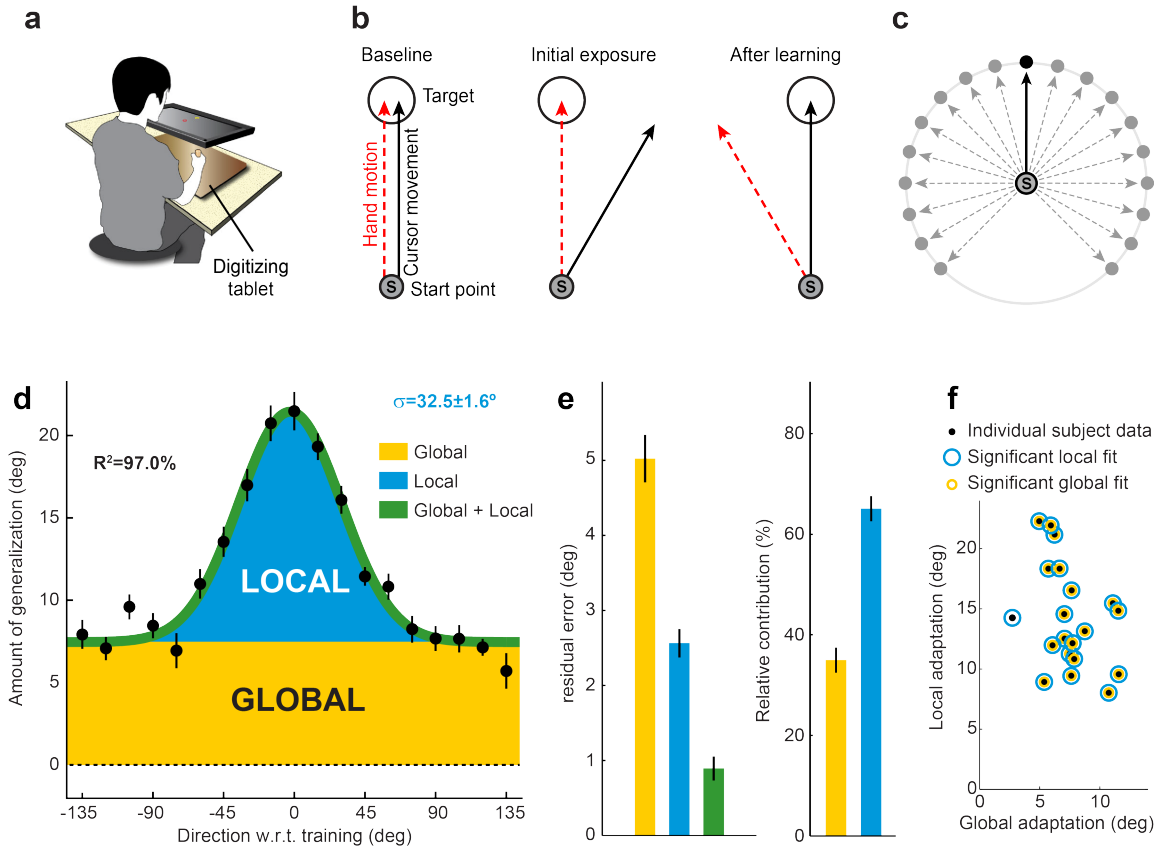

Figure 5.1: Experiment illustration and the pattern of directional generalization for VMR learning. (A) Experimental setup. A subject sits in front of a horizontally mounted computer screen. He is holding a handle containing a digitizing pen on the surface of a digitizing tablet. The tablet tracks the position of the subject's hand. The screen prevents the subject from seeing his hand and displays visual cues. (B) Visuomotor rotation learning paradigm. During baseline movements (left) the movement of the cursor (red arrow) is veridical with the motion of the subject's hand (black arrow). Note that in this diagram the two are horizontally shifted for clarity, but in reality they are co-localized. When visuomotor rotation is applied, the cursor moves in a direction 30° away from the target. At the initial introduction of the visual rotation (middle) subject's hand path goes straight to the target, however, the cursor is rotated by 30° CW and the subject perceives this as an error. After learning is complete, subject's hand path is rotated 30° CCW such that the cursor path is straight to the target. (C) Diagram of target array. All targets are located on a 9 cm circle. The trained target (black) is located in the middle of the array. Probe targets (gray) are spaced by 15° and span the range of -135 to +135° w.r.t. the trained target. (D) General shape of VMR generalization. The GF is composed of two distinct components: a local (Gaussian-like) and a global (uniform) component. (E) Individual component contributions. Left panel shows that while the local, Gaussian-like, component fits the data better than just a global offset (compare blue vs. yellow bars, a 2-fold residual error reduction), both components combined together work much better, reducing the residual error additional 2.5 times. Right panel shows that at the trained direction the global component accounts for approximately 35% of the adaptation and the global component accounts for the remaining 65%. (F) Local and global components from individual subject fits. All 20 subjects have GFs containing both components (black) and a significant local component (blue). 19 of the 20 subjects also displayed a significant global component (yellow). Significance was evaluated at α=0.01.

To more thoroughly examine how the locally-generalizing and globally-generalizing components of adaptation evolve during the course of training, we conducted a second experiment (experiment 5.2) in which the GF was measured at 3 different time points along the learning curve – after 18, 108, and 648 training trials. The results, shown in Figure 5.2C-D, demonstrate that the local and global components do evolve at different rates. Both components increase monotonically with training. However, the global component evolves more rapidly than the local component, similar to perceptual learning, reaching 75% of its asymptotic value after just 18 trials, compared to 108 trials for the local component to reach a similar relative level. Correspondingly, the local and global components contribute almost equally to adaptation after just 18 trials of training; however, as training proceeds, the contribution of the local component significantly outpaces that of the global component, as shown in Figure 5.2C-D. This is evidenced by the observation that the ratio between the local and global components significantly increases with training ($p=0.017$, $p=0.022$, and $p=0.0025$ when comparing early vs. mid training, mid vs. late, and early vs. late, respectively, paired single-sided t-tests) .

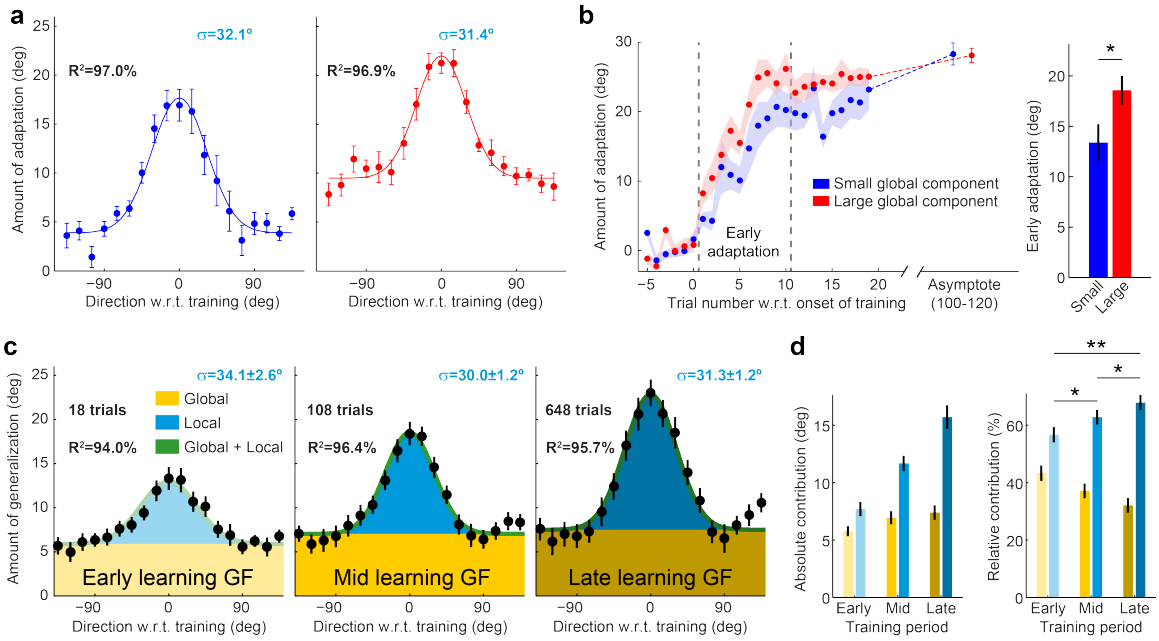

Figure 5.2: Global learning proceeds more rapidly than local learning. (A) GFs from subgroups with small (blue) and large (red) global components of generalization. Each GF is based on data from 10 subjects. (B) Learning curves for the two subgroups in (a). Early adaptation (over the first 10 trials) in the subgroup with smaller global component (blue) is significantly slower (p=0.019), despite reaching identical asymptotic levels by the end of training. (C) Temporal evolution of the GF. Each panel shows a complete GF obtained after 18, 108, and 648 rotation trials, respectively. Note that the general shape (composed of both local and global components) is present throughout training and the width (σ) of the local component does not change significantly (34.1 ±2.6° vs. 30.0 ±1.2° vs. 31.3 ±1.2°, p>0.1 for all comparisons). (D) Evolution of the individual component contributions. Left panel shows the levels (at the trained direction) of the local and global components. Note that the global component increases rapidly during early training, reaching more than 75% of its asymptotic value, but much more slowly thereafter. In contrast, the local component grows much more gradually, reaching less than 50% of its asymptote during early learning, but steadily increasing from early to mid and mid to late (p<0.001 in both cases). The right panel shows the relative contributions of the two components, demonstrating the increasing dominance of the local component as training proceeds. (* p<0.05, ** p<0.005)

The shape of the GF observed in experiment 5.1 might be explained by a single component of learning with partially local and partially global generalization. However, the differences in temporal evolution between the locally-generalizing and globally-generalizing components provide evidence that these components are distinct, because the shape of the overall generalization, in addition to its amplitude, changes during the course of training. In contrast, the shapes of the local and global components of generalization are held constant while their amplitudes evolve as training progresses. In particular, we find that although the amount of local generalization increases during training, its width is held constant ($F(2,34)=45.10$, $p=2.7\text{x}10^{-10}$ for changes in the amplitude but $F(2,34)=0.63$, $p=0.54$ for changes in the width, both based on repeated measures ANOVAs). Together, these findings show that in a visuomotor learning task, two distinct adaptive processes simultaneously contribute to the formation of motor memory. In line with the reverse-hierarchy hypothesis for perceptual learning (Ahissar and Hochstein, 1997; Hochstein and Ahissar, 2002; Ahissar and Hochstein, 2004; Ahissar et al., 2009), one learns rapidly and generalizes broadly, whereas the other learns more slowly and generalizes locally.

5.4.3 Task, effector, and awareness specificity of visuomotor adaptation.

We next investigated the effector-specificity of the local and global learning, with the hypothesis that the global process should generalize broadly across multiple movement attributes, and, in particular, display broad generalization both across different end-effectors and across different movement directions. In contrast, the local process should show little generalization across either end-effectors or movement directions. To test this hypothesis, we designed a third experiment (experiment 5.3) to compare the generalization of a 30° VMR within versus across hands. After training a single movement direction for 120 trials with the right hand, we measured generalization across different movement directions in both the trained and untrained hands. Figure 5.3A-B illustrates the corresponding GFs. Interestingly, the width of the local component

in the untrained hand was similar to the width we observed in the trained hand (σ=30.1±1.4° vs 37.8±10.4°, p=0.441). However, although intralimb generalization was primarily local [in amplitude] across movement directions consistent with the results of experiment 5.1, we found interlimb generalization to be primarily global. The amount of global learning in the untrained hand was 70.9%±9.2% from that in the trained hand, whereas the amount of local learning was significantly smaller (p = 0.001), only 24.6%±6.7% of that in the trained hand, as shown in Figure 5.3C. The findings are consistent with the idea that, across both movement directions and effectors, a fast-learning high-level process should generalize broadly, whereas a slow-learning low-level process should generalize more narrowly.

Based on these results, we hypothesized that perceptual and motor learning may rely on a single basic neural architecture for memory formation during learning. A key idea stemming from the reverse hierarchy theory in perceptual learning is that easier-to-learn tasks depend on plasticity in higher-order sensory areas, which generalizes broadly. Thus, in a fourth experiment (experiment 5.4), we examined the effect of task difficulty on the two components of motor memory, with the prediction that an easier task would display greater global generalization. We studied a visuomotor learning task known to display especially rapid adaptation: visuomotor gain (VMG) learning. Using the same training schedule as in experiment 5.1, we found that VMG learning exhibits significantly faster adaptation than VMR learning over the first 10 training trials (Figure 5.3D-E, $p=2.0 \times 10^{-7}$), in line with previous reports (Krakauer et al., 2000), and the disparity over the first 2-3 trials of adaptation appeared to be even greater. In line with our findings for VMR learning, the GF for VMG learning displayed both local and global components.

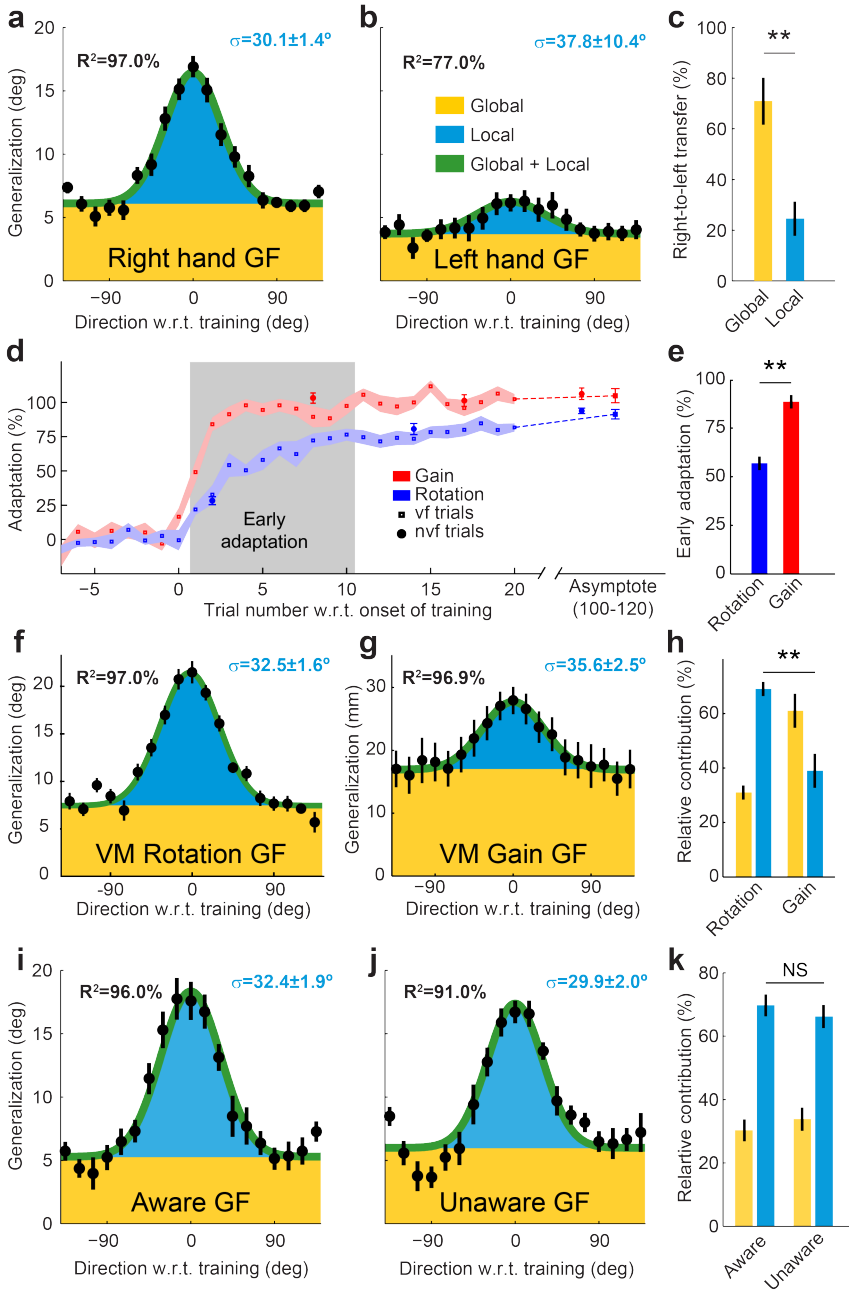

Figure 5.3: The effects of effector-specificity, task difficulty, and awareness. (A-C) Effector-specificity of VMR adaption. Rotation adaptation learned with the dominant (right) hand (A) only partially transfers to the left hand (B). Interestingly, the global component (yellow) transfers approximately 70% of its magnitude across effectors, whereas the local component (blue) transfers significantly worse (p=0.001) retaining just about 20% of its level (C). (D-H) Comparison between VMR and VMG learning. (D) Learning curves for both transformations scaled by the ideal adaptation level (30° for VMR, 38.6 mm for VMG) show that gain adaptation proceeds at a much faster rate. (E) Early adaptation (over the first 10 trials) is approximately 60%

Figure 5.3 (Continued)

higher for VMG ($p=2.0x10^{-7}$). (F) Same as Figure 5.1A. (G) The GF for VMG displays both a Gaussian-like local (blue) and uniform global (yellow) components, similar to the VMR GF. (H) Unlike VMR, the global component of VMG is larger than its local component. As a result, the relative contribution of the global component to motor memory is significantly greater in VMG than in VMR ($p=0.0015$). (I-K) Awareness of learned perturbation. Subjects presented with a 30° VMR gradually over the course of 180 trials display the same generalization pattern (J) as subjects presented with a 30° rotation abruptly (I). The overall shape (Gaussian local and uniform global components), the width of the local component, and relative contributions of the local and global components (K) are not significantly different across the two groups. (* $p<0.05$, ** $p<0.005$, NS $p>0.1$)

Interestingly, we found the widths of the local components for VMG and VMR learning to be remarkably similar (35.6±2.5° vs. 32.5±1.6°, p=0.17), suggesting a shared mechanism for the formation of these motor memories. However, we found that in VMG learning the global component dominates the local component with an amplitude that is more than 50% larger than for VMR learning, as predicted by the hypothesis that, like in sensory learning, easier motor tasks elicit broader generalization. Correspondingly, the relative contribution of global learning was 35% for VMR compared to 60% for VMG (Figure 5.3F-G, p=0.0015).

In perceptual learning, awareness has been linked to fast high-level learning (Hochstein and Ahissar, 2002; Ahissar and Hochstein, 2004) and has been shown to facilitate slow low-level learning (Ahissar and Hochstein, 1997). However, implicit motor learning has been shown to override strategic compensations resulting from awareness (Mazzoni and Krakauer, 2006; Taylor and Ivry, 2011, 2012). Therefore, in experiment 5.4, we examined whether the global and local components of motor learning might depend on awareness. To accomplish this, we trained VMR learning under conditions in which participants did not become aware of the imposed rotation. Specifically, we compared the GF when VMR learning was trained with a gradual onset, which has been shown to dramatically reduce awareness (Malfait and Ostry, 2004; Taylor et al., 2011; Wang et al., 2011) versus a sudden onset, as in experiments 5.1-5.4. In the gradual onset arm of experiment 5.5, the VMR was introduced at a rate of just 0.17° per trial and then maintained asymptotically at 30° for 120 trials to match the exposure in the sudden onset case. The sudden onset arm of experiment 5.5, where the full 30° rotation was introduced at the onset of training, was identical to experiment 5.1, except that awareness was assessed after completion. We found that all 10 sudden onset participants demonstrated awareness of the imposed rotation, whereas none of the 10 gradual onset participants reported awareness consistent with the imposed rotation. We found that the unaware and aware participants displayed remarkably similar GFs. Neither the

amplitude of the local or global components nor the width of the local component was significantly affected by awareness, as shown in Figure 5.3E ($p>0.15$ in all three cases), indicating that neither global nor local learning require awareness.

5.4.4 Two-dimensional representation of visuomotor adaptation

The adaptation to visuomotor transformations, such as rotations and gains, has generally been studied by projecting the experimentally observed adaptation onto the framework of the task. For example, during VMR learning, lateral changes in movement endpoints are generally characterized by changes in movement direction, whereas longitudinal changes are generally not analyzed. While it may be reasonable to reduce the dimensionality of the data in order to focus specifically on task-relevant changes for the trained movement, this approach may be somewhat problematic when examining generalization to untrained movements. The issue is that the trained perturbation may be associated with different tasks, which generalize in very different ways. For example, a visuomotor rotation (yellow) is equivalent to a linear shift (blue) when only a single movement direction is considered, as illustrated in the first row of Figure 5.4. However, a rotation and a shift will generalize in very different ways.

As illustrated in Figure 5.4B, a linear shift generalizes in target-vector-independent (TVI) manner in that the adaptation vector is unchanged regardless of the target vector. In contrast, visual rotation generalizes in a target-vector-dependent (TVD) manner in that the adaptation vector is consistently oriented relative to the target vector, as illustrated in Figure 5.4C. Correspondingly, TVD rotation adaptation and TVI shift adaptation are identical at the trained target direction and similar in neighboring target directions, but very different at more distal directions, when the two-dimensional adaptation vectors are compared.

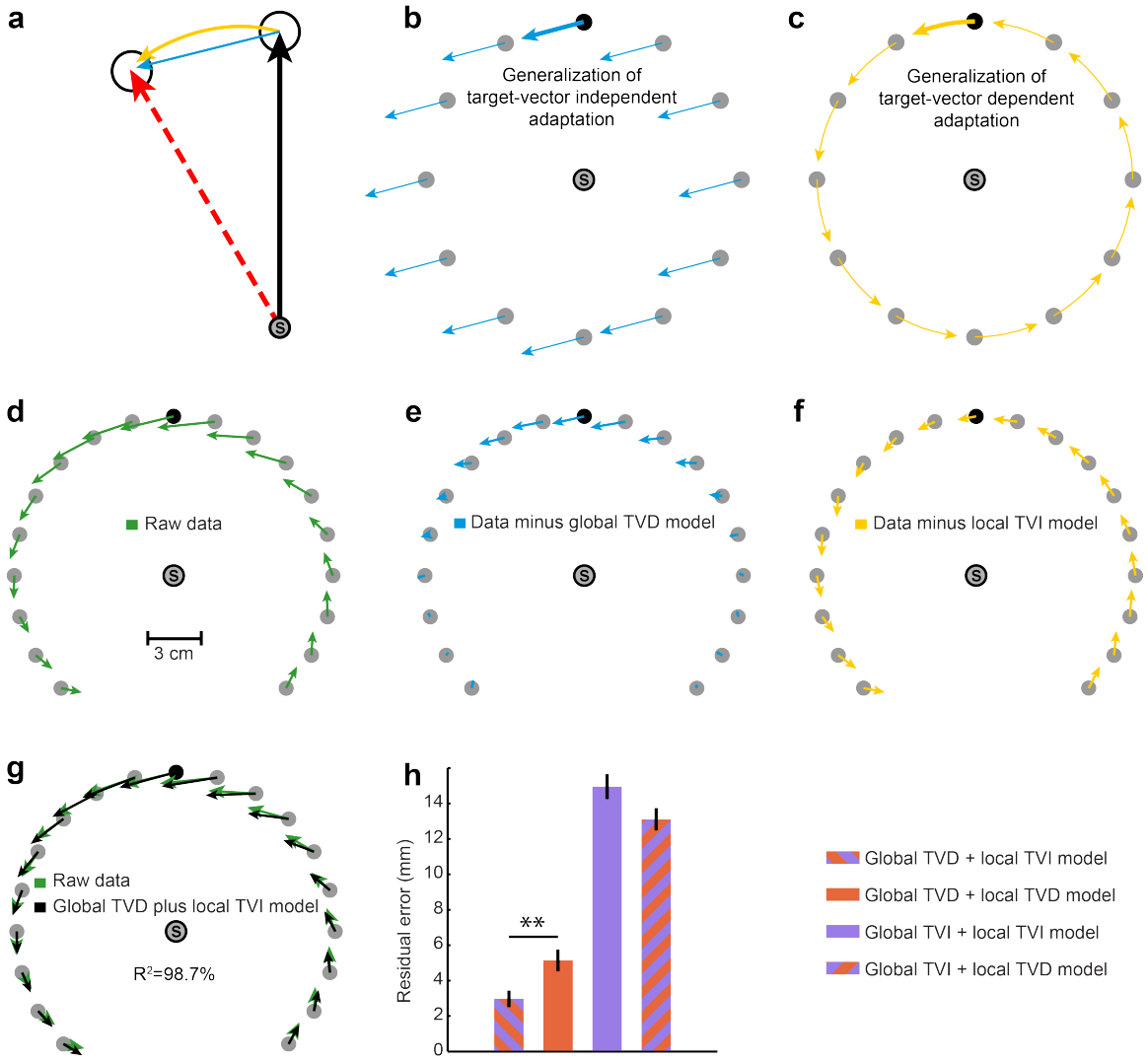

Figure 5.4: Two-dimensional analysis of generalization reveals high-level integration in global but not local generalization. (A) Two interpretations of VMR learning. Solid black line shows the ideal cursor path. Dashed green line shows the hand movement required to move the cursor along the ideal path for a 30° VMR. Note that before training the hand path follows the black arrow and after training it follows the green arrow. The thin yellow and blue arrows show two possible adaptation "vectors" which could account for the imposed visuomotor rotation. Both originate at the end-point of the pre-trained hand movement and end at the center of the end-point of the post-trained hand movement. The blue arrow represents a shift between the two centers and the yellow represents a rotation. (B) An example of how a rotation adaptation would generalize to other targets. The adapted rotation will reorient itself at different target locations, creating a "target-vector dependent" (TVD) pattern of adaptation. (C) An example of how a shift would generalize to other targets. The adapted shift would preserve its orientation at all target locations, creating a "target-vector independent" (TVI) pattern of adaptation. (D) Adaptation vectors observed in Experiment 5.1. To combine the CW and CCW data, we mirrored the CW adaptation vectors and averaged them with the CCW ones. Note that, while the vectors are

Figure 5.4 (Continued)

generally oriented along the target ring, they are neither in a perfectly circumferential pattern, as would be predicted by the TVD adaptation pattern, nor are they all parallel, as would be predicted by the TVI adaptation pattern. (E) Yellow arrows depict the result from the subtraction of a local TVI component from the data, leaving a pattern that reflects the global component of adaptation. Note that this pattern reveals adaptation vectors, which are aligned circumferentially and systematically change with movement direction. (F) Blue arrows depict the result from the subtraction of a global TVD component from the data, leaving a pattern that reflects the local component of adaptation. Note that this pattern reveals adaptation vectors, which are nearly parallel to each other and do not systematically change their orientation with movement direction. (G) A comparison between the raw data (black) and model prediction (green). The model, a combination of local TVI and global TVD adaptation, based on parameters from the 1D data fits, explains 99% of the variance in the 2D data. (H) Comparison of the 4 possible models combining local (L) and global (G) components which can either be TVD or TVI. Note that the residual error for global-TVD/local-TVI model is more than twice as small as the error for the next best model. (** $p<0.005$)

We hypothesized that a two-dimensional analysis of the adaptation vectors observed in the generalization data could isolate the TVI and TVD contributions to motor memory. In particular, we predicted that the higher-level globally-generalizing component of adaptation might display TVD adaptation based on the ability to integrate information about the errors experienced during adaptation with the direction of the planned movement. In contrast, the lower-level locally-generalizing component should display TVI adaptation that would not require such integration.

Examination of the two-dimensional adaptation vector data from experiment 5.1 (Figure 5.4D) reveals that global generalization, which dominates the more distant untrained movement directions, appears to be TVD. In particular, the adaptation vectors observed at target directions ±90° from the trained target were essentially orthogonal to the adaptation observed at the trained target in keeping with TVD adaptation. This is in line with the idea that high-level learning generalizes broadly and, though unconscious, integrates multiple sources of information – the direction of the error that drove adaptation and the direction of target. Correspondingly, a model of pure TVD global adaptation (Figure 5.4C) fitted to the generalization data explains the two-dimensional pattern of global generalization extremely well, with residuals that are essentially zero at distal directions where only global generalization would be observed (Figure 5.4E). In target directions more proximal to the trained direction, the residuals are larger, in line with the existence of a local component. Interestingly, we find that these residuals (blue) are remarkably collinear with the trained adaptation vector. This is exactly the pattern that would be predicted for local TVI learning, consistent with the idea that low-level learning generalizes narrowly and with adaptation vectors directed entirely based on training errors. We thus constructed a model of generalization that combined global TVD learning with local TVI learning. Remarkably, this simple model explained 99% of the variance in the two-dimensional adaptation vector data. The goodness of fit can be appreciated by comparing the black and green vectors in Figure 5.4G. This

model performed significantly better than models in which local and global learning were both TVD, both TVI, or TVD and TVI, respectively (residual variance was more than 2.5 fold smaller than the other three models, $p<0.001$ in all cases as shown in Figure 5.4H). In fact, considering all possible intermediate combinations of local-global TVI-TVD models offers no additional improvement over a model based on full local TVI and full global TVD adaptation.

Together, our findings indicate that the motor memory associated with visuomotor learning is based on two distinct implicit adaptive processes that evolve in parallel: (1) A globally-generalizing, high-level process which learns rapidly and integrates information about the errors that drive adaptation with the direction of the planned movement and (2) A locally-generalizing, low-level process which learns more slowly and fails to integrate information about the errors that drive adaptation with information about the planned movement.

5.5 DISCUSSION

We studied the formation and generalization of motor memories associated with the learning of movement kinematics. Using a pair of visuomotor transformations, we demonstrated that two distinct processes evolve in tandem during motor memory formation: one process learns quickly and generalizes broadly across movement directions and end effectors, whereas the other learns more slowly and generalizes locally. Remarkably, we found that not only easier-to-learn tasks elicit a larger fraction of the broadly-generalizing process, but also individuals who learn faster display a larger fraction of this process.

The existence of two distinct components of motor memory and more specifically their inherent behavior parallels what has been previously observed in perceptual learning. Interestingly, careful analysis of the special distribution of the adaptation vectors measured in experiment 5.1 conclusively demonstrated that the broadly-generalizing component of motor learning is, just like the corresponding component in perceptual learning, responsible for higher-order integration of multiple sources of information. The final finding of our manuscript ties together the observed similarities, suggesting a unified architecture across perceptual and motor learning.

BIBLIOGRAPHY

CHAPTER 1 – INTRODUCTION AND MOTIVATION

Bays, P. M., Flanagan, J. R. & Wolpert, D. M. Interference between velocity-dependent and position-dependent force-fields indicates that tasks depending on different kinematic parameters compete for motor working memory. *Exp Brain Res* **163**, 400-405 (2005).

Conditt, M. A., Gandolfo, F. & Mussa-Ivaldi, F. A. The motor system does not learn the dynamics of the arm by rote memorization of past experience. *Journal of Neurophysiology* **78**, 554-560 (1997).

Conditt, M. A. & Mussa-Ivaldi, F. A. Central representation of time during motor learning. *Proc Natl Acad Sci U S A* **96**, 11625-11630 (1999).

Diedrichsen, J., White, O., Newman, D. & Lally, N. Use-Dependent and Error-Based Learning of Motor Behaviors. *Journal of Neuroscience* **30**, 5159-5166 (2010).

Gandolfo, F., Mussa-Ivaldi, F. A. & Bizzi, E. Motor learning by field approximation. *Proc Natl Acad Sci U S A* **93**, 3843-3846 (1996).

Ghez, C., Scheidt, R. & Heijink, H. Different learned coordinate frames for planning trajectories and final positions in reaching. *Journal of neurophysiology* **98**, 3614-3626 (2007).

Halverson, H. M. *An experimental study of prehension in infants : by means of systematic cinema records.* (Clark university, 1931).

Hofsten, C. V. & Lindhagen, K. Observations on the Development of Reaching for Moving-Objects. *J Exp Child Psychol* **28**, 158-173 (1979).

Huang, V. S., Haith, A., Mazzoni, P. & Krakauer, J. W. Rethinking Motor Learning and Savings in Adaptation Paradigms: Model-Free Memory for Successful Actions Combines with Internal Models. *Neuron* **70**, 787-801 (2011).

Izawa, J. & Shadmehr, R. Learning from Sensory and Reward Prediction Errors during Motor Adaptation. *Plos Comput Biol* **7** (2011).

Kagerer, F. A., ContrerasVidal, J. L. & Stelmach, G. E. Adaptation to gradual as compared with sudden visuo-motor distortions. *Exp Brain Res* **115**, 557-561 (1997).

Krakauer, J. W. Motor Learning and Consolidation: The Case of Visuomotor Rotation. *Adv Exp Med Biol* **629**, 405-421 (2009).

Krakauer, J. W., Ghilardi, M. F. & Ghez, C. Independent learning of internal models for kinematic and dynamic control of reaching. *Nature neuroscience* **2**, 1026-1031 (1999).

Krakauer, J. W., Pine, Z. M., Ghilardi, M. F. & Ghez, C. Learning of visuomotor transformations for vectorial planning of reaching trajectories. *J Neurosci* **20**, 8916-8924 (2000).

Mazzoni, P. & Krakauer, J. An Implicit Plan Overrides an Explicit Strategy during Visuomotor Adaptation. *The Journal of Neuroscience* **26**, 3642-3645 (2006).

Melendez-Calderon, A., Masia, L., Gassert, R., Sandini, G. & Burdet, E. Force Field Adaptation Can Be Learned Using Vision in the Absence of Proprioceptive Error. *Ieee T Neur Sys Reh* **19**, 298-306 (2011).

Scheidt, R. A., Conditt, M. A., Secco, E. L. & Mussa-Ivaldi, F. A. Interaction of visual and proprioceptive feedback during adaptation of human reaching movements. *Journal of Neurophysiology* **93**, 3200-3213 (2005).

Scheidt, R. A., Reinkensmeyer, D. J., Conditt, M. A., Rymer, W. Z. & Mussa-Ivaldi, F. A. Persistence of motor adaptation during constrained, multi-joint, arm movements. *J Neurophysiol* **84**, 853-862 (2000).

Shadmehr, R. & Mussa-Ivaldi, F. A. Adaptive Representation of Dynamics during Learning of a Motor Task. *Journal of Neuroscience* **14**, 3208-3224 (1994).

Sing, G. C., Joiner, W. M., Nanayakkara, T., Brayanov, J. B. & Smith, M. A. Primitives for motor adaptation reflect correlated neural tuning to position and velocity. *Neuron* **64**, 575-589 (2009).

Smith, M. A., Ghazizadeh, A. & Shadmehr, R. Interacting adaptive processes with different timescales underlie short-term motor learning. *PLoS Biol* **4**, e179 (2006).

Thoroughman, K. A. & Shadmehr, R. Learning of action through adaptive combination of motor primitives. *Nature* **407**, 742-747 (2000).

White, B. L., Castle, P. & Held, R. Observations on the Development of Visually-Directed Reaching. *Child Dev* **35**, 349-364 (1964).

Wolpert, D. M., Diedrichsen, J. & Flanagan, J. R. Principles of sensorimotor learning. *Nat Rev Neurosci* **12**, 739-751 (2011).

CHAPTER 2: BAYESIAN AND "ANTI-BAYESIAN" BIASES IN SENSORY INTEGRATION FOR ACTION AND PERCEPTION IN THE SIZE-WEIGHT ILLUSION

Aglioti S, DeSouza JFX, and Goodale MA. Size-Contrast Illusions Deceive the Eye but Not the Hand. Curr Biol 5: 679-685, 1995.

Albers J. Interaction of Color. Yale University Press, 1975, p. 86.

Barlow H. The Exploitation of Regularities in the Environment by the Brain. Behav Brain Sci 24: 602-607, 2001.

Barlow HB. A Theory About the Functional Role and Synaptic Mechanism of Visual after-Effects. In: Vision: Coding and Efficiency, edited by Blakemore CB Cambridge University Press. , 1990.

Bays PM, Wolpert DM, and Flanagan JR. Perception of the Consequences of Self-Action Is Temporally Tuned and Event Driven. Current Biology 15: 1125-1128, 2005.

Blakemore SJ, Wolpert D, and Frith C. Why Can't You Tickle Yourself? Neuroreport 11: R11-R16, 2000.

Bouisset S, and Zattara M. A Sequence of Postural Movements Precedes Voluntary Movement. Neurosci Lett 22: 263-270, 1981.

Brenner E, and Smeets JBJ. Size Illusion Influences How We Lift but Not How We Grasp an Object. Exp Brain Res 111: 473-476, 1996.

Brown JE, and Frank JS. Influence of Event Anticipation on Postural Actions Accompanying Voluntary Movement. Exp Brain Res 67: 645-650, 1987.

Byblow WD, Coxon JP, Stinear CM, Fleming MK, Williams G, Muller JFM, and Ziemann U. Functional Connectivity between Secondary and Primary Motor Areas Underlying Hand-Foot Coordination. J Neurophysiol 98: 414-422, 2007.

Campbell FW, and Maffei L. Tilt after-Effect - Fresh Look. Vision Res 11: 833-&, 1971.

Chang EC, Flanagan JR, and Goodale MA. The Intermanual Transfer of Anticipatory Force Control in Precision Grip Lifting Is Not Influenced by the Perception of Weight. Exp Brain Res 185: 319-329, 2008.

Charpentier A. Analyse Experimentale Quelques De La Sensation De Poids [Experimental Study of Some Aspects of Weight Perception]. Arch Physiol Norm Pathol 3: 122-135, 1891.

Chouinard PA, Large ME, Chang EC, and Goodale MA. Dissociable Neural Mechanisms for Determining the Perceived Heaviness of Objects and the Predicted Weight of Objects During Lifting: An Fmri Investigation of the Size-Weight Illusion. Neuroimage 44: 200-212, 2009.

Chouinard PA, Leonard G, and Paus T. Role of the Primary Motor and Dorsal Premotor Cortices in the Anticipation of Forces During Object Lifting. J Neurosci 25: 2277-2284, 2005.

Cisek P, Crammond DJ, and Kalaska JF. Neural Activity in Primary Motor and Dorsal Premotor Cortex in Reaching Tasks with the Contralateral Versus Ipsilateral Arm. J Neurophysiol 89: 922-942, 2003.

Cordo PJ. Kinesthetic Control of a Multijoint Movement Sequence. J Neurophysiol 63: 161-172, 1990.

Cordo PJ, and Nashner LM. Properties of Postural Adjustments Associated with Rapid Arm Movements. J Neurophysiol 47: 287-382, 1982.

Cross DV, and Rotkin L. The Relation between Size and Apparent Heaviness. Perception and Psychophysics 18: 79-87, 1975.

Davare M, Andres M, Cosnard G, Thonnard JL, and Olivier E. Dissociating the Role of Ventral and Dorsal Premotor Cortex in Precision Grasping. J Neurosci 26: 2260-2268, 2006.

Davis CM, and Roberts W. Lifting Movements in the Size-Weight Illusion. Percept Psychophys 20: 33-36, 1976.

de Grave DDJ, Biegstraaten M, Smeets JBJ, and Brenner E. Effects of the Ebbinghaus Figure on Grasping Are Not Only Due to Misjudged Size. Exp Brain Res 163: 58-64, 2005.

Diedrichsen J, Verstynen T, Hon A, Lehman SL, and Ivry RB. Anticipatory Adjustments in the Unloading Task: Is an Efference Copy Necessary for Learning? Exp Brain Res 148: 272 - 276, 2003.

Diedrichsen J, Verstynen T, Hon A, Zhang Y, and Ivry RB. Illusions of Force Perception: The Role of Sensori-Motor Predictions, Visual Information, and Motor Errors. J Neurophysiol 97: 3305-3313, 2007.

Diedrichsen J, Verstynen T, Lehman SL, and Ivry RB. Cerebellar Involvement in Anticipating the Consequences of Self-Produced Actions During Bimanual Movements. J Neurophysiol 93: 801-812, 2005.

Dufossae M, Hugon M, and Massion J. Postural Forearm Changes Induced by Predictable in Time or Voluntary Triggered Unloading in Man. Exp Brain Res 60: 330-334, 1985.

Ellis RR, and Lederman SJ. The Golf-Ball Illusion: Evidence for Top-Down Processing in Weight Perception. Perception 27: 193-201, 1998.

Ellis RR, and Lederman SJ. The Material–Weight Illusion Revisited. Percept Psychophys 61: 1564-1576, 1999.

Ernst MO. Perceptual Learning: Inverting the Size-Weight Illusion. Curr Biol 19: R23-R25, 2009.

Ernst MO, and Banks MS. Humans Integrate Visual and Haptic Information in a Statistically Optimal Fashion. Nature 415: 439-443, 2002.

Flanagan JR, and Beltzner MA. Independence of Perceptual and Sensorimotor Predictions in the Size-Weight Illusion. Nature Neuroscience 3: 737-741, 2000.

Flanagan JR, Bittner JP, and Johansson RS. Experience Can Change Distinct Size-Weight Priors Engaged in Lifting Objects and Judging Their Weights. Curr Biol 18: 1742-1747, 2008.

Flanagan JR, Bowman MC, and Johansson RS. Control Strategies in Object Manipulation Tasks. Curr Opin Neurobiol 16: 650-659, 2006.

Flanagan JR, King S, Wolpert DM, and Johansson RS. Sensorimotor Prediction and Memory in Object Manipulation. Can J Exp Psychol-Rev Can Psychol Exp 55: 87-95, 2001.

Flanagan JR, Vetter P, Johansson RS, and Wolpert DM. Prediction Precedes Control in Motor Learning. Curr Biol 13: 146-150, 2003.

Fogassi L, Gallese V, Buccino G, Craighero L, Fadiga L, and Rizzolatti G. Cortical Mechanism for the Visual Guidance of Hand Grasping Movements in the Monkey - a Reversible Inactivation Study. Brain 124: 571-586, 2001.

Franz VH. Action Does Not Resist Visual Illusions. Trends Cogn Sci 5: 457-459, 2001.

Gahery Y, and Nieoullon A. Postural and Kinetic Coordination Following Cortical Stimuli Which Induce Flexion Movements in Cats Limbs. Brain Res 149: 25-37, 1978.

Ganel T, Tanzer M, and Goodale MA. A Double Dissociation between Action and Perception in the Context of Visual Illusions - Opposite Effects of Real and Illusory Size. Psychol Sci 19: 221-225, 2008.

Gibson JJ. Adaptation, after-Effect, and Contrast in the Perception of Tilted Lines. Ii. Simultaneous Contrast and the Areal Restriction of the after-Effect. Journal of Experimental Psychology 20: 553-569, 1937.

Goodale MA, and Milner DA. Separate Visual Pathways for Perception and Action. Trends Neurosci 15: 20-25, 1992.

Grandy MS, and Westwood DA. Opposite Perceptual and Sensorimotor Responses to a Size-Weight Illusion. J Neurophysiol 95: 3887-3892, 2006.

Gregory RL. Editorial Essay. Perception 35: 431-432, 2006.

Haffenden AM, Schiff KC, and Goodale MA. The Dissociation between Perception and Action in the Ebbinghaus Illusion: Nonillusory Effects of Pictorial Cues on Grasp. Curr Biol 11: 177-181, 2001.

Harshfield SP, and DeHardt DC. Weight Judgment as a Function of Apparent Density of Objects. Psychon Sci 20: 365-366, 1970.

Horak FB, and Diener HC. Cerebellar Control of Postural Scaling and Central Set in Stance. J Neurophysiol 72: 479-493, 1994.

Horak FB, Diener HC, and Nashner LM. Influence of Central Set on Human Postural Responses. J Neurophysiol 62: 841-853, 1989.

Hoshi E, and Tanji J. Differential Involvement of Neurons in the Dorsal and Ventral Premotor Cortex During Processing of Visual Signals for Action Planning. J Neurophysiol 95: 3596-3616, 2006.

Hoshi E, and Tanji J. Distinctions between Dorsal and Ventral Premotor Areas: Anatomical Connectivity and Functional Properties. Curr Opin Neurobiol 17: 234-242, 2007.

Jackson SR, and Shaw A. The Ponzo Illusion Affects Grip-Force but Not Grip-Aperture Scaling During Prehension Movements. J Exp Psychol Hum Percept Perform 26: 418-423, 2000.

Jones LA. Perception of Force and Weight: Theory and Research. Psychological Bulletin 100: 29-42, 1986.

Kaas JH. Evolution of Somatosensory and Motor Cortex in Primates. Anatomical Record Part a-Discoveries in Molecular Cellular and Evolutionary Biology 281A: 1148-1156, 2004.

Körding KP, Ku S-p, and Wolpert DM. Bayesian Integration in Force Estimation. J Neurophysiol 92: 3161-3165, 2004.

Körding KP, and Wolpert DM. Bayesian Integration in Sensorimotor Learning. Nature 427: 244-247, 2004.

Koseleff P. Studies in the Perception of Heaviness. Acta Psychol 13: 242-252, 1957.

Krakauer JW. Motor Learning and Consolidation: The Case of Visuomotor Rotation. edited by Sternad DSpringer, 2009, p. 405-421.

Krakauer JW, Pine ZM, Ghilardi MF, and Ghez C. Learning of Visuomotor Transformations for Vectorial Planning of Reaching Trajectories. J Neurosci 20: 8916-8924, 2000.

Lu MT, Preston JB, and Strick PL. Interconnections between the Prefrontal Cortex and the Premotor Areas in the Frontal-Lobe. Journal of Comparative Neurology 341: 375-392, 1994.

Lum PS, Reinkensmeyer DJ, Lehman SL, Li PY, and Stark LW. Feedforward Stabilization in a Bimanual Unloading Task. Exp Brain Res 89: 172-180, 1992.

Marsden CD, Merton PA, and Morton HB. Stretch Reflex and Servo Action in a Variety of Human Muscles. J Physiol 259: 531-560, 1976.

Massion J. Movement, Posture and Equilibrium - Interaction and Coordination. Progress in Neurobiology 38: 35-56, 1992.

Milner AD, and Goodale MA. Visual Pathways to Perception and Action. Prog Brain Res 95: 317-337, 1993.

Mishkin M, and Ungerleider LG. Contribution of Striate Inputs to the Visuospatial Functions of Parieto-Preoccipital Cortex in Monkeys. Behavioural Brain Research 6: 57, 1982.

Müller GE, and Schumann F. Über Die Psychologischen Grundlagen Der Vergleichung Gehobener Gewichte. Arch Gesamte Psychol 45: 37-112, 1889.

Norris D, and Kinoshita S. Perception as Evidence Accumulation and Bayesian Inference: Insights from Masked Priming. Journal of Experimental Psychology: General 137: 434-455, 2008.

Rabe K, Brandauer B, Li Y, Gizewski ER, Timmann D, and Hermsdorfer J. Size-Weight Illusion, Anticipation, and Adaptation of Fingertip Forces in Patients with Cerebellar Degeneration. J Neurophysiol 101: 569-579, 2009.

Rispal-Padel L, Cicirata F, and Pons C. Cerebellar Nuclear Topography of Simple and Synergistic Movements in the Alert Baboon (Papio-Papio). Exp Brain Res 47: 365-380, 1982.

Rizzolatti G, and Luppino G. The Cortical Motor System. Neuron 31: 889-901, 2001.

Ross HE. Sensory Information Necessary for the Size-Weight Illusion. Nature 212: 650-650, 1966.

Rothwell JC, Traub MM, and Marsden CD. Influence of Voluntary Intent on the Human Long-Latency Stretch Reflex. Nature 286: 496-498, 1980.

Sakreida K, Schubotz RI, Wolfensteller U, and von Cramon DY. Motion Class Dependency in Observers' Motor Areas Revealed by Functional Magnetic Resonance Imaging. J Neurosci 25: 1335-1342, 2005.

Sato Y, Toyoizumi T, and Aihara K. Bayesian Inference Explains Perception of Unity and Ventriloquism Aftereffect: Identification of Common Sources of Audiovisual Stimuli. Neural Comput 19: 3335-3355, 2007.

Scheidt RA, Dingwell JB, and Mussa-Ivaldi FA. Learning to Move Amid Uncertainty. J Neurophysiol 86: 971-985, 2001.

Scheidt RA, Reinkensmeyer DJ, Conditt MA, Rymer WZ, and Mussa-Ivaldi FA. Persistence of Motor Adaptation During Constrained, Multi-Joint, Arm Movements. J Neurophysiol 84: 853-862, 2000.

Schmitz C, Jenmalm P, Ehrsson HH, and Forssberg H. Brain Activity During Predictable and Unpredictable Weight Changes When Lifting Objects. J Neurophysiol 93: 1498-1509, 2005.

Schwartz O, Hsu A, and Dayan P. Space and Time in Visual Context. Nat Rev Neurosci 8: 522-535, 2007.

Shergill SS, Bays PM, Frith CD, and Wolpert DM. Two Eyes for an Eye: The Neuroscience of Force Escalation. Science 30: 187-187, 2003.

Shiratori T, and Latash ML. Anticipatory Postural Adjustments During Load Catching by Standing Subjects. Clin Neurophysiol 112: 1250-1265, 2001.

Simoncelli EP. Optimal Estimation in Sensory Systems. In: The New Cognitive Neurosciences, edited by Gazzaniga M. Cambridge, MA: MIT Press, 2009.

Smeets JBJ, and Brenner E. 10 Years of Illusions. J Exp Psychol Hum Percept Perform 32: 1501-1506, 2006.

Smeets JBJ, and Brenner E. Grasping Weber's Law. Curr Biol 18: R1089-R1090, 2008.

Smeets JBJ, and Brenner E. A New View on Grasping. Motor Control 3: 237-271, 1999.

Smith MA, Ghazizadeh A, and Shadmehr R. Interacting Adaptive Processes with Different Timescales Underlie Short-Term Motor Learning. PLoS Biol 4: 1035-1043, 2006.

Sperry RW. Neural Basis of the Spontaneous Optokinetic Response Produced by Visual Inversion. J Comp Physiol Psychol 43: 482-489, 1950.

Stocker AA, and Simoncelli EP. Noise Characteristics and Prior Expectations in Human Visual Speed Perception. Nature Neuroscience 9: 578-585, 2006a.

Stocker AA, and Simoncelli EP. Sensory Adaptation within a Bayesian Framework for Perception. Advances in Neural Information Processing Systems 18: 1291-1298, 2006b.

Thoroughman KA, and Shadmehr R. Learning of Action through Adaptive Combination of Motor Primitives. Nature 407: 742-747, 2000.

Ungerleider LG, and Mishkin M. Two Cortical Visual Systems. In: Analysis of Visual Behavior1982, p. 549–586.

Usnadze D. Uber Die Gewichtstauschung Und Ihre Analoga [Aspects of Weight Illusions]. Psychol Forsch 14: 366-379, 1931.

Wainwright MJ. Visual Adaptation as Optimal Information Transmission. Vision Res 39: 3960-3974, 1999.

Webster MJ, Bachevalier J, and Ungerleider LG. Connections of Inferior Temporal Areas Teo and Te with Parietal and Frontal-Cortex in Macaque Monkeys. Cerebral Cortex 4: 470-483, 1994.

Weiskrantz L, Elliott J, and Darlington C. Preliminary Observations on Tickling Oneself. Nature 230: 598-599, 1971.

Weiss Y, Simoncelli EP, and Adelson EH. Motion Illusions as Optimal Percepts. Nat Neurosci 5: 598-604, 2002.

Wing AM, Flanagan JR, and Richardson J. Anticipatory Postural Adjustments in Stance and Grip. Exp Brain Res 116: 122-130, 1997.

Wolpert DM, Ghahramani Z, and Jordan MI. An Internal Model for Sensorimotor Integration. Science 269: 1880-1882, 1995.

CHAPTER 3 – GENERALIZATION OF MOTOR ADAPTATION: EXAMINATION OF STATE AND CONTEXT DEPENDENCE

Bays PM, Wolpert DM (2006) Actions and consequences in bimanual interaction are represented in different coordinate systems. J Neurosci 26:7121-7126.

Conditt, M. A., Gandolfo, F. & Mussa-Ivaldi, F. A. The motor system does not learn the dynamics of the arm by rote memorization of past experience. Journal of Neurophysiology 78, 554-560 (1997).

Conditt, M. A. & Mussa-Ivaldi, F. A. Central representation of time during motor learning. Proc Natl Acad Sci U S A 96, 11625-11630 (1999).

Hwang, E. J., Smith, M. A. & Shadmehr R. Adaptation and generalization in acceleration dependent force fields. Exp Brain Res, 169:496-506, 2006

Hwang, E. J., Donchin, O., Smith, M.A. & Shadmehr, R. A gain-field encoding of limb position and velocity in the internal model of arm dynamics. PLoS Biol 1, 209-220, 2003

Gonzalez-Castro, L. N., Monsen, C. B. & Smith, M. A. The Binding of Learning to Action in Motor Adaptation. Plos Comput Biol 7 (2011).

Goodbody S. J. & Wolpert D. M. Temporal and amplitude generalization in motor learning. J Neurophysiol 79: 1825–1838, 1998.

Joiner, W. M., Ajayi, O., Sing, G. C. & Smith, M. A. Linear Hypergeneralization of Learned Dynamics Across Movement Speeds Reveals Anisotropic, Gain-Encoding Primitives for Motor Adaptation. *Journal of Neurophysiology* **105**, 45-59 (2011)

Krakauer, J. W., Pine, Z. M., Ghilardi, M. F. & Ghez, C. Learning of visuomotor transformations for vectorial planning of reaching trajectories. *J Neurosci* **20**, 8916-8924 (2000).

Malfait N, Shiller DM, Ostry DJ (2002) Transfer of motor learning across arm configurations. J Neurosci 22:9656-9660.

Scheidt, R. A., Reinkensmeyer, D. J., Conditt, M. A., Rymer, W. Z. & Mussa-Ivaldi, F. A. Persistence of motor adaptation during constrained, multi-joint, arm movements. J Neurophysiol 84, 853-862 (2000).

Shadmehr R, Mussa-Ivaldi FA (1994) Adaptive Representation of Dynamics during Learning of a Motor Task. J Neurosci 14:3208-3224.

Shadmehr R, Moussavi ZMK (2000) Spatial generalization from learning dynamics of reaching movements. J Neurosci 20:7807-7815.

Sing, G. C., Joiner, W. M., Nanayakkara, T., Brayanov, J. B. & Smith, M. A. Primitives for motor adaptation reflect correlated neural tuning to position and velocity. Neuron 64, 575-589 (2009).

Sing, G. C. & Smith, M. A. Reduction in Learning Rates Associated with Anterograde Interference Results from Interactions between Different Timescales in Motor Adaptation. Plos Comput Biol 6 (2010).

Smith, M. A., Ghazizadeh, A. & Shadmehr, R. Interacting adaptive processes with different timescales underlie short-term motor learning. PLoS Biol 4, e179 (2006).

CHAPTER 4 – MOTOR MEMORY IS ENCODED AS A GAIN-FIELD COMBINATION OF INTRINSIC AND EXTRINSIC ACTION REPRESENTATIONS

Ahmed AA, Wolpert DM, Flanagan JR (2008) Flexible representations of dynamics are used in object manipulation. Curr Biol 18:763-768.

Akaike H (1981) Citation Classic - a New Look at the Statistical-Model Identification. Cc/Eng Tech Appl Sci:22-22.

Andersen RA, Mountcastle VB (1983) The influence of the angle of gaze upon the excitability of the light-sensitive neurons of the posterior parietal cortex. J Neurosci 3:532-548.

Andersen RA, Essick GK, Siegel RM (1985) Encoding of Spatial Location by Posterior Parietal Neurons. Science 230:456-458.

Andersen RA, Buneo C, Pesaran B (2004) Coordinate transformations for sensory-guided movements. Perception 33:10-10.

Andersen RA, Batista AP, Buneo CA, Snyder LH, Cohen YE (1998) Common spatial reference frames for reach and eye movements in posterior parietal cortex. Perception 27:16-16.

Anderson DR, Burnham KP, White GC (1998) Comparison of Akaike information criterion and consistent Akaike information criterion for model selection and statistical inference from capture-recapture studies. J Appl Stat 25:263-282.

Baraduc P, Wolpert DM (2002) Adaptation to a visuomotor shift depends on the starting posture. J Neurophysiol 88:973-981.

Bays PM, Wolpert DM (2006) Actions and consequences in bimanual interaction are represented in different coordinate systems. J Neurosci 26:7121-7126.

Berniker M, Kording K (2008) Estimating the sources of motor errors for adaptation and generalization. Nat Neurosci 11:1454-1461.

Berniker M, Kording KP (2011) Estimating the relevance of world disturbances to explain savings, interference and long-term motor adaptation effects. Plos Comput Biol 7:e1002210.

Brainard DH (1997) The psychophysics toolbox. Spatial Vision 10:433-436.

Buneo CA, Andersen RA (2006) The posterior parietal cortex: Sensorimotor interface for the planning and online control of visually guided movements. Neuropsychologia 44:2594-2606.

Burnham KP, Anderson DR (2004) Multimodel inference - understanding AIC and BIC in model selection. Sociol Method Res 33:261-304.

Chang SWC, Papadimitriou C, Snyder LH (2009) Using a Compound Gain Field to Compute a Reach Plan. Neuron 64:744-755.

Cohen DA, Pascual-Leone A, Press DZ, Robertson EM (2005) Off-line learning of motor skill memory: A double dissociation of goal and movement. P Natl Acad Sci USA 102:18237-18241.

Conditt MA, Mussa-Ivaldi FA (1999) Central representation of time during motor learning. Proc Natl Acad Sci U S A 96:11625-11630.

Conditt MA, Gandolfo F, Mussa-Ivaldi FA (1997) The motor system does not learn the dynamics of the arm by rote memorization of past experience. J Neurophysiol 78:554-560.

de Xivry JJO, Marko MK, Pekny SE, Pastor D, Izawa J, Celnik P, Shadmehr R (2011) Stimulation of the Human Motor Cortex Alters Generalization Patterns of Motor Learning. J Neurosci 31:7102-7110.

Donchin O, Rabe K, Diedrichsen J, Lally N, Schoch B, Gizewski ER, Timmann D (2012) Cerebellar regions involved in adaptation to force field and visuomotor perturbation. J Neurophysiol 107:134-147.

Fine MS, Thoroughman KA (2006) Motor adaptation to single force pulses: sensitive to direction but insensitive to within-movement pulse placement and magnitude. J Neurophysiol 96:710-720.

Galea JM, Vazquez A, Pasricha N, de Xivry JJO, Celnik P (2011) Dissociating the Roles of the Cerebellum and Motor Cortex during Adaptive Learning: The Motor Cortex Retains What the Cerebellum Learns. Cereb Cortex 21:1761-1770.

Gandolfo F, MussaIvaldi FA, Bizzi E (1996) Motor learning by field approximation. P Natl Acad Sci USA 93:3843-3846.

Ghahramani Z, Wolpert DM, Jordan MI (1996) Generalization to local remappings of the visuomotor coordinate transformation. J Neurosci 16:7085-7096.

Ghez C, Scheidt R, Heijink H (2007) Different learned coordinate frames for planning trajectories and final positions in reaching. J Neurophysiol 98:3614-3626.

Ghez C, Krakauer JW, Sainburg RL, Ghilardi M (2000) Spatial representation and internal models of limb dynamics in motor learning. In: The new cognitive neurosciences, 2nd edition Edition (Gazzaniga MS, ed), pp 501-513. Cambridge, Mass.: MIT Press.

Gonzalez Castro LN, Monsen CB, Smith MA (2011) The binding of learning to action in motor adaptation. Plos Comput Biol 7:e1002052.

Haswell CC, Izawa J, Dowell LR, Mostofsky SH, Shadmehr R (2009) Representation of internal models of action in the autistic brain. Nat Neurosci 12:970-972.

Hatsopoulos NG (2005) Encoding in the motor cortex: Was evarts right after all? Focus on "Motor cortex neural correlates of output kinematics and kinetics during isometric-force and arm-reaching tasks". J Neurophysiol 94:2261-2262.

Hikosaka O, Nakamura K, Sakai K, Nakahara H (2002) Central mechanisms of motor skill learning. Current Opinion in Neurobiology 12:217-222.

Hwang EJ, Smith MA, Shadmehr R (2006) Adaptation and generalization in acceleration-dependent force fields. Exp Brain Res 169:496-506.

Joiner WM, Ajayi O, Sing GC, Smith MA (2011) Linear hypergeneralization of learned dynamics across movement speeds reveals anisotropic, gain-encoding primitives for motor adaptation. J Neurophysiol 105:45-59.

Kakei S, Hoffman DS, Strick PL (1999) Muscle and movement representations in the primary motor cortex. Science 285:2136-2139.

Kakei S, Hoffman DS, Strick PL (2001) Direction of action is represented in the ventral premotor cortex. Nat Neurosci 4:1020-1025.

Kalaska JF (2009) From Intention to Action: Motor Cortex and the Control of Reaching Movements. Progress in Motor Control: A Multidisciplinary Perspective 629:139-178.

Kalaska JF, Cohen DAD, Hyde ML, Prudhomme M (1989) A Comparison of Movement Direction-Related Versus Load Direction-Related Activity in Primate Motor Cortex, Using a Two-Dimensional Reaching Task. J Neurosci 9:2080-2102.

Kleiner M, Brainard D, Pelli D (2007) What's new in Psychtoolbox-3? Perception 36:14-14.

Krakauer JW, Pine ZM, Ghilardi MF, Ghez C (2000) Learning of visuomotor transformations for vectorial planning of reaching trajectories. J Neurosci 20:8916-8924.

Malfait N, Shiller DM, Ostry DJ (2002) Transfer of motor learning across arm configurations. J Neurosci 22:9656-9660.

MATLAB (2010) version 7.10.0 (R2010a). Natick, Massachusetts: The MathWorks Inc.

Mattar AAG, Ostry DJ (2007) Modifiability of generalization in dynamics learning. J Neurophysiol 98:3321-3329.

Mattar AAG, Ostry DJ (2010) Generalization of Dynamics Learning Across Changes in Movement Amplitude. J Neurophysiol 104:426-438.

Morton SM, Bastian AJ (2004) Prism adaptation during walking generalizes to reaching and requires the cerebellum. J Neurophysiol 92:2497-2509.

Morton SM, Lang CE, Bastian AJ (2001) Inter- and intra-limb generalization of adaptation during catching. Exp Brain Res 141:438-445.

Noto CT, Watanabe S, Fuchs AF (1999) Characteristics of simian adaptation fields produced by behavioral changes in saccade size and direction. J Neurophysiol 81:2798-2813.

Pesaran B, Nelson MJ, Andersen RA (2006) Dorsal premotor neurons encode the relative position of the hand, eye, and goal during reach planning. Neuron 51:125-134.

Pine ZM, Krakauer JW, Gordon J, Ghez C (1996) Learning of scaling factors and reference axes for reaching movements. Neuroreport 7:2357-2361.

Poggio T, Bizzi E (2004) Generalization in vision and motor control. Nature 431:768-774.

Pouget A, Snyder LH (2000) Computational approaches to sensorimotor transformations. Nat Neurosci 3 Suppl:1192-1198.

Quaia C, Joiner WM, Fitzgibbon EJ, Optican LM, Smith MA (2010) Eye movement sequence generation in humans: Motor or goal updating? J Vis 10.

Rabe K, Livne O, Gizewski ER, Aurich V, Beck A, Timmann D, Donchin O (2009) Adaptation to Visuomotor Rotation and Force Field Perturbation Is Correlated to Different Brain Areas in Patients With Cerebellar Degeneration. J Neurophysiol 101:1961-1971.

Scott SH, Kalaska JF (1997) Reaching movements with similar hand paths but different arm orientations .1. Activity of individual cells in motor cortex. J Neurophysiol 77:826-852.

Sergio LE, Kalaska JF (2003) Systematic changes in motor cortex cell activity with arm posture during directional isometric force generation. J Neurophysiol 89:212-228.

Sergio LE, Hamel-Paquet C, Kalaska JF (2005) Motor cortex neural correlates of output kinematics and kinetics during isometric-force and arm-reaching tasks. J Neurophysiol 94:2353-2378.

Shadmehr R, Mussa-Ivaldi FA (1994) Adaptive Representation of Dynamics during Learning of a Motor Task. J Neurosci 14:3208-3224.

Shadmehr R, Moussavi ZMK (2000) Spatial generalization from learning dynamics of reaching movements. J Neurosci 20:7807-7815.

Smith MA, Shadmehr R (2005) Intact ability to learn internal models of arm dynamics in Huntington's disease but not cerebellar degeneration. J Neurophysiol 93:2809-2821.

Snyder LH, Batista AP, Andersen RA (1998a) Spatially aligned saccade and intended reach responses in monkey posterior parietal cortex. J Cognitive Neurosci 10:90-90.

Snyder LH, Grieve KL, Brotchie P, Andersen RA (1998b) Separate body- and world-referenced representations of visual space in parietal cortex. Nature 394:887-891.

Spong MW, Hutchinson S, Vidyasagar M (2006) Forward and Inverse Kinematics. In: Robot Modelling and Control, pp 74-118. Hoboken, NJ: John Wiley & Sons, Inc.

Tanaka H, Sejnowski TJ, Krakauer JW (2009) Adaptation to Visuomotor Rotation Through Interaction Between Posterior Parietal and Motor Cortical Areas. J Neurophysiol 102:2921-2932.

Thoroughman KA, Shadmehr R (2000) Learning of action through adaptive combination of motor primitives. Nature 407:742-747.

Vetter P, Goodbody SJ, Wolpert DM (1999) Evidence for an eye-centered spherical representation of the visuomotor map. J Neurophysiol 81:935-939.

Vindras P, Viviani P (1998) Frames of reference and control parameters in visuomanual pointing. J Exp Psychol Human 24:569-591.

Vuong QH (1989) Likelihood Ratio Tests for Model Selection and Non-Nested Hypotheses. Econometrica 57:307-333.

Wagner MJ, Smith MA (2008) Shared internal models for feedforward and feedback control. J Neurosci 28:10663-10673.

Wang JS, Sainburg RL (2005) Adaptation to visuomotor rotations remaps movement vectors, not final positions. J Neurosci 25:4024-4030.

Wu W, Hatsopoulos N (2006) Evidence against a single coordinate system representation in the motor cortex. Exp Brain Res 175:197-210.

Yokoi A, Hirashima M, Nozaki D (2011) Gain field encoding of the kinematics of both arms in the internal model enables flexible bimanual action. J Neurosci 31:17058-17068.

CHAPTER 5 – A UNIFORM ARCHITECTURE FOR PROCEDURAL LEARNING IN THE HUMAN NERVOUS SYSTEM

Ahissar M, Hochstein S (1997) Task difficulty and the specificity of perceptual learning. Nature 387:401-406.

Ahissar M, Hochstein S (2004) The reverse hierarchy theory of visual perceptual learning. Trends Cogn Sci 8:457-464.

Ahissar M, Nahum M, Nelken I, Hochstein S (2009) Reverse hierarchies and sensory learning. Philos Trans R Soc Lond B Biol Sci 364:285-299.

Brainard DH (1997) The psychophysics toolbox. Spatial Vision 10:433-436.

Donchin O, Francis JT, Shadmehr R (2003) Quantifying generalization from trial-by-trial behavior of adaptive systems that learn with basis functions: Theory and experiments in human motor control. J Neurosci 23:9032-9045.

Ghahramani Z, Wolpert DM, Jordan MI (1996) Generalization to local remappings of the visuomotor coordinate transformation. J Neurosci 16:7085-7096.

Ghez C, Krakauer JW, Sainburg RL, Ghilardi M (2000) Spatial representation and internal models of limb dynamics in motor learning. In: The new cognitive neurosciences, 2nd edition Edition (Gazzaniga MS, ed), pp 501-513. Cambridge, Mass.: MIT Press.

Gonzalez Castro LN, Monsen CB, Smith MA (2011) The binding of learning to action in motor adaptation. Plos Comput Biol 7:e1002052.

Haswell CC, Izawa J, Dowell LR, Mostofsky SH, Shadmehr R (2009) Representation of internal models of action in the autistic brain. Nat Neurosci 12:970-972.

Hochstein S, Ahissar M (2002) View from the top: hierarchies and reverse hierarchies in the visual system. Neuron 36:791-804.

Kleiner M, Brainard D, Pelli D (2007) What's new in Psychtoolbox-3? Perception 36:14-14.

Krakauer JW, Pine ZM, Ghilardi MF, Ghez C (2000) Learning of visuomotor transformations for vectorial planning of reaching trajectories. J Neurosci 20:8916-8924.

Malfait N, Ostry DJ (2004) Is interlimb transfer of force-field adaptation a cognitive response to the sudden introduction of load? J Neurosci 24:8084-8089.

Mattar AAG, Ostry DJ (2007) Modifiability of generalization in dynamics learning. J Neurophysiol 98:3321-3329.

Mazzoni P, Krakauer JW (2006) An implicit plan overrides an explicit strategy during visuomotor adaptation. J Neurosci 26:3642-3645.

Morton SM, Bastian AJ (2004) Prism adaptation during walking generalizes to reaching and requires the cerebellum. J Neurophysiol 92:2497-2509.

Pine ZM, Krakauer JW, Gordon J, Ghez C (1996) Learning of scaling factors and reference axes for reaching movements. Neuroreport 7:2357-2361.

Poggio T, Bizzi E (2004) Generalization in vision and motor control. Nature 431:768-774.

Shadmehr R, Mussa-Ivaldi FA (1994) Adaptive Representation of Dynamics during Learning of a Motor Task. J Neurosci 14:3208-3224.

Shadmehr R, Moussavi ZMK (2000) Spatial generalization from learning dynamics of reaching movements. J Neurosci 20:7807-7815.

Tanaka H, Sejnowski TJ, Krakauer JW (2009) Adaptation to Visuomotor Rotation Through Interaction Between Posterior Parietal and Motor Cortical Areas. J Neurophysiol 102:2921-2932.

Taylor JA, Ivry RB (2011) Flexible cognitive strategies during motor learning. Plos Comput Biol 7:e1001096.

Taylor JA, Ivry RB (2012) The role of strategies in motor learning. Ann N Y Acad Sci 1251:1-12.

Taylor JA, Wojaczynski GJ, Ivry RB (2011) Trial-by-trial analysis of intermanual transfer during visuomotor adaptation. J Neurophysiol 106:3157-3172.

Wang J, Joshi M, Lei Y (2011) The extent of interlimb transfer following adaptation to a novel visuomotor condition does not depend on awareness of the condition. J Neurophysiol 106:259-264.

Yokoi A, Hirashima M, Nozaki D (2011) Gain field encoding of the kinematics of both arms in the internal model enables flexible bimanual action. J Neurosci 31:17058-17068.